A Coupled Soil Hydrology Model and Terrestrial Ecology Scheme for the MIT Integrated Global Systems Model

by

Susan Dunne

Submitted to the Department of Civil and Environmental Engineering
in partial fulfillment of the requirements for the degree of

Master of Science in
Civil and Environmental Engineering

at the

MASSACHUSETTS INSTITUTE OF TECHNOLOGY

June 2002

Author .....

Susan Dunne
Department of Civil and Environmental Engineering
26th February 2002

Certified by.....

Professor Dara Entekhabi
Department of Civil and Environmental Engineering
Thesis Supervisor

Accepted by.....

Oral Buyukozturk
Chairman, Departmental Committee on Graduate Studies

A Coupled Soil Hydrology and Terrestrial Ecology Scheme for the MIT Integrated Global Systems Model

by

Susan Dunne

Submitted to the Department of Civil and Environmental Engineering on 26th February 2002, in partial fulfillment of the requirements for the degree of Master of Science in Civil and Environmental Engineering

Abstract

In order to investigate the evolution of climate and land-cover, in particular the interactions and feedbacks between them, the land hydrology and terrestrial ecology modules of any integrated global system model must be physically consistent. The atmosphere and the terrestrial biosphere must be considered as a system, coupled through chemical cycles, and acting on a range of spatial and time-scales. The MIT Integrated Global System Model (IGSM) includes coupled models of atmospheric chemistry, physical climate and human activity, and it is a framework within which variability and change in the water cycle may be quantitatively assessed. The objective of this project is to determine whether the National Center for Atmospheric Research Land Surface Model could be successfully incorporated into the MIT Integrated Global Systems Model. This would enable a synchronous coupling of the hydrologic and ecological cycles to yield consistent surface energy, water and CO_2 fluxes at each time step.

One of the major changes in employing the NCAR LSM in the MIT IGSM is that the representation of the land surface will be more detailed. Whereas the current model has just four surface type categories (ocean, ocean ice, land and land ice), the new model will have up to fifteen land cover and biome surface types. Factors were derived by which precipitation could be adjusted to reflect the variation in precipitation over different cover types in each zonal band. As the NCAR LSM is vectorized, the atmospheric forcing applied to each individual cover type could be factored without any increase in computational effort.

Results from a 50-year simulation demonstrate that the models could be coupled to yield improved estimates of surface fluxes at the terrestrial component of the Earth's surface. This was achieved without a discernable increase in CPU time for hydrological parameterization calculations. Since the NCAR LSM also calculates carbon flux, there are further potential savings by eliminating the need for asynchronous terrestrial ecology model integrations. Successful incorporation of the NCAR LSM into the MIT IGSM may facilitate expansion of the role of the climate model to include estimation of biogeochemical fluxes in addition to standard climatological outputs.

Thesis Supervisor: Dara Entekhabi
Title: Professor

Acknowledgements

Many thanks to those who provided me with sponsorship during this project, notably the National University of Ireland, the Fulbright Commission of Ireland, MIT Rosenblith Fellowship, and MIT Center for Global Change Science.

I wish to acknowledge the Climate and Global Dynamics Division of the National Center for Atmospheric Research in Boulder, Colorado, for allowing the use of the Land Surface Model (NCAR LSM, Version 1.0).

For his guidance, encouragement and patience, I am very thankful to my advisor, Professor Dara Entekhabi.

For the hours he spent demystifying the GISS model, his patience and generosity, many thanks to Andrei Sokolov. Thanks to Radhika DeSilva for sharing her experience with the NCAR LSM. I am very grateful to Steve Margulis and Gary Steele for their help in clearing many software hurdles.

I am most grateful for the constant support and encouragement of family and friends in Dublin and Boston.

Table of Contents

List of Figures

List of Tables

Chapter 1

Introduction

The atmosphere and the terrestrial biosphere comprise a system coupled through chemical, energy and water cycles and acting on a range of temporal and spatial scales. Science questions abound in the field of climate change, and few if any can be addressed by considering one cycle without reference to the others.

In order to address the science questions about the Earth System and about future climate impacts on the global ecosystem based on models, there needs to be tighter coupling between the terrestrial ecology processes and hydrologic processes.

While climate change may be manifested in changes in surface temperature, sea level, ocean circulation patterns and occurrence of extreme climatic events, its origins rest not only in natural variability, but also in anthropogenic processes. Integrated climate models are used to simulate global environmental changes that may result from anthropogenic causes. They also allow us to study the uncertainties associated with projected changes, and the impact of proposed policies on such changes. The MIT Integrated Global System Model (IGSM) includes coupled models of atmospheric chemistry, physical climate and human activity, and it is an example of a framework within which the variability and change in climate may be quantitatively assessed. In the MIT IGSM, the combined anthropogenic and natural emissions model outputs are driving forces for the coupled atmospheric chemistry and climate model, the essential components of which are

chemistry, atmospheric chemistry, atmospheric circulation and ocean circulation. The climate outputs drive a terrestrial ecosystems model predicting land vegetation changes, land CO_2 changes, and soil composition, which feed back to the coupled chemistry/climate, and natural emissions models.

A shortcoming of the MIT IGSM is the asynchronous coupling of the land surface hydrology component and the terrestrial ecology model. At each hourly time-step the land surface hydrology component is forced with precipitation, wind, temperature, humidity and radiation input from the atmospheric component. In turn, the land surface model generates the surface moisture, energy, momentun and radiative fluxes required by the next step of the atmospheric model. On the other hand, the TEM is run on a monthly time-step, forced with monthly average precipitation, temperature and cloudiness, as well as a description of soil texture, elevation and water availability. The TEM estimates carbon and nitrogen fluxes, which are inputs to the coupled chemistry-climate model and the natural emissions model. An advantage of the NCAR LSM is that it estimates the carbon dioxide flux at each time-step, yielding a value that is consistent with the rate of evapotranspiration.

A major goal of the MIT Joint Program for Global Change Science is the evaluate uncertainties in climate change prediction (Jacoby and Prinn, 1994). Typically, numerous versions of an atmospheric model will be used to study several scenarios for changes in greenhouse gas concentrations, resulting in a large number of 50-100 year simulations being carried out for typical studies. As Global Circulation Models (GCMs) require an

enormous amount of computer time, the current MIT Climate Model couples a two-dimensionsal (2D – zonally and vertically) land and ocean-resolving (LO) statistical-dynamical model of the atmosphere to a 3D ocean model. This simplified 2D atmosphere/3D ocean model successfully reproduces many characteristics of the current zonally-averaged climate (Sokolov and Stone, 1995), while being twenty times faster than 3D models with similar latitudinal and vertical resolutions.

The objective of this research was to determine if the NCAR LSM could be introduced within the framework of the MIT IGSM, as a first step towards having a truly consistent coupling between the terrestrial ecosystem and the climate model. A detailed description of the relevant components of the MIT IGSM and the NCAR LSM is given in Chapters 2 and 3. Particular attention is drawn to the similarities and differences between the NCAR model and the climate and terrestrial ecology components of the MIT model.

In order to use the NCAR LSM within the framework of the MIT IGSM, it must be included as a zonally averaged model. One of the major changes in employing the NCAR LSM is the representation of the land surface. Whereas the current climate model distinguishes between ocean, ocean ice, land and land ice, the new model will have up to fifteen land cover types within each zonal band. Model inputs that had to be adapted include geographical location, land surface parameterization, land surface type, soil color and percentage lake and wetlands. These changes are described in detail in Chapter 5, along with the changes to model architecture required to accommodate them. Factors were derived by which zonal precipitation could be adjusted to reflect the variation in

precipitation over these cover types. It is noteworthy that as the NCAR LSM is vectorized, the atmospheric forcing applied to each individual cover type could be factored without any increase in computational effort.

In order to determine the land cover distribution and the precipitation, data was downloaded from the Global Ecosystems Database II, and used in conjunction with the data provided with NCAR LSM. These datasets are discussed in full in Chapter 4, and the resultant characterization of the global land surface and development of the precipitation scheme is described in Chapter 5.

In Chapter 6 the results from a fifty-year simulation are presented, to demonstrate that the NCAR Land Surface Model, when coupled to the GISS model produces a satisfactory climatology. The annual mean and seasonality in net radiation show that the exchange of forcing data is correct, while those of temperature and precipitation indicate that the new model yields a satisfactory meteorology while showing the same artifacts of zonal averaging as those from the old model. Some improvement is seen in the estimates of latent and sensible heat fluxes compared to those calculated by the GISS model. The estimated carbon dioxide flux from the land surface exhibits the trends associated with changing seasons and surface type distribution.

Chapter 7 contains the conclusions from this research, primarily that the NCAR LSM could be successfully coupled into the MIT IGSM. The implications of this success, in

particular the potential to expand the scope of the climate model to include estimation of biogeochemical fluxes in addition to standard climatological outputs, are also discussed. In addition, several prospective areas of future research are outlined.

Chapter 2

Coupled Climate and Ecosystem Modeling for Integrated Assessment : The MIT IGSM

2.1 Introduction

Projected changes in future climate associated with an increase in greenhouse gases, and other chemical species such as nitrogen, phosphorous and potassium, are expected to be large enough to cause fundamental changes in ecological function and even global vegetation distribution.

Studies have also shown that changes in land cover can have a profound effect on regional climate, and possibly global climate. Therefore, the atmosphere and the terrestrial biosphere must be considered as a system, coupled through water, energy and chemical cycles, and acting on a range of spatial and time-scales.

A typical land surface model estimates the exchange of water and energy through the turbulent sensible and latent heat fluxes and radiative transfers. A terrestrial ecology model, on the other hand is used to predict the states of plants and soils as they respond to climate change, changes in CO_2 concentrations, nitrogen availability and land-use. In particular, they simulate the carbon and nitrogen fluxes from the terrestrial biosphere when forced with climate data and a description of the land surface.

In order to investigate the evolution of climate and land-cover, in particular the interactions and feedbacks between them, the land surface parameterization and terrestrial ecology modules of any integrated global system model must be physically consistent. Typically they differ significantly in how they consider the water and energy balances, so water and energy calculations are not always consistent.

In addition, the co-evolution of the hydroclimate and biospheric systems suggests that coupled ecological-climate models may have different equilibrium climate-vegetations regimes, and may be sensitive to ecotone initialization (Pielke, 1998).

Results from preliminary studies carried out using the existing Terrestrial Ecology Model (TEM), the MIT Joint Program on the Science and Policy of Global Change have shown that carbon storage in terrestrial ecosystems results from the superposition of a number of factors that are related to the physical climate system, biogeochemical cycles and land-use changes.

For example, when run with the land-use dataset of Ramankutty and Foley (1999), they found that historical change in land-use has led to a reduction in terrestrial carbon. During the 1980s and 1990s, terrestrial ecosystems behaved as a net carbon sink, due to the effects of CO_2 fertilization. Furthermore, they have found that changes in nitrogen dynamics and water use efficiencies caused feedbacks in the terrestrial carbon cycle, such that interactions between climate and atmospheric CO_2 concentrations led to an enhancement of this terrestrial carbon sink.

2.2 Integrated Modeling

The results discussed above prompted the need to develop the MIT IGSM to consider feedbacks between the fundamental physical and land-atmosphere processes, for example feedbacks related to carbon storage, albedo, trace gases and transpiration. Important science questions in this field include:

1) Can changes in land ecosystems caused by climate change and human activity feed back to climate and air quality through changes in albedo, terrestrial carbon storage, and trace gas exchange rates?
2) Nitrogen is a growth-limiting factor in many diverse aquatic and terrestrial ecosystems. Can coupling of the nitrogen, carbon and water cycles in land atmosphere interactions improve the ability to estimate regional evaporative fluxes in terrestrial ecosystems?
3) How do the combined effects of land-use change, atmospheric pollution, and climate change affect the productivity, carbon storage capacity and distribution of major vegetation types over the globe?

The central hypothesis of this research is that variability and change in the terrestrial component of the water cycle should be characterized in the context of the global cycles of several key macro- and micro- nutrient chemical species. The MIT Integrated Global System Model (IGSM) includes coupled models of atmospheric chemistry, physical

climate and human activity, and it is the framework within which the variability and change in the water cycle may be quantitatively assessed.

2.3 MIT Integrated Global Integrated Systems Model (IGSM)

The IGSM consists of a set of coupled sub-models of economic development and associated emissions, natural biogeochemical cycles, climate, and natural ecosystems. It attempts to include each of the major areas in the natural and social sciences that are relevant to the issue of climate change, and is designed to illuminate key issues linking science and policy.

Refer to Figure 2.1, a schematic illustrating the framework and components of the MIT Integrated Global Systems Model. Feedbacks between the submodels which are currently included are shown by solid lines, while those that are under development for future inclusion are shown by dashed lines. Output from both anthropogenic and natural emissions models drive the coupled atmospheric chemistry and climate model, which in turn drive a terrestrial ecosystems model (TEM). The TEM then predicts vegetation changes, land carbon dioxide (CO2) fluxes and soil composition, which can feed back to the coupled chemistry-climate model and the natural emissions model.

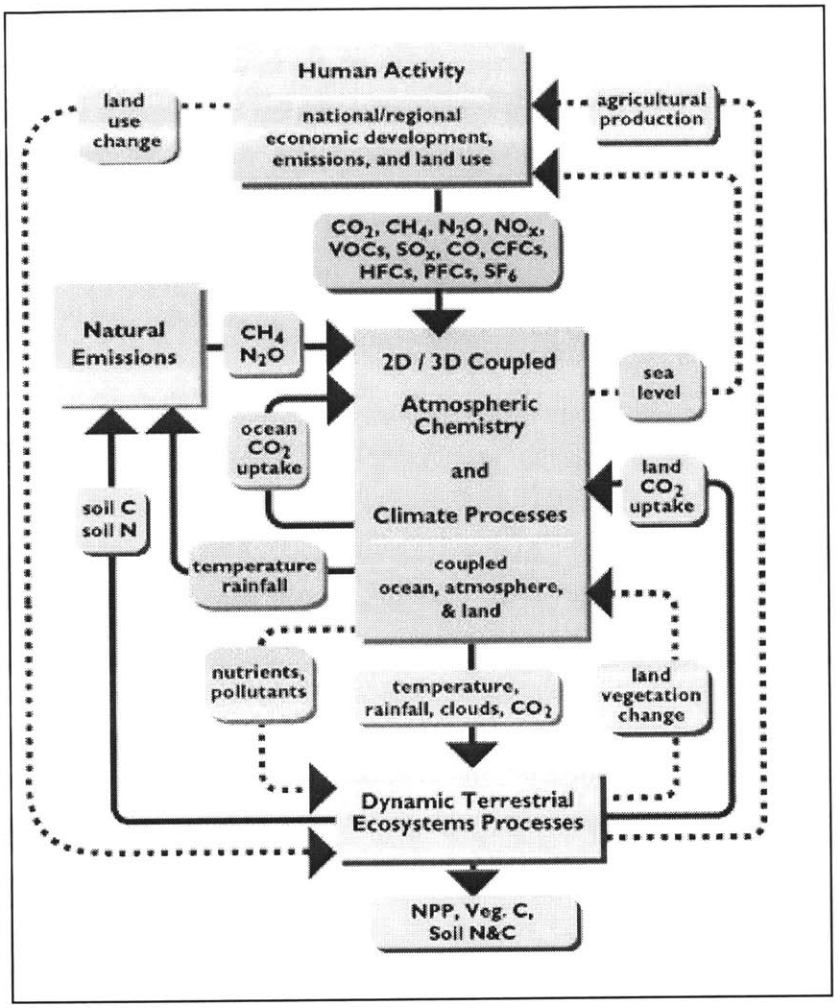

Figure 2.1 Schematic Diagram of The MIT Integrated Global Systems Model (IGSM).
Source: http://web.mit.edu/globalchange/www

By carefully selecting key processes in each of the sub-models and defining the level of detail in which it must be represented, complex models for all the relevant processes can be coupled in a computationally efficient form. Such efficiency allows us to identify and understand important feedbacks between model components and to compute sensitivities of policy-relevant variables (e.g. rainfall, temperature, ecosystem state) to assumptions in the various components and subcomponents in the coupled models.

Furthermore, the IGSM must be computationally feasible for use in multiple 100-year simulations, so that the future impacts on climate due to proposed policies can be examined. For simulations of this length, intra-storm variability need not be studied, so the model can be zonally averaged without any loss in accuracy.

In the following sections we will briefly introduce the components of the MIT IGSM, paying particular attention to the climate dynamics component. It is this element which we seek to improve through introduction of the NCAR Land Surface Model. Information in this chapter is largely drawn from Prinn et al. (1999), which provides descriptions of all components of the MIT IGSM.

2.4 MIT IGSM Climate dynamics (MIT 2D-LO)

The coupled climate-chemistry model is shown in Figure 2.2. The objective of the climate model is to simulate the present climate as well as reproducing the climate change patterns predicted by three-dimensional General Circulation Models (GCMs) in a more computationally efficient manner. The current MIT climate model consists of a two-dimensional (2D) land and ocean (LO) resolving statistical dynamical model of the atmosphere coupled to a three-dimensional ocean general circulation model.

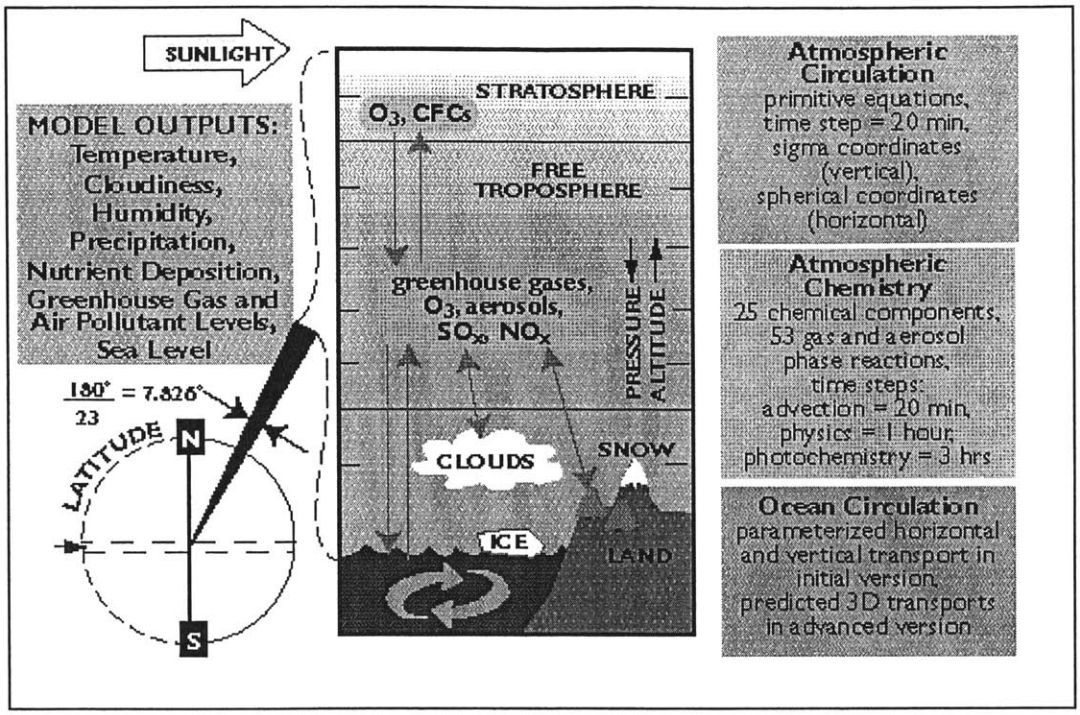

Figure 2.2 Schematic Diagram of the MIT IGSM Coupled Climate-Atmospheric Chemistry Model
Source: http://web.mit.edu/globalchange/www

The 2D-LO climate model is coupled to the atmospheric chemistry model, and by running interactively and simultaneously they are capable of predicting the atmospheric concentrations of radiatively and chemically significant trace species. The coupled climate and chemistry model is 2D (latitude and altitude) with separate predictions over land and ocean at each latitude. The grid used in the model consists of 24 points in latitude, corresponding to a resolution of 7.826 degrees. The model has nine layers in the vertical, notably two in the planetary boundary layer, five in the troposphere, and two in the stratosphere. Longitudinal variations are obtained from a combination of observed climate data and selected transient runs of 3D climate models.

Two-dimensional models certainly have some limitations when compared to 3D GCMs. For example, they are incapable of simulating features of the atmospheric circulation attributed to the temperature contrast between land and ocean. They also fail to take real topography into account. However, 2D models can be used to model climate change scenarios reasonably well if certain modifications are made.

The two-dimensional statistical dynamical model was originally developed at the NASA Goddard Institute for Space Studies (GISS). It was derived from the GISS GCM of Hansen et al. (1983). Yao and Stone (1987) provide a detailed description of the original 2D model, which they found to be 23 times faster than the GISS full GCM with similar latitudinal and vertical resolution. The most important feature of the 2D model is that it incorporates the radiation code from the GISS GCM. This code incorporates all of the significant greenhouse gases such as H_2O, CO_2, CH_4, N_2O, CFCs and aerosols. For use within the MIT IGSM, several modifications were made to the GISS 2D model. These changes will be discussed below.

The name "MIT 2D-LO" derives from the first necessary change. The GISS 2D model assumed that the terrestrial boundary consisted entirely of ocean. The MIT 2D-LO, like the GISS GCM, allows up to four different kinds of surface in the same grid cell, namely ocean, ocean ice, land and land ice. The surface characteristics such as temperature and soil moisture as well as surface turbulent fluxes are calculated separately for each kind of surface while the atmosphere is assumed to be well-mixed horizontally in each grid cell.

The weighted averages of fluxes from the four surface types are used to calculate changes of temperature, humidity, and wind speed in the model's first layer due to the air-surface interaction. The same applies to the surface albedo used in radiative flux calculations.

The MIT 2D-LO model explicitly solves the primitive equations for zonal mean flow and includes parameterizations of heat, moisture, and momentum transport by large scale eddies based on baroclinic instability theory. It also includes parameterizations of all the main physical processes such as radiation, convection and cloud formation. It is thus capable of reproducing many of the nonlinear interactions taking place in GCMs.

The surface flux calculation scheme is based on Monin-Obukhov Similarity Theory, and uses the approximation for transfer coefficients derived by Deardorff (1978). Details of this scheme, and those used for ground temperature and moisture calculations are given in Hansen et al. (1983).

The main difference between the approaches of the MIT 2D-LO and that of the original GISS GSM lies in the definition of variables at the top boundary of the surface layer. In the GISS GCM, the surface layer is assumed to be in equilibrium. The numerical realization of this assumption results in a complicated algorithm including nested iterations. This algorithm can be used in the GISS GCM and 2D-LO without land, but results in computational difficulties when land is included. Therefore in the MIT 2D-LO the assumption of surface layer equilibrium is replaced by the assumption that the layer between the surface and the model's first layer is well-mixed.

Other differences between the MIT 2D-LO and the original GISS 2D model are a simplified wind speed calculation in the MIT model, as well as a modification to the cloud parameterization. In the original GISS 2D model, condensation occurs when humidity reaches 100%. In the MIT 2D-LO model, condensation is allowed to occur in partly saturated cells to allow for subgrid-scale variation in relative humidity. The criterion for condensation, h_{con}, is therefore reduced to 90%. This small changes has a significant impact on the model's sensitivity, insofar as the model produces a negative cloud feedback when h_{con} is 100%, whereas it produces a positive cloud feedback if h_{con} is reduced to 90%.

Sokolov and Stone (1995) presented results of simulations with the MIT 2D-LO model, demonstrating that it could reproduce the main features of the present climate reasonably well. The objective of this project is to further improve the performance of the MIT 2D-LO by incorporating the NCAR land surface model to perform the surface flux, ground temperature and moisture calculations over the land component of each grid cell.

2.5 MIT IGSM Terrestrial Ecology Model, TEM

The carbon cycle and the nitrogen cycle play significant roles in tying changes in climate change to changes in the terrestrial biosphere. Climate change forces changes in the terrestrial biosphere, which in turn impact climate dynamics. These feedbacks are analyzed in the MIT IGSM using the Terrestrial Ecosystems Model (TEM) developed at

the Marine Biology Laboratory (MBL). A schematic diagram of TEM is given below in Figure 2.3.

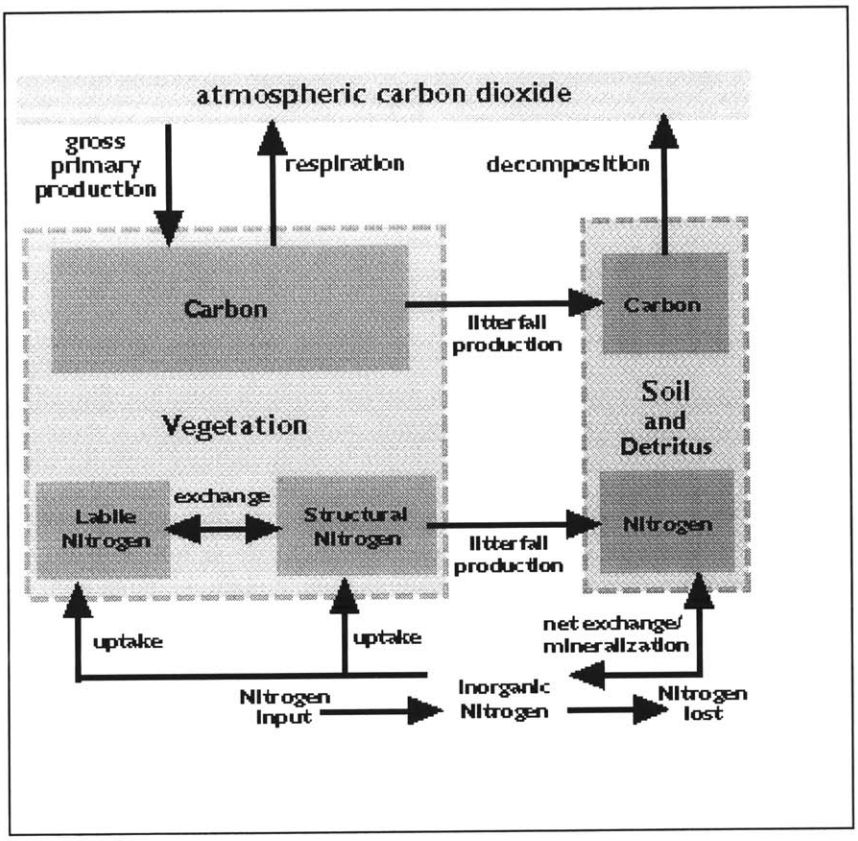

Figure 2.3 Schematic Diagram of the MIT IGSM Terrestrial Ecology Model (TEM)
Source: http://web.mit.edu/globalchange /www/

The Terrestrial Ecology Model is used in the IGSM to predict the states of plants and soils as they respond to climatic variability, atmospheric CO_2 concentrations, nitrogen availability and changes in land-use. Its use within the MIT IGSM allows us to study how climate-driven changes in the terrestrial biosphere affect climate dynamics through feedbacks on both the carbon cycle and the natural emissions of trace gases.

The TEM is run on a monthly time-step, forced with monthly average precipitation, temperature and cloudiness (derived from the MIT 2D-LO model), as well as a description of soil texture, elevation and water availability. An inbuilt water balance model generates the required hydrological inputs to simulate the carbon and nitrogen fluxes over 18 terrestrial ecosystems.

The estimated carbon and nitrogen fluxes, as well as changes in vegetation cover and soil composition, are inputs to the coupled chemistry/climate model and the natural emissions model. Furthermore, this information is useful in its own right, as changes in land cover will lead to economic and ecological impacts. Climate change is reflected in changes to the carbon and nitrogen cycles, in particular carbon storage in vegetation and soils.

2.6 MIT IGSM Natural Emissions Model (NEM)

Natural terrestrial fluxes of methane (CH_4) and nitrous oxide (N_2O) from soils and wetlands are significant contributors to the global budgets for these gases. Due to their dependence on climate, these fluxes must be modeled within the MIT IGSM. This takes place in the Natural Emissions Model.

The driving variables for the global model for N_2O emissions include vegetation type, total soil organic carbon, soil texture and climate parameters. Recall from Figure 2.1 that soil carbon and soil nitrogen were inputted to NEM from TEM, while temperature and

precipitation data was received from the climate model. In turn the CH_4 and N_2O fluxes calculated in NEM are used as input to the atmospheric chemistry model.

Climatic influences, particularly temperature and precipitation, determine dynamic soil temperature and moisture profiles and shifts of aerobic-anaerobic conditions. The N_2O model can predict daily emissions of N_2O, N_2, NH_3 and CO_2 as well as the daily soil uptake of CH_4. The N_2O emissions model has a spatial resolution of 2.5 degrees.

The methane emission model was developed specifically to estimate fluxes of methane from wetlands and wet tundra. In high-latitude and tropical wetlands methane flux is modeled based on soil temperature and bog soil temperature. Methane emissions from wet tundra are calculated by assuming a constant small methane flux and an emission season based on the time period for which the surface temperature is above the freezing point.

2.7 The MIT IGSM Emissions Prediction and Policy Analysis (EPPA) Model

The Emissions Prediction and Policy Analysis (EPPA) Model shown in Figure 2.4 is a model of economic growth, international trade and greenhouse gas emissions. It is used to compute predictions of anthropogenic emissions of the key gases from twelve economic regions, and to provide economic analysis of proposed control measures.

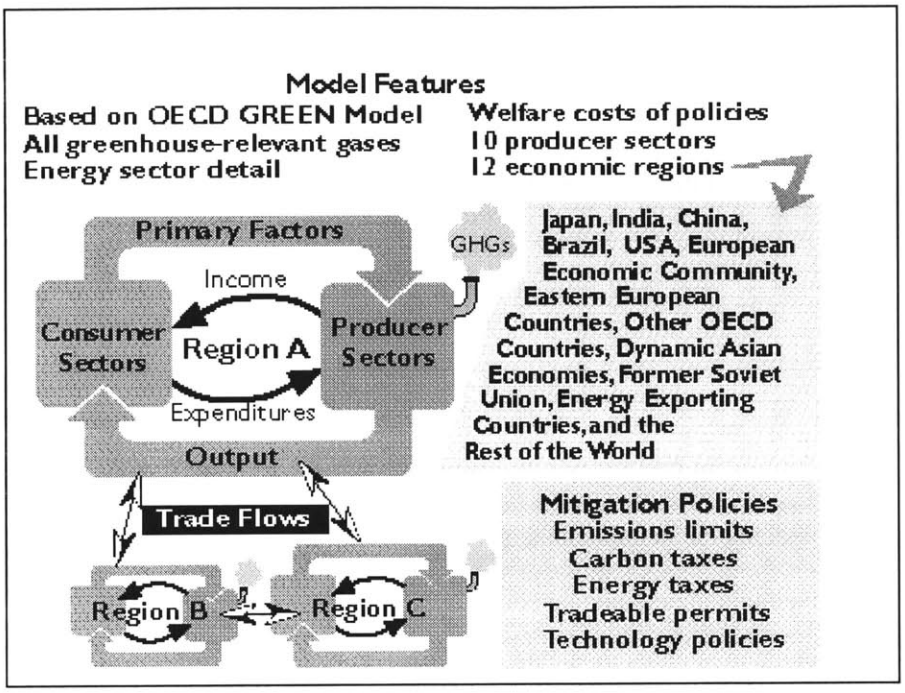

Figure 2.4 Schematic Diagram of the MIT Emissions Prediction and Policy Analysis (EPPA) Model
Source: http://web.mit.edu/globalchange/www

EPPA has been formulated to support analysis of a host of emissions control policies, providing estimates of the magnitude and distribution among nations of the costs, and clarifying the ways that changes are mediated through international trade. Special provision is made for analysis of uncertainty in key elements, such as the growth of population and economic activity, and the pace and direction of technical change.
In addition to predicting future levels of emissions of greenhouse gases and aerosols, future economical and technological change are modeled in some detail. Economic development and the consequent emissions of trace gases are predicted as functions of geographic location and time, in order to capture the impact of chemical species that exist in the atmosphere for only a short period of time.

2.8 Asynchronous coupling of hydrologic and ecological models within the MIT IGSM

This framework has one fundamental shortcoming in that some components are linked sequentially. Therefore because the components are linked asynchronously, the output from the climate model is used to force the terrestrial ecology model. In reality, however, there are significant feedbacks between the physical climate, atmospheric chemistry and biosphere that can only be captured if these components are integrated synchronously and with coupled exchanges of mass, heat and chemical species.

Chapter 3

National Center for Atmospheric Research Land Surface Model, Version 1.0.(NCAR LSM)

3.1 Introduction

Recall from Chapter 2 that we wish to capture the significant feedbacks between the physical climate, atmospheric chemistry and biosphere. We hope to achieve this through synchronous integration of these component models, thereby obtaining coupled exchanges of mass, heat and chemical species.

The NCAR LSM Version 1.0 was initially developed to combine "the relevant biogeophysical, biogeochemical, hydrologic and ecosystem processes into a comprehensive model of land-atmosphere interactions that was physically and biologically realistic and also internally self-consistent", so in principle it seems ideal for our purposes.

Furthermore, a feasibility study by deSilva (1998) using data from the FIFE experiment (Betts and Ball, 1998) demonstrated that using the same atmospheric forcing in uncoupled mode, it provided improved estimates of surface fluxes compared to the existing climate and terrestrial ecology models. Partitioning of surface energy between latent and sensible heat in the NCAR LSM was consistently better than the MIT 2D-LO

and the climate module of TEM at different levels of saturation. It was also found that the hydrological models in MIT 2D-LO and TEM were inconsistent; the MIT 2D-LO sub-surface was often too dry restricting evaporation, and resulting in erroneous ground temperature. The climate component of TEM, on the other hand resulted in excessive evaporation during rainy periods. DeSilva also found that as NCAR LSM calculates all fluxes and ground temperature simultaneously, its errors in ground heat flux were smaller than those of the other two models. Furthermore, the employment of a multi-layer soil column in NCAR LSM facilitated accurate ground temperature, soil moisture and surface flux calculations at both diurnal and seasonal cycles. The layered soil column was found to perform better than a merely deep soil column.

It is anticipated that the greater coupling between the climate, atmospheric chemistry and terrestrial ecology achieved by using the NCAR LSM to model the land ("L") component of the MIT 2D-LO model will allow full development of physical feedbacks, and improved estimates of surface fluxes of energy, momentum, water and CO_2.

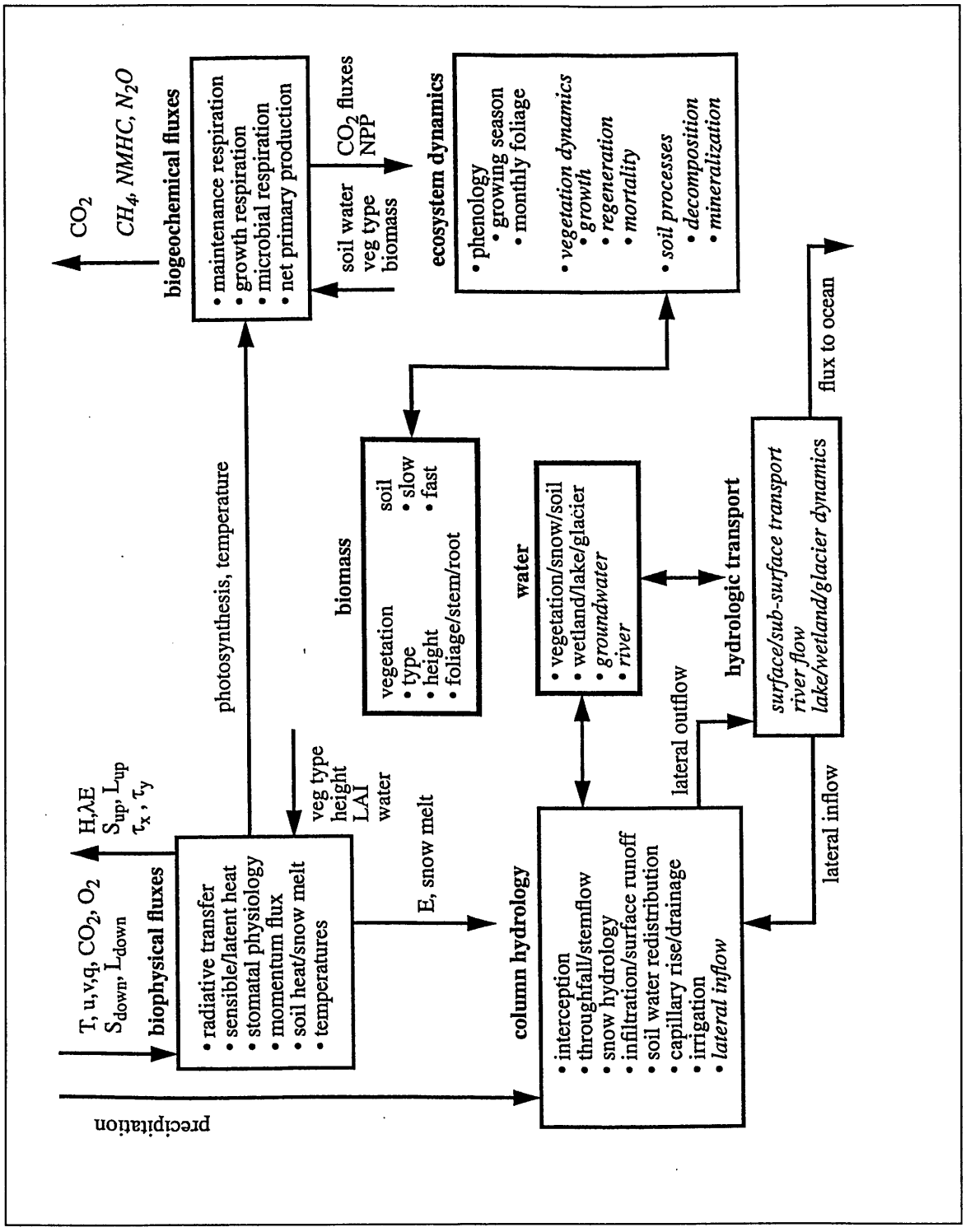

Figure 3.1 **Schematic diagram of hydrologic and ecological processes modeled in NCAR LSM and the interactions between them**

In the NCAR Land Surface Model (Version 1.0), land surface processes are described in terms of biophysical, and biogeochemical fluxes which depend on both the ecological and hydrologic state of the land. Biophysical fluxes include latent and sensible heat, momentum, reflected solar radiation and emitted longwave radiation. The flux of carbon dioxide is the main biogeochemical flux considered by the model. The processes at work in the ecological and hydrologic sub-models are shown in Figure 3.1, along with the interactions between them.

The objective of this chapter is to introduce the NCAR LSM Version 1.0.
Land Surface Characterization, typical model input and output requirements and model physics shall be discussed. For further detail the reader is referred to the Technical Description and User's Guide (Bonan, 1996).

3.2 Land Surface Characterization in NCAR LSM Version 1.0.

Each grid cell is characterized by one of twenty-eight surface classes, one of nine soil colors, soil texture information, and the fractions of the grid cell covered by lake and wetlands.

3.2.1 Land Surface Class

Each grid cell is assigned a land surface class (1-28), from those listed in Table 3.1. A surface class of zero indicates that the cell is entirely ocean, so it will not be modeled by NCAR LSM.

Table 3.1 NCAR LSM Surface Classes and their constituent sub-grid cover types

	NCAR LSM Classification	bare	net	ndt	bdt	tst	wg	ag	c	cg	ads	es	ds	bet
1	Land ice	1	0	0	0	0	0	0	0	0	0	0	0	0
2	Desert	1	0	0	0	0	0	0	0	0	0	0	0	0
3	Cool needleleaf evergreen tree	0.25	0.75	0	0	0	0	0	0	0	0	0	0	0
4	Cool needleleaf deciduous tree	0.5	0	0.5	0	0	0	0	0	0	0	0	0	0
5	Cool broadleaf deciduous tree	0.25	0	0	0.75	0	0	0	0	0	0	0	0	0
6	Cool mixed needleleaf evergreen & broadleaf deciduous trees	0.26	0.37	0	0.37	0	0	0	0	0	0	0	0	0
7	Warm needleleaf evergreen tree	0.25	0.75	0	0	0	0	0	0	0	0	0	0	0
8	Warm broadleaf deciduous tree	0.25	0	0	0.75	0	0	0	0	0	0	0	0	0
9	Warm mixed needleleaf evergreen & broadleaf deciduous trees	0.26	0.37	0	0.37	0	0	0	0	0	0	0	0	0
10	Tropical broadleaf evergreen tree	0.05	0	0	0	0	0	0	0	0	0	0	0	0.95
11	Tropical seasonal deciduous tree	0.25	0	0	0	0.75	0	0	0	0	0	0	0	0
12	Savanna	0	0	0	0	0.3	0.7	0	0	0	0	0	0	0
13	Evergreen forest tundra	0.5	0.25	0	0	0	0	0.25	0	0	0	0	0	0
14	Deciduous forest tundra	0.5	0	0.25	0	0	0	0.25	0	0	0	0	0	0
15	Cool forest crop	0	0.3	0	0.3	0	0	0	0.4	0	0	0	0	0
16	Warm forest crop	0	0.3	0	0.3	0	0	0	0.4	0	0	0	0	0
17	Cool grassland	0.2	0	0	0	0	0.2	0	0	0.6	0	0	0	0
18	Warm grassland	0.2	0	0	0	0	0.6	0	0	0.2	0	0	0	0
19	Tundra	0.4	0	0	0	0	0	0.3	0	0	0.3	0	0	0
20	Evergreen shrub	0.2	0	0	0	0	0	0	0	0	0	0.8	0	0
21	Deciduous shrub	0.2	0	0	0	0	0	0	0	0	0	0	0.8	0
22	Semi-desert	0.9	0	0	0	0	0	0	0	0	0	0	0.1	0
23	Cool irrigated crop	0.15	0	0	0	0	0	0	0.85	0	0	0	0	0
24	Cool crop	0.15	0	0	0	0	0	0	0.85	0	0	0	0	0
25	Warm irrigated crop	0.15	0	0	0	0	0	0	0.85	0	0	0	0	0
26	Warm crop	0.15	0	0	0	0	0	0	0.85	0	0	0	0	0
27	Forest wetland	0.2	0	0	0	0	0	0	0	0	0	0	0	0.8
28	Non-forest wetland	1	0	0	0	0	0	0	0	0	0	0	0	0

Each of the 28 surface classes consists of combination of plant types and bare soill, as shown in Table 3.1. These 13 fundamental cover types, named in full in Table 3.2, differ in important properties that influence surface fluxes, for example:

- Leaf and stem areas
- Root profile, canopy height, leaf dimension, stem and root biomass
- Physiological properties that determine stomatal resistance and CO_2 fluxes
- and roughness length, displacement height, and other aerodynamic properties.

The significance of this parameterization is that the model performs separate flux calculations for each fractional cover type and then averages the fluxes, instead of using bulk parameters to characterize the whole cell. Surface types were derived from the 0.5^{o} x 0.5^{o} dataset of Olson et al. (1983). Vegetation composition and fractional areas are currently time-invariant.

It is apparent from Table 3.1 that several surface classes are comprised of the same fractions of sub-grid cover. For example cool broadleaf deciduous forest is identical to warm broadleaf deciduous forest. This is because in the current version of the model there is no physiological differences between cool and warm plant types, except cool C_3 and warm C_4 grasses.

	Cover type	Abbreviated title
1	Bare	bare
2	Needleleaf Evergreen Tree	net
3	Needlelear Deciduous Tree	ndt
4	Broadleaf Deciduous Tree	bdt
5	Tropical Seasonal Tree	tst
6	Warm Grass (C4)	wg
7	Arctic Grass	ag
8	Crop	c
9	Cool Grass (C3)	cg
10	Arctic Deciduous Shrub	ads
11	Evergreen Shrub	es
12	Deciduous Shrub	ds
13	Broadleaf Evergreen Tree	bet

Table 3.2 NCAR LSM Fundamental cover types and their abbreviated titles

3.2.2 Soil Color

The soil in each grid cell must be assigned a color, 1 to 9. The color of the soil determines its albedo in a dry or saturated state, at visible and near-infrared wavelengths as shown in Table 3.3. The first eight color classes are as in BATS (Dickenson et al., 1993). The ninth class is particular to desert and semi-desert surface types in North Africa and the Arabian Peninsula. In order to match ERBE clear-sky albedos, albedo was increased by 0.1.

Soil Color Class	Vis (Saturated)	Nir(Saturated)	Vis(Unsaturated)	Nir(Unsaturated)
1 = light	0.24	0.48	0.12	0.24
2	0.22	0.44	0.11	0.22
3	0.20	0.40	0.10	0.20
4	0.18	0.36	0.09	0.18
5	0.16	0.32	0.08	0.16
6	0.14	0.28	0.07	0.14
7	0.12	0.24	0.06	0.12
8 = dark	0.10	0.20	0.05	0.10
9	0.27	0.55	0.15	0.31

Table 3.3 NCAR LSM Dry and Saturated Albedos as a function of soil color

3.2.3 Soil Texture

The soil texture within each grid cell is inputted to the model by prescribing the percentages of sand, silt and clay in the grid cell. Describing soil texture in this form enables the model to account for the effect of different soil types. Thermal properties such as heat capacity and thermal conductivity, and hydraulic properties such as porosity, saturated hydraulic conductivity, saturated matric potential and the slope of the retention curve, are functions of soil texture.

3.2.4 Percentage Lakes and Wetlands

The fraction the grid cell covered in lake or wetlands must also be prescribed to fully characterize the cell. If present, lake and/or wetlands form additional sub-grid patches. Lakes may be either deep (50m) or shallow (10m). In Version 1.0, all lakes are modeled as deep lakes.

3.3 Required Atmospheric Forcing, and Typical Output of NCAR LSM

The NCAR LSM Version 1.0 was designed to be coupled with the NCAR CCM3. Full coupling between the atmospheric model and the land surface model is achieved through a fully explicit time-stepping procedure.

The current state of the atmosphere is used to force the land model. The required inputs are listed in Table 3.4. The Land Surface Model uses these to calculate the surface energy, constituent (water vapor and carbon dioxide), momentum and radiative fluxes required by the next step of the atmospheric model. When coupled to CCM3, the outputs from NCAR LSM listed in Table 3.5 are used to force the next step of the CCM3.

Quantity	Symbol	Units
Reference height	z_{atm}	m
Temperature at z_{atm}	T_{atm}	K
Zonal wind at z_{atm}	u_{atm}	M s^{-1}
Meridional wind at z_{atm}	v_{atm}	M s^{-1}
Specific Humidity at z_{atm}	q_{atm}	kg kg^{-1}
Pressure at z_{atm}	P_{atm}	Pa
Partial pressure CO_2 at z_{atm}	355 x 10^{-6}	mol mol^{-1}
Partial pressure O_2 at z_{atm}	0.209	mol mol^{-1}
Surface pressure	P_{srf}	Pa
Convective precipitation	q_{prcc}	mm H_2O s^{-1}
Large-scale precipitation	q_{prcl}	mm H_2O s^{-1}
Incident direct bean solar radiation < 0.7μm	$S_{atm}\downarrow_{vis}^{\mu}$	W m^{-2}
Incident direct beam solar radiation ≥ 0.7 μm	$S_{atm}\downarrow_{nir}^{\mu}$	W m^{-2}
Incident diffuse solar radiation < 0.7μm	$S_{atm}\downarrow_{vis}$	W m^{-2}
Incident diffuse solar radiation ≥ 0.7 μm	$S_{atm}\downarrow_{nir}$	W m^{-2}
Incident longwave radiation	$L_{atm}\downarrow$	W m^{-2}

Table 3.4 NCAR LSM Required Inputs

Quantity	Symbol	Units
Latent heat flux	λE	W m^{-2}
Sensible heat flux	H	W m^{-2}
Constituent flux	H_2O, CO_2	kg m^{-2} s^{-1}
Zonal momentum flux	τ_x	kg m^{-2} s^{-1}
Meridional momentum flux	τ_y	kg m^{-2} s^{-1}
Emitted longwave radiation	$L\uparrow$	W m^{-2}
Direct beam albedo <0.7μm	$I\uparrow^{\mu}_{vis}$	
Direct beam albedo ≥ 0.7μm	$I\uparrow^{\mu}_{nir}$	
Diffuse albedo <0.7μm	$I\uparrow_{vis}$	
Diffuse albedo ≥ 0.7μm	$I\uparrow_{nir}$	

Table 3.5 NCAR LSM Output to Atmospheric Model, when coupled to NCAR Community Climate Model

3.4 NCAR LSM Model Physics

3.4.1 Radiative fluxes

The net radiation at the surface R_n is given by

$$R_n = \left(\vec{S}_v + \vec{S}_g \right) + \left(\vec{L}_v + \vec{L}_g \right) \tag{3.1}$$

where $\vec{S}$ and $\vec{L}$ are the net solar and net longwave fluxes absorbed by vegetation (subscript v) and (subscript g).

Photosynthesis and transpiration depend non-linearly on solar radiation, via the light response of stomata. A common way of approaching the closely related CO_2 and H_2O fluxes within the canopy is to divide the canopy into a sunlit fraction f_{sun} and a shaded fraction, f_{sha}, defined in

$$f_{sun} = \frac{1 - e^{-K(L+S)}}{K(L+S)} \tag{3.2}$$

$$f_{sha} = 1 - f_{sun} \tag{3.3}$$

The leaf and stem index is denoted (L+S), K is a function of the amount of scattering within the canopy (Sellers, 1985), and the term $e^{-K(L+S)}$ is the fractional area of "sunflecks" on a horizontal plane below the leaf and stem index.

The solar radiation absorbed by the vegetation in the visible waveband is partitioned between the sunlit and shaded leaves to calculate the average absorbed photosynthetically

active radiation for sunlit (ϕ^{sun}) and shaded (ϕ^{sha}) leaves. It is assumed that the sunlit leaves absorb the direct beam radiation, that all leaves absorb diffuse radiation, and that leaves absorb $\frac{L}{L+S}$ of the radiation absorbed by the vegetation.

The net longwave radiation ($\vec{L}$) at the surface is calculated differently for vegetated and non-vegetated surfaces. For non-vegetated surfaces it is given by Equation 3.4:

$$\vec{L} = -\alpha_g L_{atm} \uparrow + \varepsilon_g \sigma T_g^4 \tag{3.4}$$

where α_g is the ground absorptivity, ε_g is the ground emissivity, T_g is the ground temperature in Kelvin, and σ is the Stefan-Boltzmann constant ($Wm^{-2}K^{-4}$).

For vegetated surfaces, the net longwave radiation flux has components from the vegetation and the ground:

$$\vec{L} = \vec{L_v} + \vec{L_g} \tag{3.5}$$

where

$$\vec{L_v} = -\alpha_v (L_{atm} \downarrow + L_g \uparrow) + 2\varepsilon_v \sigma T_v^4 \tag{3.6}$$

$$\vec{L_g} = -\alpha_g (L_v \downarrow) + \varepsilon_g \sigma T_g^4 \tag{3.7}$$

The subscrips *v* denote from the canopy, and *g* denotes from the ground. The downward flux from the canopy is given by

$$L_v \downarrow = (1 - \alpha_v) L_{atm} \downarrow + \varepsilon_v \sigma T_v^4 \tag{3.8}$$

The upward radiation from the ground is given by

$$L_g \uparrow = (1-\alpha_g) L_v \downarrow + \varepsilon_g \sigma T_g^4 \tag{3.9}$$

3.4.2 Turbulent fluxes

The expressions used to estimate the surface fluxes are derived by applying Monin-Obukhov similarity theory separately to the vegetated and non-vegetated surfaces and combining the results.

The zonal and meridional momentum fluxes, τ_x and τ_y are given by

$$\tau_x = -\rho_{atm} \frac{(u_{atm} - u_s)}{r_{am}} \tag{3.10}$$

$$\tau_y = -\rho_{atm} \frac{(v_{atm} - v_s)}{r_{am}} \tag{3.11}$$

where u_{atm} and v_{atm} are the zonal and meridional winds (ms^{-1}) at a reference height z_{atm}, u_s and v_s are the zonal and meridional winds ($m\ s^{-1}$) at the surface, and r_{am} is the aerodynamic resistance ($s\ m^{-1}$) for momentum between the surface and the reference height $z_{0m}+d$ (the apparent sink for momentum).

For non-vegetation surfaces (where L+S=0), the sensible and latent heat fluxes are given by

$$H = -\rho_{atm} C_p \frac{(\theta_{atm} - T_g)}{r_{ah}} \tag{3.12}$$

$$\lambda E = -\frac{\rho_{atm} C_p}{\gamma} \frac{[e_{atm} - e_*(T_g)]}{r_{aw} + r_{srf}} \tag{3.13}$$

where in Equation (3.12) T_g is the ground temperature(K) and is equivalent to the surface temperature T_s here, θ_{atm} is the potential temperature (K) at the reference height z_{atm}, ρ_{atm}

is the density of moist air (kg m^{-3}), C_p is the heat capacity of air (J kg^{-1} K^{-1}), r_{ah} is the aerodynamic resistance to sensible heat transfer between the atmosphere at height z_{atm} and the surface at height $z_{0h}+d$ (the apparent sink for heat). In Equation (3.13), γ is the psychrometric constant (Pa K^{-1}), e_{atm} is the vapor pressure (Pa) at height z_{atm}, $e_*(T_g)$ is the saturation vapor pressure (Pa) at the ground temperature, r_{aw} is the aerodynamic resistance to water vapor transfer between the atmosphere at a height z_{atm} and the surface at a height $z_{0m}+d$ (the apparent sink for water vapor), r_{srf} is a surface resistance (s m^{-1}) that accounts for water vapor transfer between the soil with water vapor pressure $e_*(T_g)$ and the apparent sink for water vapor with a vapor pressure e.

For vegetated surfaces, H and λE are partitioned into vegetation and ground fluxes that depend on vegetation T_v and ground T_g temperatures in addition to surface temperature T_s and vapor pressure e_s. Sensible heat flux is given by

$$H = H_v + H_g \tag{3.14}$$

where

$$H_v = -\rho_{atm} C_p (T_s - T_v) \frac{2(L+S)}{\overline{r_b}} \tag{3.15}$$

$$H_g = -\rho_{atm} C_p \frac{(T_s - T_g)}{r'_{ah}} \tag{3.16}$$

where L and S are the leaf and stem area indices, $\overline{r_b}$ is the average leaf boundary layer resistance (s m^{-1}), and r'_{ah} is the aerodynamic resistance (s m^{-1}) between the ground z'_{0h} and $d+z_{0h}$.

The latent heat flux for vegetated surfaces is given by Equations (3.17) to (3.19):

$$\lambda E = \lambda E_v + \lambda E_g \tag{3.17}$$

where

$$\lambda E_v = -\frac{\rho_{atm} C_p}{\gamma}\left[e_s - e_*(T_v)\right]\left[f_{wet}\left(\frac{L+S}{\overline{r_b}}\right) + (1-f_{wet})\left(\frac{L^{sun}}{\overline{r_b}+r_s^{sun}} + \frac{L^{sha}}{\overline{r_b}+r_s^{sha}}\right)\right] \tag{3.18}$$

$$\lambda E_g = -\frac{\rho_{atm} C_p}{\gamma}\frac{\left[e_s - e_*(T_g)\right]}{r_{aw}' + r_{srf}} \tag{3.19}$$

In Equations (3.18) and (3.19), $e_*(T_v)$ and $e_*(T_g)$ are the saturated vapor pressures at T_v and T_g respectively, L^{sun} and L^{sha} are the sunlit and shaded leaf area indices, r_s^{sun} and r_s^{sha} are the sunlit and shaded stomatal resistances (s m^{-1}), f_{wet} is the wetted fraction of the canopy, r_{aw}' is the aerodynamic resistance between the ground z_{0w}' and $d+z_{0w}$.

The second bracketed term of Equation (3.18) is the evaporation of intercepted water from the wetted fraction of the canopy, transpiration from sunlit leaves and transpiration from shaded leaves.

The aerodynamic resistances to sensible heat (r_{ah}') and latent heat (r_{aw}') transfer within the canopy, as well as the bulk leaf boundary layer resistance $\overline{r_b}$ are from Choudhury and Monteith (1988). They are derived using so-called "K-theory", which assumes that the eddy diffusivity (m^2 s^{-1}) appropriate to each quantity has an exponential profile within the canopy. This assumption simplifies the surface flux parameterization considerably.

3.4.3 Vegetation and Ground Temperatures

For non-vegetated surfaces, surface fluxes and temperatures are calculated by finding the ground temperature T_g that balances the energy budget:

$$-\overrightarrow{S_g} + \vec{L}(T_g) + H(T_g) + \lambda E(T_g) + G(T_g) + M = 0 \qquad (3.20)$$

where $\overrightarrow{S_g}$ is the net solar radiation at the ground, $\vec{L}$, H, and λE (positive upwards) are the net longwave radiative, sensible and latent heat fluxes at the ground surface respectively. G is the soil heat flux, positive into the soil, and M is the snowmelt flux. All fluxes are in W m^{-2}.

The case for the vegetated surface is more complicated as the fluxes depend on vegetation temperature (T_v) as well as ground temperature (T_g). These are the temperatures that balance the canopy and ground energy budgets as follows:

$$-\overrightarrow{S_v} + \overrightarrow{L_v}(T_v, T_g) + H_v(T_v, T_g) + \lambda E_v(T_v, T_g) = 0 \qquad (3.21)$$

and

$$-\overrightarrow{S_g} + \overrightarrow{L_g}(T_v, T_g) + H(T_v, T_g) + \lambda E_g(T_v, T_g) + G(T_g) + M = 0 \qquad (3.22)$$

3.4.4 Soil Temperature profile

The heat flux at a depth z, F_z (W m^{-2}) is given by Equation (3.23):

$$F_z = -k\frac{\partial T}{\partial z} \qquad (3.23)$$

Energy conservation in the soil column requires that Equation (3.24) holds:

$$\rho c\frac{\partial T}{\partial t} = -\frac{\partial F_z}{\partial z} = \frac{\partial}{\partial z}\left[k\frac{\partial T}{\partial z}\right] \qquad (3.24)$$

where ρc is the volumetric soil heat capacity (J m^{-3} K^{-1}), T is the soil temperature in Kelvin, and k is the thermal conductivity (W m^{-1} K^{-1}). Equation (3.24) is solved numerically to calculate soil temperatures in each of the six layers of the soil column, subject to the boundary conditions of G, the ground heat flux into the soil at the top of the column, and zero heat flux at the bottom of the soil column.

3.4.5 Hydrology

The hydrological fluxes parameterized by the model are illustrated in Figure 3.2. The model parameterizes interception, throughfall, snow accumulation and melt, infiltration, surface run-off, sub-surface drainage, and redistribution within the soil column to simulate canopy water W_{can}, snow water W_{sno}, and soil water $\sum_i \theta_i \Delta z_i$, where θ_i is the volumetric soil water content, and Δz_i is the soil thickness (mm). Total water is conserved for all but irrigated soils.

Bonan (1996) points to three significant features of the surface hydrology component of the NCAR LSM:

1) Spatial heterogeneity in precipitation is accounted for by assuming that a fraction ($1-k_c=0.4$) of the land surface receives only large-scale precipitation at a mean rate q_{prcl} and the remainder of the surface receives both convective and large-scale precipitation at a mean rate $q_{prcl} + \frac{q_{prcc}}{k_c}$. Interception and throughfall differ in these two regions as a result of the different precipitation rates.
2) In both precipitation regions, throughfall and soil water have stochastic spatial distributions similar to those of Entekhabi and Eagleson (1989) which affects

surface run-off by determining the net flux of water at the surface and the infiltration capacity.

3) Canopy, snow, and water pools are updated using the surface averaged fluxes of interception, throughfall and infiltration so that there is no distinction of water pools between the two precipitation regions.

3.4.6 Surface CO_2 flux

Surface CO_2 fluxes account for photosynthetic uptake, maintenance and growth respiration losses, as well as CO_2 losses due to microbial respiration. Leaf stomatal resistance is needed for the latent heat flux, and is coupled to leaf photosynthesis in a manner similar to Collatz et al. (1991). The formulations differ only in that the NCAR LSM uses photosynthesis not net photosynthesis. Net photosynthesis causes stomatal conductance to be less than the minimum conductance at night or in winter, when plants do not photosynthesize but still respire. The use of photosynthesis instead, ensures that stomatal conductance equals *b* when there is no photosynthesis.

The canopy integration technique used in NCAR LSM allows both sunlit and shaded leaves to photosynthesize, although at different rates depending on the amount of absorbed photosynthetically active radiation. Photosynthesis and stomatal resistance depend on incident light, temperature, CO_2 concentration, soil water, vapor pressure and foliage nitrogen, according to plant type.

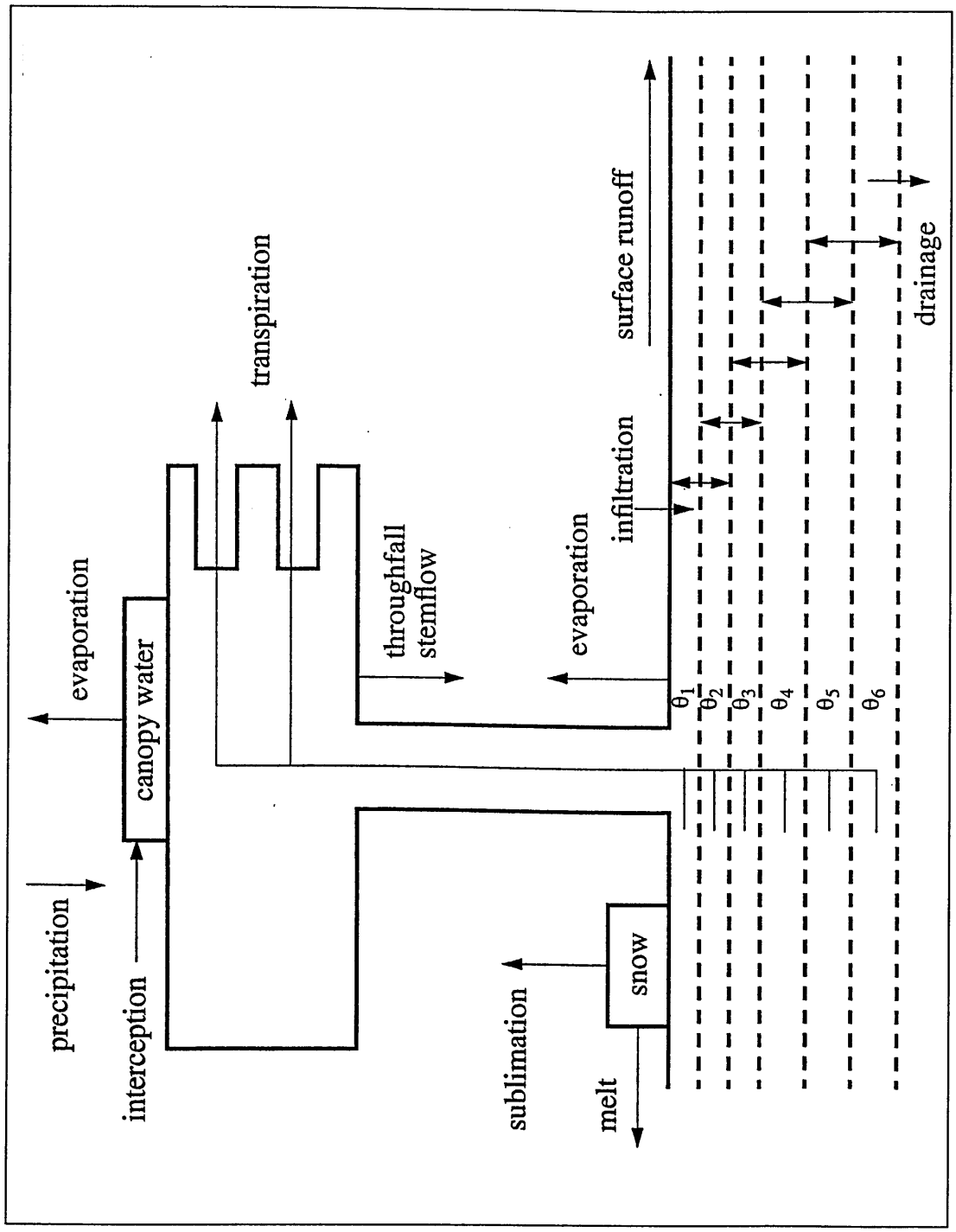

Figure 3.2 **Schematic diagram of the water fluxes modeled in the NCAR LSM, namely interception, throughfall, snow accumulation and melt, infiltration, surface run-off, subsurface drainage and redistribution within the soil column**

3.5 Incorporating the NCAR LSM within the MIT IGSM

In this chapter, we have examined how the land surface is characterized in the NCAR Land Surface Model by assigning a surface type, soil color, soil texture and percentage lake and wetlands. We have also discussed the atmospheric forcing variables required by the NCAR LSM, and the fluxes and quantities it typically outputs when coupled to an atmospheric model. The model physics used to estimate these quantities has been briefly introduced. For further information the reader is referred to Bonan (1996 and 1996a).

We wish to use the NCAR LSM to model the land ("L") component of the MIT 2D-LO model. This will entail calling the NCAR LSM as a subroutine from the MIT-2D-LO. To use the NCAR LSM in this manner, we must describe the global land surface in terms of the characteristics discussed in Section 3.2. In addition, we must ensure that at each call to the NCAR LSM it is supplied with the appropriate atmospheric forcing as discussed in Section 3.3, and that the forcing required by the next time step of the atmospheric model is outputted correctly. This subject will be the focus of Chapter 4.

Chapter 4

Datasets used to characterize the global land surface for use in a zonally averaged NCAR Land Surface Model

4.1 Introduction

Atmospheric forcing is applied over each grid cell in the NCAR LSM, so that each sub-grid cover type is subject to equal amounts of precipitation, incident radiation, and is understood to have the same bottom-level temperature. The current MIT 2D-LO is zonally-averaged, with each grid cell consisting of a 8 degree latitudinal band, with uniform atmospheric forcing. One of the major changes in employing the NCAR LSM in the MIT 2D-LO is that the representation of the land surface will be more detailed. Whereas the current model (MIT 2D-LO) has just four categories, namely ocean, ocean ice, land and land ice, incorporating the NCAR LSM will increase this to fifteen. Land and land ice will be described in terms of the 13 fundamental cover types of the NCAR LSM. As the NCAR LSM is vectorized, the atmospheric forcing applied to each individual cover type could be factored without any increase in computational effort.

It is unreasonable to assume that the mean zonal precipitation can be applied across all land cover types at the same latitude. If we consider, for example, a zonal band which includes grasslands and desert. Clearly, the grassland is sustained by precipitation, while the absence of precipitation yields desert conditions. By applying a mean precipitation to

both cover types, we would be undersupplying the grassland, and oversupplying the desert. Through its impact on soil moisture, this would also affect the partitioning of surface energy between latent and sensible heat fluxes. This would lead to reduced evaporation in the grassland, and increased evaporation in the desert.

Using the datasets described in this chapter, factors were derived by which precipitation could be adjusted to reflect the variation in precipitation over different cover types in each latitudinal band. A description of the algorithm used and the resultant factors follow in Chapter 5.

4.2 Global Ecosystems Database, Version 2.

Both the land-cover dataset and the climatology dataset used in this project were obtained from the Global Ecosystems Database (Version 2). The GED 2 provides an integrated version of commonly used global and regional research datasets related to landscape ecological characterization and modeling for a variety of uses in various disciplines.

The Global Ecosystems Database (GED) project began in 1990 as an interagency project between the National Geophysical Data Center (NGDC) of the U.S. National Oceanic and Atmospheric Administration (NOAA), and the U.S. Environmental Protection Agency's (EPA) Environmental Research Laboratory in Corvallis, Oregon (ERL-C). The goals of the project were to:

- Prepare and document important global change research datasets for intercomparison, verification, further research, and applied use related to global climate change and landscape ecology.
- Integrate and publish these datasets to improve their transfer between disciplines and to the broadest possible user base.
- Collaborate in developing useful ecosystem indices and meeting data integration requirements of specific user groups.

GED Version 2 is a combined database consisting of the original GED published in September 1992, and the additional datasets contributed through 1997. The original data ("disk A") was upgraded to meet the standards of the new data ("disk B"). A further advantage of GED Version 2 is that the user can download data and documentation directly from the GED 2 web page, or order them as a two CD set.

To allow their inter-comparison (comparison between datasets) and use in combination, the datasets are provided in geographically and temporally compatible vector and raster GIS form (i.e., registered to common origins, cell boundary conventions, projection, and in comparable time steps).

Integrated datasets are provided within geographically defined databases. Each database has a common geographical "window," spatial reference system, and projection. The global database (GLGEO) is in a flat "geographic" projection (longitude/latitude

reference system mapped to a Cartesian coordinate system: also referred to as "platte carree").

4.3 The Major World Ecosystem Complexes Ranked by Carbon in Live Vegetation

The Major World Ecosystem Complexes Ranked by Carbon in Live Vegetation database was compiled by Olson, Watts and Allison at the Oak Ridge National Laboratory, Oak Ridge, TN. The database involves the spatial distribution of 44 ecosystem complexes. The World Ecosystem complexes are defined to reflect the major topographic, climatic and land-use patterns. All vegetation-bearing land masses are represented.

The objective of the database is to provide the user community a basis for making improved estimates of vegetation areas and carbon quantities, natural biological exchanges of CO_2, and eventually the net historic shifts in carbon between the biosphere and the atmosphere. The World Ecosystem database consists of a grid of 360 rows (latitude bands), and 720 columns (longitude bands). Each grid cell is 0.5^{o} x 0.5^{o} so the map plots at a scale of 1:30,000,000 at the equator.

The Olson World Ecosystems dataset on the GED 2 consists of 3 thematic coverages:

- Ecosystems 30 minute resolution (Version 1.3),

- Ecosystems 10 and 30 minute composite resolution (version 1.4) and
- Ecosystems resolution codes for (version 1.4; b).

Version 1.3, as used in this project, contains 14 Major Ecosystem classes and 8 fringe classes, plus ocean. It was derived from WE1.4D by editing, aggregating classes, and modal filtering to 0.5^{o}. All three of the thematic coverages were derived from the same source, as described above. The classes in Version 1.3 are given in Table 4.1 below:

Class	Description
0	Seas
1	Conifer Forest
2	Broadleaf Forest
3	Mixed Forest
4	Grass/Shrub/Herb complexes
5	Tropical/Subtropical moist or Broadleaf Humid Forest
6	Scrub/woods complexes
7	Semi-desert/Tundra
8	Field/woods mosaic or savanna
9	Northern Taiga
10	Forest/field or dry evergreen mixtures
11	Wetland mires marshes or swamps
12	Deserts
13	Shrub/tree or thicket
14	Crop/settlement/commercial
15	Conifer rainforest fringe coast
16	reserved for later use
17	reserved for later use
18	reserved for later use
19	Mangrove
20	Water/land mixtures and coastal systems
21	reserved for later use
22	reserved for later use
23	Island/shore water fringe
24	Land/water combinations (31%<water<50%)
25	Ice
26	Polar Desert
27	Wooded tundra or Moorland/Heath types
28	reserved for later use
29	Inland Water

Table 4.1 Olson Ecosystem Classifications, Version 1.3.

4.4 The IIASA Database for Mean Monthly Values of Temperature, Precipitation, and Cloudiness on a Global Terrestrial Grid

The IIASA (International Institute for Applied Systems Analysis) Database is a global database for terrestrial climate derived from instrumental weather records containing monthly averaged values for temperature, precipitation, and cloudiness. The data has a resolution of 0.5^{o} in longitude and latitude. The coverage for Europe, USA, Japan, India and Africa is considered good, and interpolation techniques can be used reliably to estimate the intermediate values between stations. Climate data from other regions, have been derived from sparser weather station networks, rendering interpolation less reliable.

Leemans and Cramer (1991) attempted to define a typical climate for each terrestrial cell in relation to topographical and ecological features, limited to weather records for which no greenhouse effect has been recognized.

They defined "current climate" as the average climate of the period 1941-1960. The climate of this period was rather stable (Jones et al., 1986) and probably no anthropogenic greenhouse effect was detectable. Global coverage of measurements series for this period is relatively good and there are several sources with digitized weather records available for this period. Where appropriate data was accepted on the grounds that coverage was more important than the constraint on observation period.

Creating the global climate database involved a quality check and selection algorithm, spatial interpolation, and application of a correction scheme for altitudinal differences. All data sets were transformed to the IIASA Biosphere Dynamics Project file standard. All stations were separately tested for inaccuracies by evaluating extreme values and comparison between neighboring stations. The longitude, latitude and altitude of each station were checked before the stations were all merged into a single database sorted by longitude and latitude. Stations with multiple entries in the database were eliminated, and the remaining stations were ranked according to quality based on the observation period 1931-1960. A terrestrial 0.5^{o} longitude and latitude grid was created, and the most typical station of each terrestrial cell was selected as representative of that whole cell. The resulting data set consisted of 6,280 records with temperature values, 6,090 records with precipitation values, and only 1,507 records with cloudiness values.

The interpolation technique used was a triangulation of all data points (according to the algorithm developed by Green and Sibson, 1978) followed by a smooth surface fitting (Akima, 1978). A cartesian two-dimensional space was used, in which they directly used the actual longitude and latitude values to define a sinusoidal projection for both the data points and the resulting grid.

Precipitation data was interpolated without accounting for differences in altitude, as a satisfactory global orographic lapse rate could not be defined. A moist adiabatic lapse rate for temperature was implemented, i.e. before any monthly temperature was used in

the interpolation, the value was corrected as if the station was located at sea level using a lapse rate of -0.6° Celsius per 100m altitude.

A sample image is provided in Figure 4.1, which illustrates the mean monthly precipitation for the month of December.

Precipitation and temperature data from Leemans and Cramer (1991) will also be used in Chapter 6 to validate the performance of NCAR LSM when it is used to model the land ("L") portion of the MIT 2D-LO.

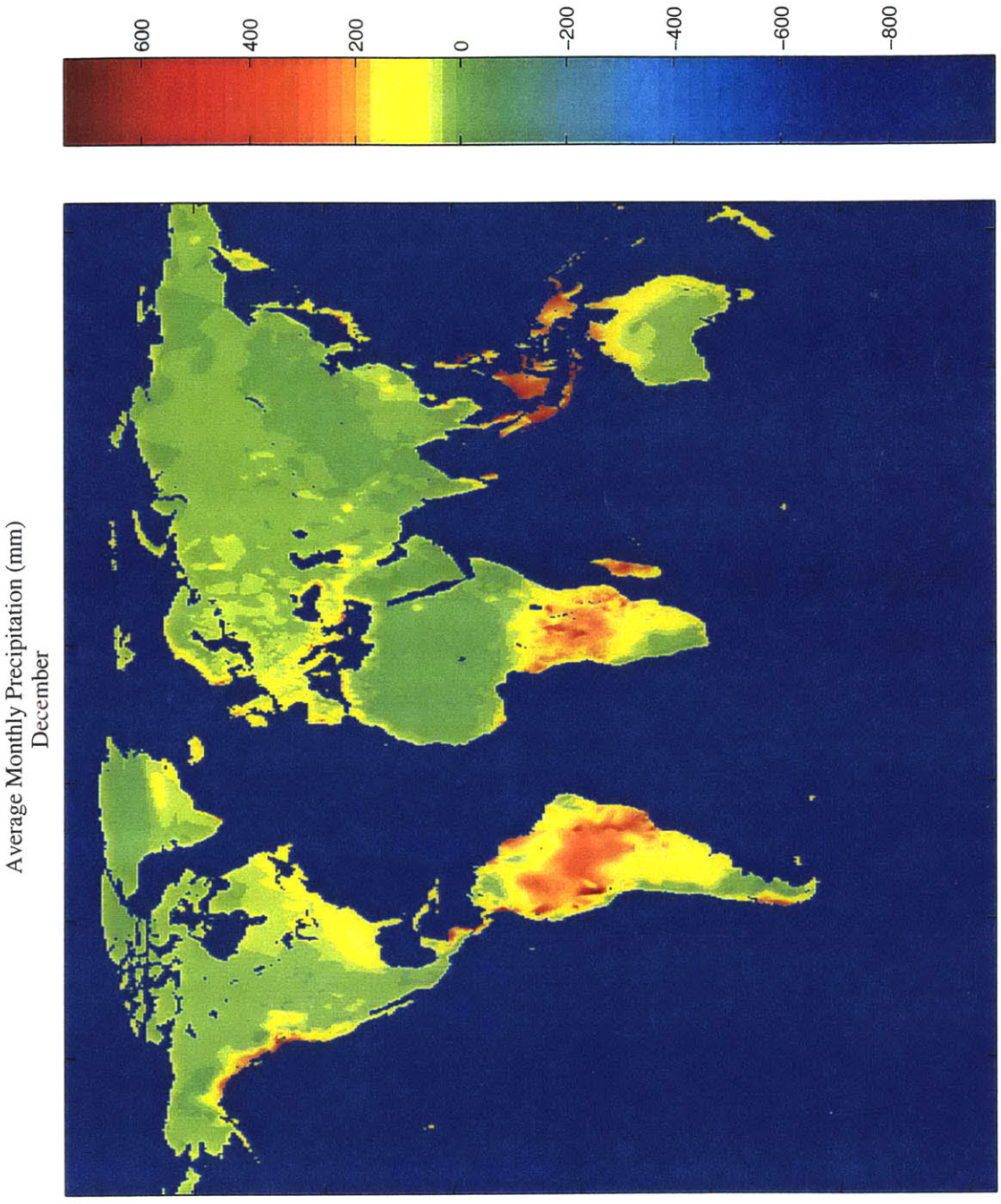

Figure 4.1 Sample of Leemans and Cramer Precipitation Data

Chapter 5

Zonal Characterization

5.1 Introduction

In order to use the NCAR LSM as a zonally averaged model, several changes were made to the input data set describing the land surface. In particular, the file **fsurdatsd** was generated to describe the land surface for use in NCAR LSM. It differs from the original input data set, **fsurdat**, in the manner in which land cover and soil color are defined. The generation of **fsurdatsd**, and the differences between it and **fsurdat** are explained in Section 5.2.

Changes were also made to the model architecture to accommodate the new surface parameterization, and to allow for coupling between NCAR LSM and MIT 2D-LO.These are discusses in Section 5.3. An improved precipitation scheme was also implemented, whereby zonal precipitation is multiplied by a factor to account for variability in precipitation between different cover types. This is discussed in Section 5.4.

5.2 Input Dataset describing the global land surface for use in NCAR LSM

In NCAR LSM the file **fsurdat** contains all the information required to completely describe the land surface. Its format is best described using an example. Consider a study area which consists of 3 x 1 grid cells. The file **fsurdat** will have a format like that given in Figure 5.1.

```
1     1     1
0     50    17    3     0.34 0.27 0.29 0.1  0.0
10    50    18    3     0.40 0.3  0.3  0.2  0.1
20    50    17    4     0.5  0.23 0.27 0.0  0.0
```

Figure 5.1 Sample of the land description file "fsurdat" for a simple 3 x 1 grid

The first three values are the number of longitude points for each latitude, so we have one point at each latitude. The remaining data describes the three individual grid cells:

- Column 1: Latitude at the center of grid cell (degrees)
- Column 2: Longitude at the center of grid cell (degrees)
- Column 3: NCAR surface type (integer 0 to 28).
- Column 4: NCAR soil color (integer 1 to 9).
- Column 5: Soil texture: Percentage of sand
- Column 6: Soil texture: Percentage of silt

- Column 7: Soil texture: Percentage of clay
- Column 8: Percentage of cell covered by lake.
- Column 9: Percentage of cell covered by wetland.

The relevance of each of these characteristics was discussed in Section 3.2.

The dataset **fsurdat_t42** is a sample dataset available to download with the NCAR LSM Version 1.0. It consists of the surface types derived from Olson et al.'s (1983) 0.5^0 by 0.5^0 data, overlaid onto the NCAR CCM T42 grid (2.8^0 by 2.8^0). Soil colors taken from the BATS T42 data set for use with the CCM (Dickinson et al. 1993) are also included, as well as sand, silt and clay proportions from Webb et al.'s 1.0^0 by 1.0^0 data set. Inland lake and wetland data is derived from 1.0^0 by 1.0^0 data (Cogley, 1991). This data was developed to use with the NCAR CCM T42 grid, in a coupled NCAR LSM and NCAR CCM run, for example.

This data could not be used directly in coupling the NCAR LSM to the MIT 2D-LO because the grids are not aligned. The longitude and latitude at the center of each land surface model grid point, must match exactly that of the overlying general circulation model. The MIT 2D-LO has grid points centered on the poles, with a resolution of 7.826^0. We can however base our input files on the information in fsurdat_t42, and attempt to realign it by weighting bounding grid points accordingly.

Furthermore, it is apparent from **fsurdat_t42** that a single land surface type or soil color will be insufficient to represent each latitudinal band.

In order to use NCAR LSM with MIT 2D-LO, the file **fsurdatsd** was created to describe the 24 zonal bands of the MIT IGSM grid. It is included in Appendix A, for reference. Its generation is discussed in the following sections 5.2.1 through 5.2.4.

5.2.1 Geographical Location

The geographical location of any grid cell is described by its latitude and longitude. Obviously, the longitude and latitude values used in the Land Surface Model (e.g. MIT 2D-LO or NCAR LSM) must exactly match those of the overlying General Circulation Model.

Furthermore, we are calling the NCAR LSM to model the land ('L') portion of the MIT 2D-LO in each grid cell, so the grid used will be that of the MIT 2D-LO. This consists of 24 points in latitude, corresponding to a resolution of 7.826 degrees. The polar grid points are centred on the poles.

5.2.2 Land Surface Type

For illustration purposes, we zonally aggregated the 2.8^{o} x 2.8^{o} cells of the NCAR CCM T42 to investigate the distribution of the 28 NCAR LSM land surface types as described in fsurdat_t42. The results are shown in Figure 5.2.

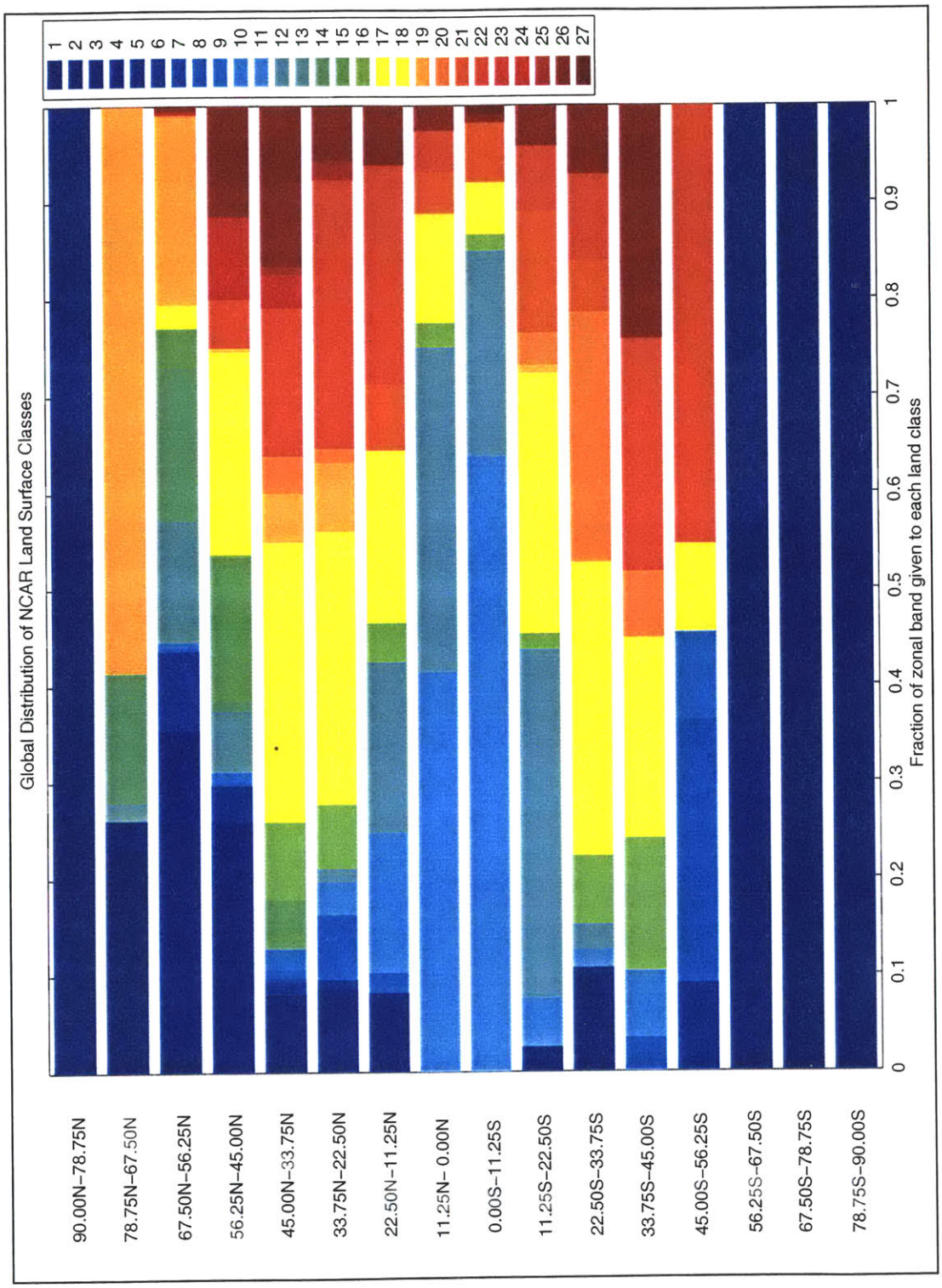

Figure 5.2 **Global Distribution of 28 NCAR Land Surface Classes (NCAR CCM T42 grid). NCAR surface classes are described in Section 3.2.1 and Table 3.1.**

The figure illustrates the occurrence of the land surface types as a fraction of total land in each latitudinal band, as we are not concerned with the ocean. There are no grid points covered by non-forest wetland, so the 28^{th} class has been discarded.

We can see however, with many of the 27 classes occurring in each latitudinal band, significant errors would be induced if the entire zonal band were assigned just one class. We know, however, that each of the 28 land classes is a combination of the 12 fundamental plant types and bare soil. The data from fsurdat_t42 may therefore be represented as in Figure 5.3, without sacrificing any information. The 13 cover types have to be retained as they differ in important properties that influence surface fluxes. The NCAR cover types are discussed in Section 3.2.1 and are listed in Table 3.2. As they are used in several figures in this chapter, Table 3.2 is reproduced for convenience, as Table 5.1.

	Cover type	Abbreviated title
1	Bare	bare
2	Needleleaf Evergreen Tree	net
3	Needlelear Deciduous Tree	ndt
4	Broadleaf Deciduous Tree	bdt
5	Tropical Seasonal Tree	tst
6	Warm Grass (C4)	wg
7	Arctic Grass	ag
8	Crop	c
9	Cool Grass (C3)	cg
10	Arctic Deciduous Shrub	ads
11	Evergreen Shrub	es
12	Deciduous Shrub	ds
13	Broadleaf Evergreen Tree	bet

Table 5.1 NCAR LSM Fundamental cover types and their abbreviated titles

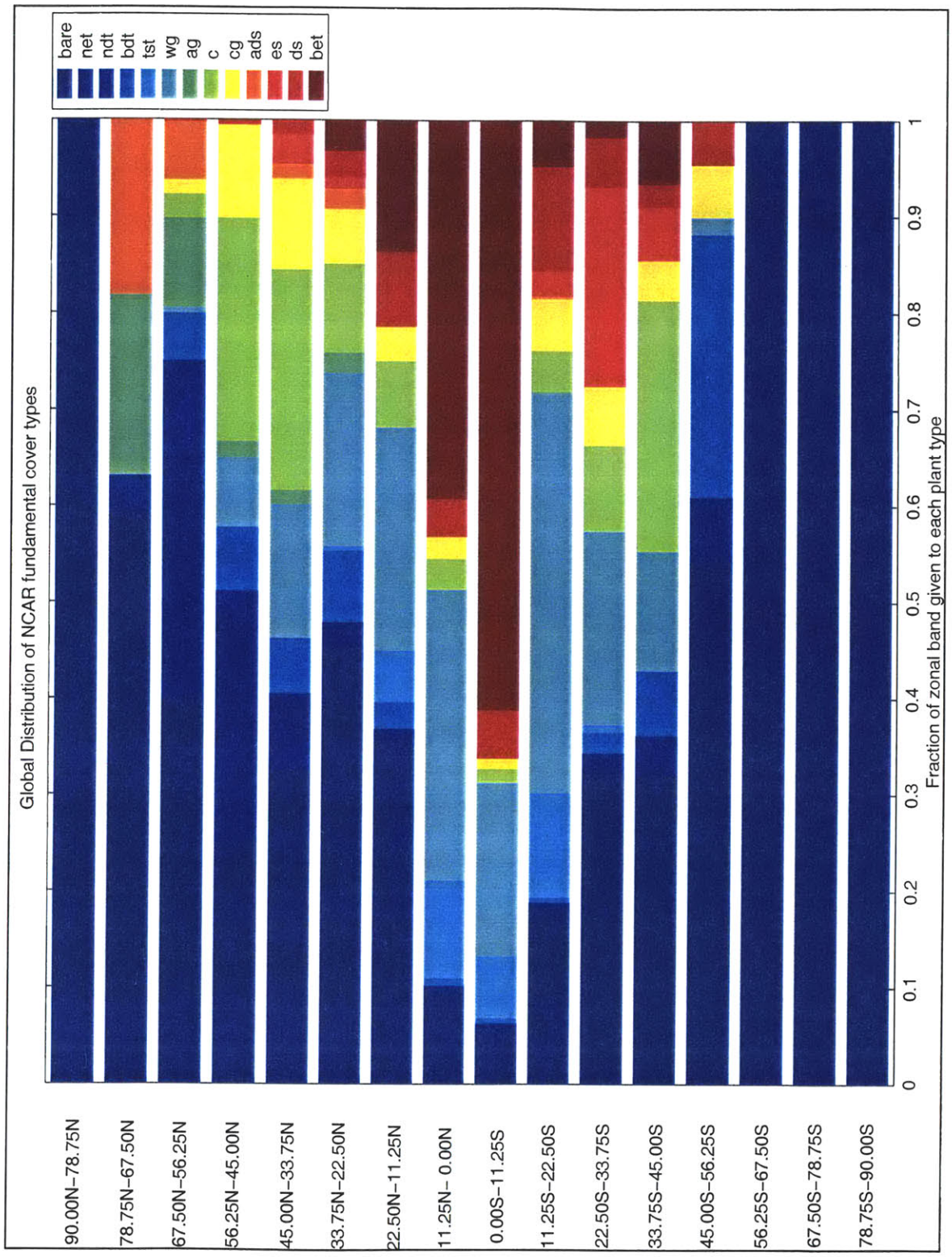

Figure 5.3 **Global Distribution of 13 NCAR sub-grid cover types (NCAR CCM T42 grid). NCAR cover types are discussed in Section 3.2.1. Their names, which are abbreviated in the legend,are given in full in Table 5.1.**

Using the data from fsurdat42, combined with finer resolution input from the Olson dataset, the global land surface can be described as a combination of bare ground and the fundamental plant types on the MIT IGSM grid as in Figure 5.4 below.

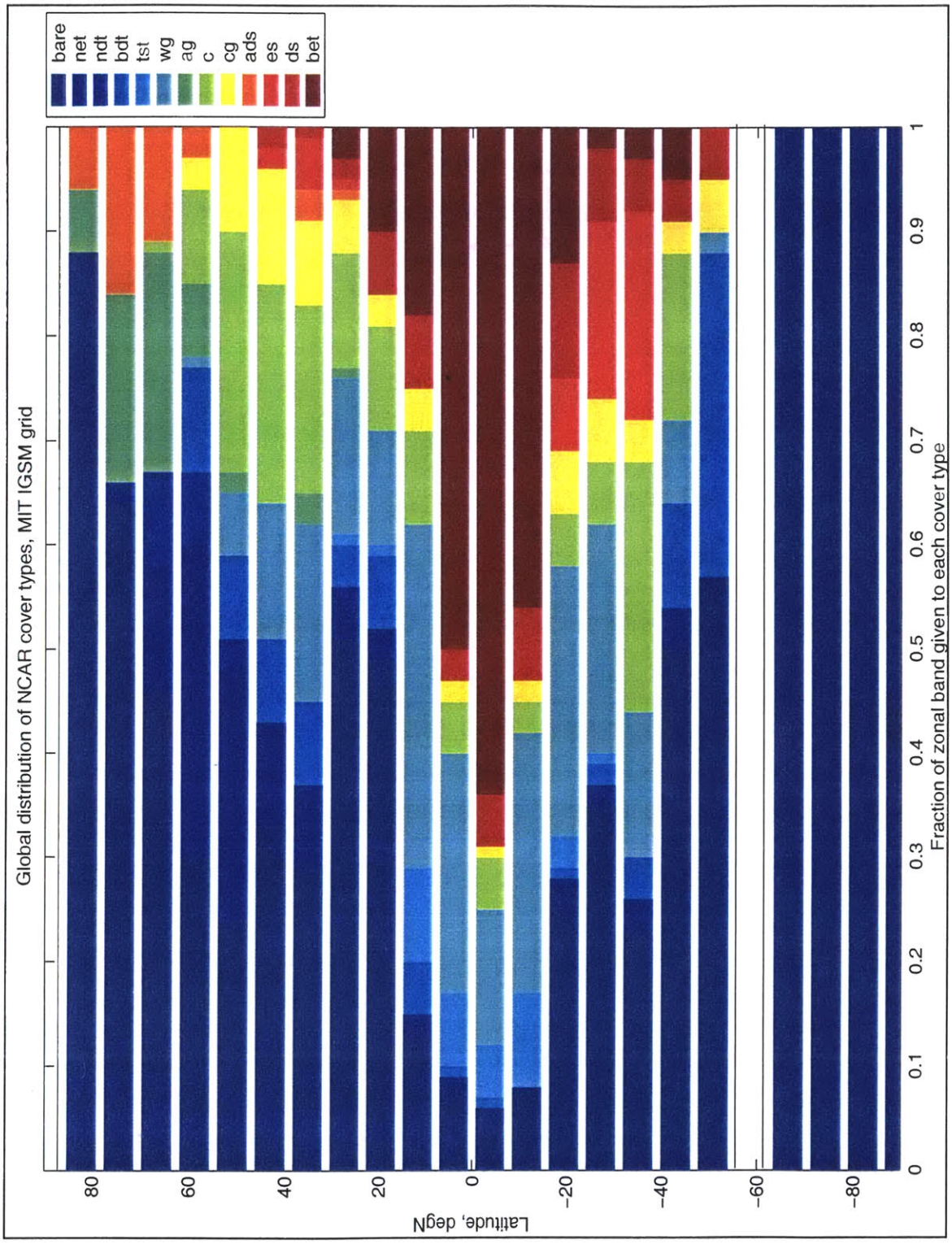

Figure 5.4 **Global Distribution of 13 NCAR sub-grid cover types (MIT IGSM grid) NCAR cover types are discussed in Section 3.2.1. Their names, which are abbreviated in the legend,are given in full in Table 5.1.**

5.2.3 Soil Color

In NCAR LSM, soil color is a required input for each grid cell. Each grid cell can be assigned one of nine soil colors, as discussed in Section 3.2.3. In the subroutine **radconi.F** the dry and saturated albedos, in the visible and near infared region, are given for each of the nine colors.

Figure 5.4 shows the distribution of the nine soil colors in the 11.2^{o} latitudinal bands derived from the NCAR CCM T42 grid. It is clear that it would be incorrect to assign just one color to an entire zonal band.

Instead, when coupling the NCAR LSM to MIT 2D-LO each zonal band will have its own "color", an index corresponding to the average albedo over that band. The average albedo was determined for each 2.8^{o} zonal band from fsurdat_t42, and then realigned with the grid of the MIT IGSM. The resultant albedo figures assigned to the 24 grid points of the coupled NCAR LSM/MIT 2D-LO model are shown in Figure 5.5. The block data subroutine **radconi.F** has therefore been adapted to contain 24 soil "colors" defining the dry and saturated albedos in the near infrared and visible ranges, instead of the original 9 in the NCAR LSM Version 1.0.

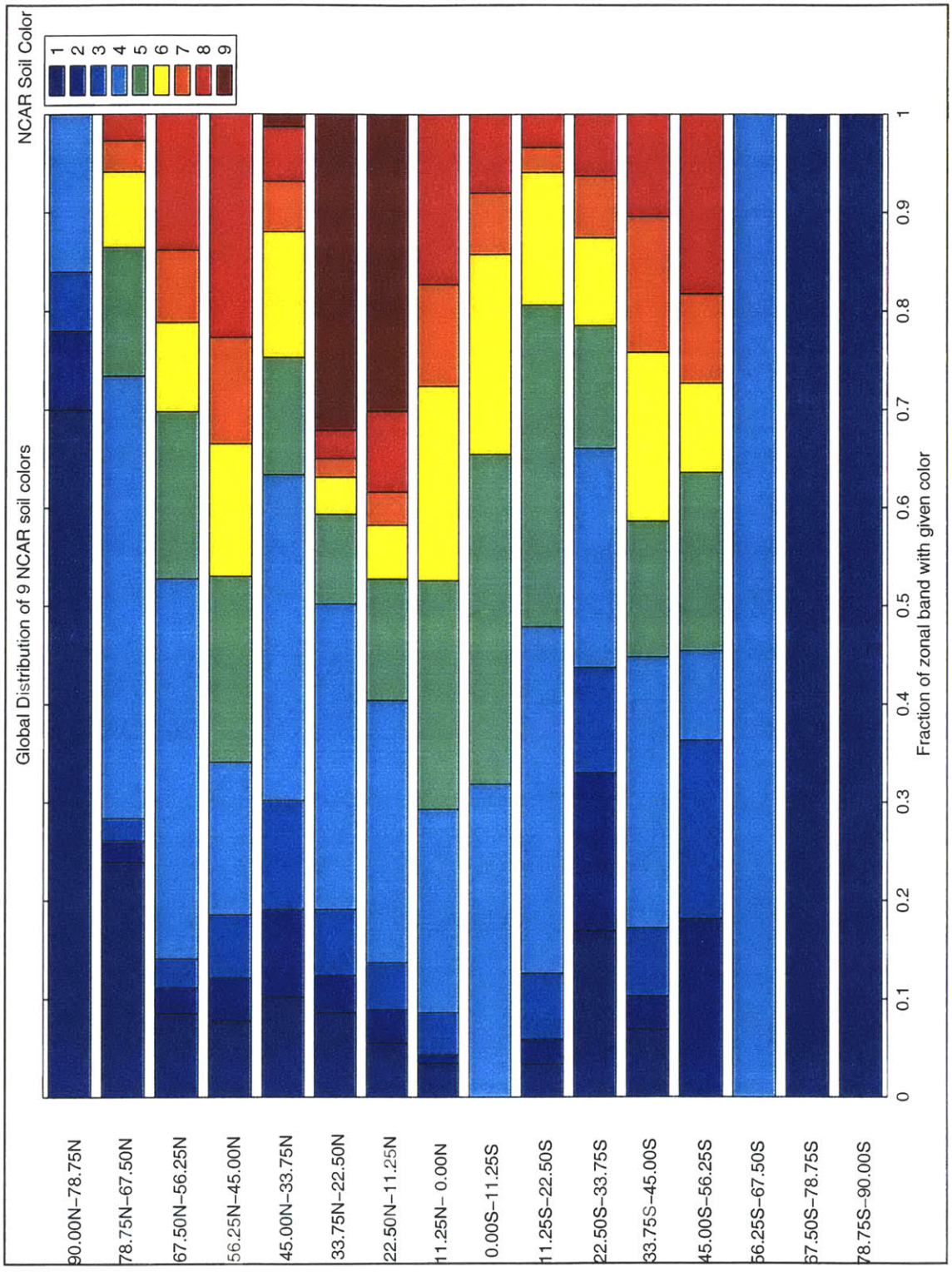

Figure 5.5 **Global Distribution of 9 soil colors (NCAR CCM T42 grid, fsurdat42) NCAR soil colors in the legend are described in Section 3.2.3, and Table 3.3.**

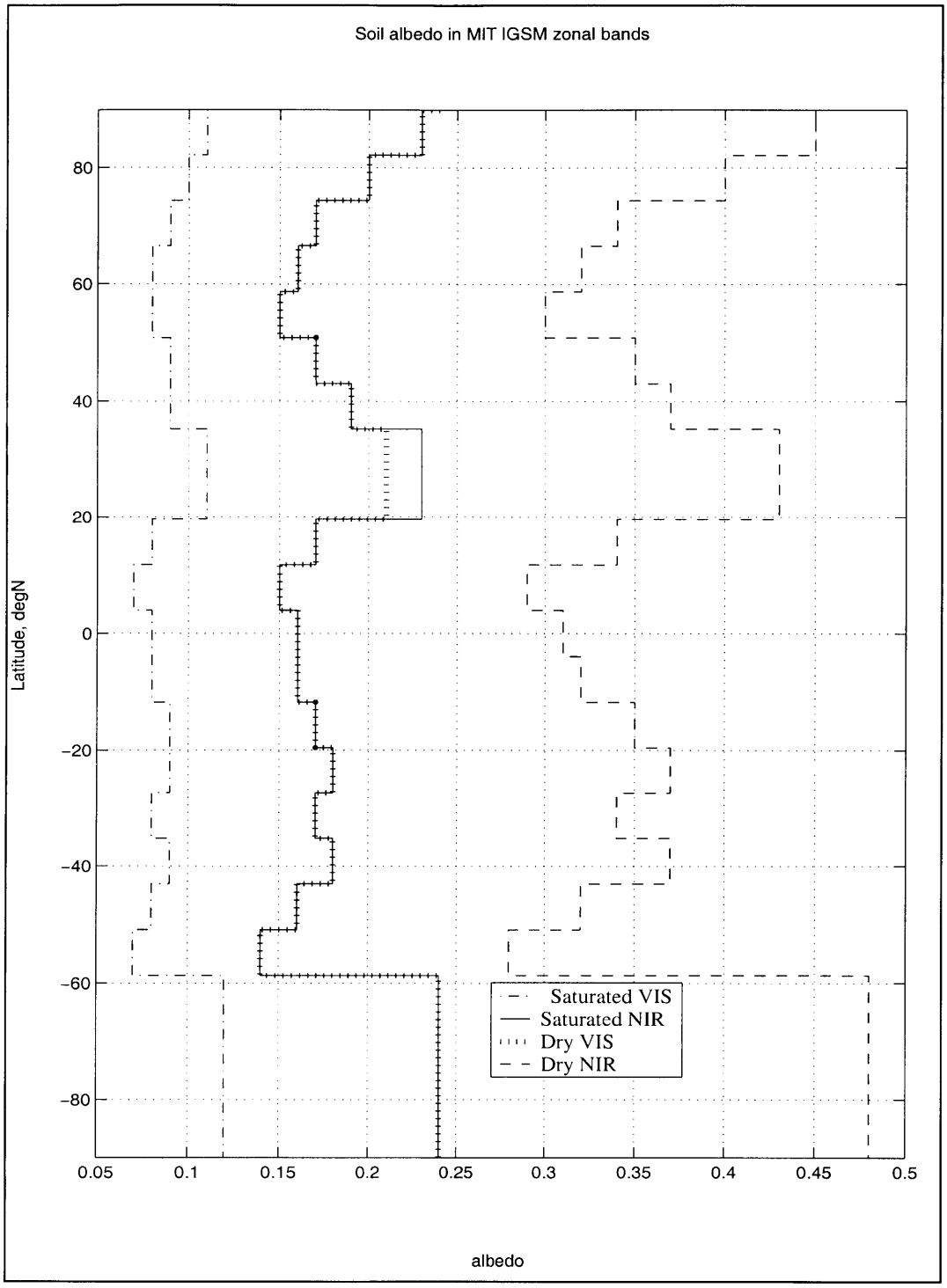

Figure 5.6 **Dry and saturated soil albedo on the MIT IGSM grid, for visible and near infrared wavelengths**

5.2.4 Lake and Wetlands

The proportion of lake and wetlands in each latitudinal band of the MIT IGSM was estimated from fsurdat_t42 in a similar manner, and the results inputted to the model in **fsurdatsd**.

5.3 Model Architecture

In NCAR LSM, **lsmmain.F** is an "off-line" driver that mimics how the land surface model is coupled to the NCAR CCM atmospheric driver. This program can be used to run the model uncoupled from the NCAR CCM atmospheric model, if the appropriate atmospheric forcing is provided in the subroutine **atm.F**. The subroutine atm.F consists of a short code to obtain atmospheric forcing for the land surface model. Typically, in an off-line use of the NCAR LSM, atmospheric forcing data would be read from a file using **atm.F**.

In our application, we wish to fully couple the NCAR LSM to the MIT 2D-LO. This means that at each time step the required atmospheric forcing is generated by the atmospheric component of MIT 2D-LO, and the resultant output from NCAR LSM is then provided as input for the next step of the atmospheric model.

As we are sharing variables at each time step, the obvious solution is to use common blocks. For clarity we established two common blocks, **GCM2LSM** and **TOATM**. As

the name suggests, **GCM2LSM** contains the atmospheric forcing data provided to the land surface model from the atmospheric component of MIT 2D-LO. The data required from the atmospheric component of the MIT 2D-LO is listed in Table 5.1 below.

Similarly **TOATM** contains the data required by the atmospheric component of MIT 2D-LO that is provided as output from the NCAR LSM. This data required as output from the NCAR LSM to force the atmospheric component of MIT 2D-LO is listed in Table 5.3 below.

Quantity	Units
Atmospheric Bottom Pressure	pa
Atmospheric Surface Pressure	pa
Atmospheric bottom level zonal wind - at center of grid cell	$m\ s^{-1}$
Atmospheric bottom level meridional wind	$m\ s^{-1}$
Atmospheric bottom level temperature	K
Atmospheric bottom level specific humidity	kg/kg
Atmospheric bottom level height above surface, derived from temperature at bottom level	m
Convective precipitation rate	$mm\ water\ s^{-1}$
Large-scale precipitation rate	$mm\ water\ s^{-1}$
Downward LW radiation onto surface	$W\ m^{-2}$
Solar radiation onto surface (visible)	$W\ m^{-2}$
Solar radiation onto surface (near infrared)	$W\ m^{-2}$
Cosine of the solar zenith at each time step	-

Table 5.2 Required atmospheric forcing from MIT 2D-LO to NCAR LSM

Quantity	Units
Sensible heat flux	$W\ m^{-2}$
Latent heat flux	$W\ m^{-2}$
Water and Carbon dioxide fluxes	$kg\ m^{-2}\ s^{-1}$
Zonal surface stress	$W\ m^{-2}$
Meridional surface stress	$W\ m^{-2}$
Emitted longwave radiation	$W\ m^{-2}$
Ground skin temperature	K
Ground temperature for each of 6 layers in soil column	K
Volumetric soil water content for each of the 6 layers of the soil column*	-

Table 5.3 Required outputs from NCAR LSM to MIT 2D-LO

*Note: While the NCAR LSM soil profile consists of six layers, the MIT 2D-LO has just two. So, the temperature and moisture content of the 6 layers of the soil column in the NCAR LSM are weighted according to thickness to give the corresponding quantities for the two soil layers of the MIT IGSM.

In the NCAR LSM, the subroutine **lsmzen.F** uses the longitude and the current seconds of day at Greenwich, to calculate the zenith angle at the grid cell at each time step. Because we are interested in running the model as a zonally averaged model, we must use a single longitude value for the entire latitudinal band. The zenith angle is also calculated in the MIT 2D-LO, as it is required by the ocean and ocean ice components too. This value will be provided along with the atmospheric forcing data when the NCAR LSM is called. The forcing data and cosine of the zenith angle are outputted to the **GSM2LSM** common block before the NCAR LSM is called. Instead of actually calculating the solar zenith angle, the subroutine **lsmzen.F** will now read the current value as calculated by in MIT 2D-LO from the **GSM2LSM** common block . The zenith angle is required in the

radiation calculations, and this approach ensures that these calculations are consistent with the GCM.

So, while **lsmmain.F** is the main driver program for simulations uncoupled to CCM3, we can use it to couple the LSM to the atmospheric component of MIT 2D-LO. This will be achieved by using **atm.F** to read the atmospheric forcing data from the **GCM2LSM** common block, updated with each time step. At the end of each model run the variables required by the next step of the GCM will be written to the **TOATM** common block in **lsmmain.F**.

5.4 Determination of precipitation factors for direct use in the zonally averaged LSM.

The existence of an ecosystem depends on the climate, so it is reasonable to expect that climatic forcing such as precipitation might vary across land cover types. Where tropical forest and desert exist in the same latitudinal band, it is likely that the contribution to the zonal mean precipitation from the precipitation over desert is far less than that from the tropical forest. Furthermore, the response of the surface to precipitation will depend on the plant type. For this reason, applying the zonal mean precipitation over all land cover type is unrealistic.

In Section 5.2.2, we described the parameterization of the land surface in the 24 latitudinal bands in terms of the 13 fundamental cover types of the NCAR LSM. The

number of sub-grid points, or land points, in a latitudinal band may vary from 0 (all ocean) to 13. The total number of landpoints is 172. As the NCAR LSM is a vectorized model, all calculations are performed on the vector of 172 landpoints. In contrast, the MIT 2D-LO model performs all calculations zone by zone. The use of the vector approach in the NCAR LSM facilitates the implementation of weighting factors to distribute the zonal average precipitation over the individual cover types without incurring considerable computational cost.

The objective of this section is to define a matrix of "precipitation factors" which represent the multiple of the zonal mean precipitation which falls over each land point. The precipitation factor will vary throughout the year, so we will have a 172 x 12 matrix.

The Olson World Ecosystem Database and the IIASA precipitation are defined on the same grid, so it is straightforward to calculate the precipitation factors for use with the 31 Olson land classes. However, the following obstacles must be overcome before they can be applied to the NCAR LSM:

1) The Olson data is on a considerably finer scale (0.5^0 x 0.5^0), identical to the precipitation data. The NCAR LSM coupled to the Community Climate Model (denoted NCAR-LSM-CCM) uses a land surface description file (fsurdat_t42) which is on a grid similar, but not identical, to the MIT model. These grids will have to be aligned during the calculations.

2) As we have seen, the surface types in the NCAR LSM differ from the Olson classification system. Each Olson class needs to be expressed as a combination of NCAR surface types.

By grouping the latitudinal bands of the Olson database into bands of 7.5 or 8degrees, based on the approximate bands of the MIT 2D-LO model and those of the NCAR CCM T42 grid, the Olson classes could be compared to those of the NCAR LSM. Using a spreadsheet, the Olson classes were expressed as combination of the NCAR surface types, such that the proportions of the 13 fundamental cover types matched as closely as possible.

This resulted in each ~8° band being represented as a combination of the 13 fundamental cover types used in the NCAR LSM to specify aerodynamic and physiological properties that determine stomatal resistance and carbon dioxide fluxes. It was assumed that these combinations would be valid over the MIT resolution of 7.826.

If we assume that the precipitation over any pixel is distributed evenly over the pixel, the precipitation factors for the 13 surface types in each band can be determined using the following algorithm. Consider a latitudinal band of N pixels such as that in Figure 5.6. Let each pixel have area $A_p = 1$, for simplicity.

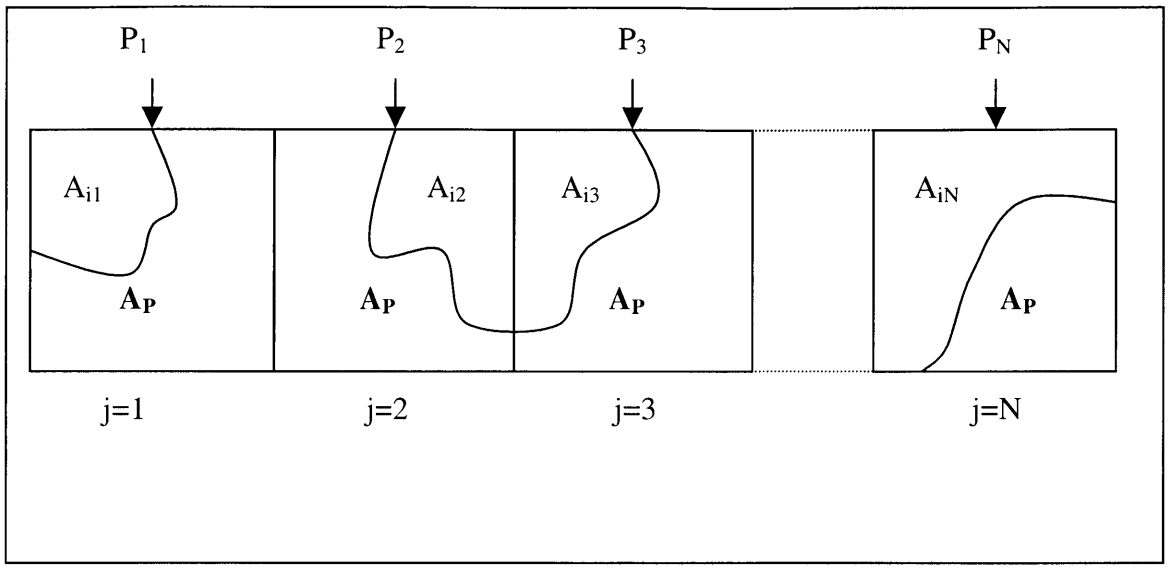

Figure 5.7 Schematic of N pixels in each zonal band, for use in precipitation factor algorithm

Each pixel is one of the 31 Olson Surface types. We have previously expressed the Olson surface types in terms of the 13 NCAR cover types, so we can determine for each pixel (j) , the area A_{ij} of cover type i at the appropriate latitude.

Hence the ratio of precipitation over a given cover type (i) to the zonal mean precipitation is given by:

$$\frac{\sum_{j=1}^{N}\{A_{ij}P_j\}}{\overline{P}\sum_{j=1}^{N}A_{ij}} \qquad (5.1)$$

where $\overline{P}$ is the zonal mean precipitation.

Using this expression, monthly precipitation factors were derived for each cover type in latitudinal bands of 7.826^{o}, the resolution of the MIT model.

The results, which consist of a 172 by 12 matrix are plotted overleaf in Figures 5.7 to 5.11 and discussed in Section 5.5. The figure legends contain the abbreviated titles of the cover types, but recall that the names are given in full in Table 5.1. Note that below 54.783S, the land surface consists entirely of bare ground, and so the precipitation is unity everywhere.

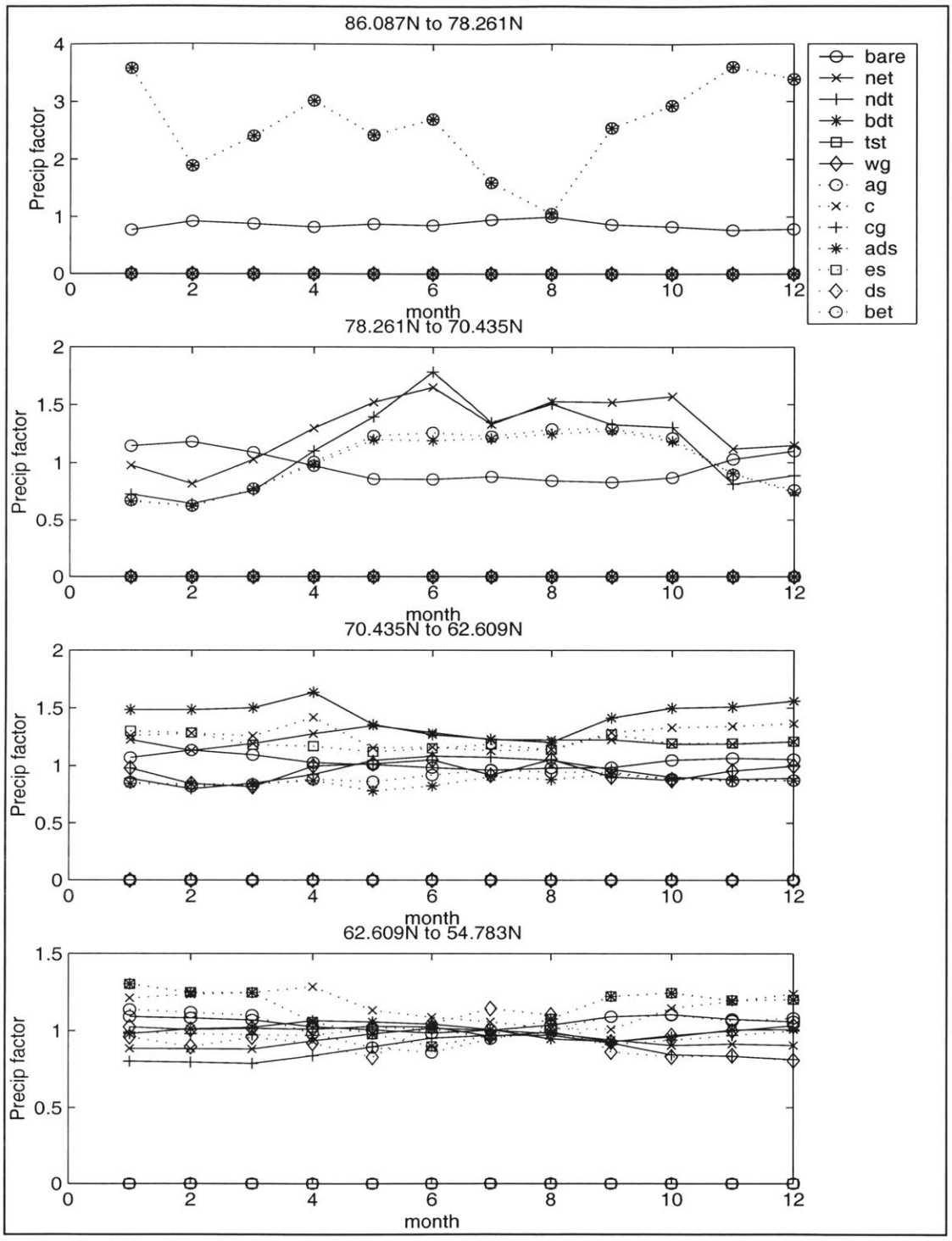

Figure 5.8 Precipitation factors to be applied to the 13 NCAR fundamental cover types between 86.087N and 54.783N. The abbreviated cover types in the legend are named in full in Table 5.1.

(Note that above this latitude there are no land points).

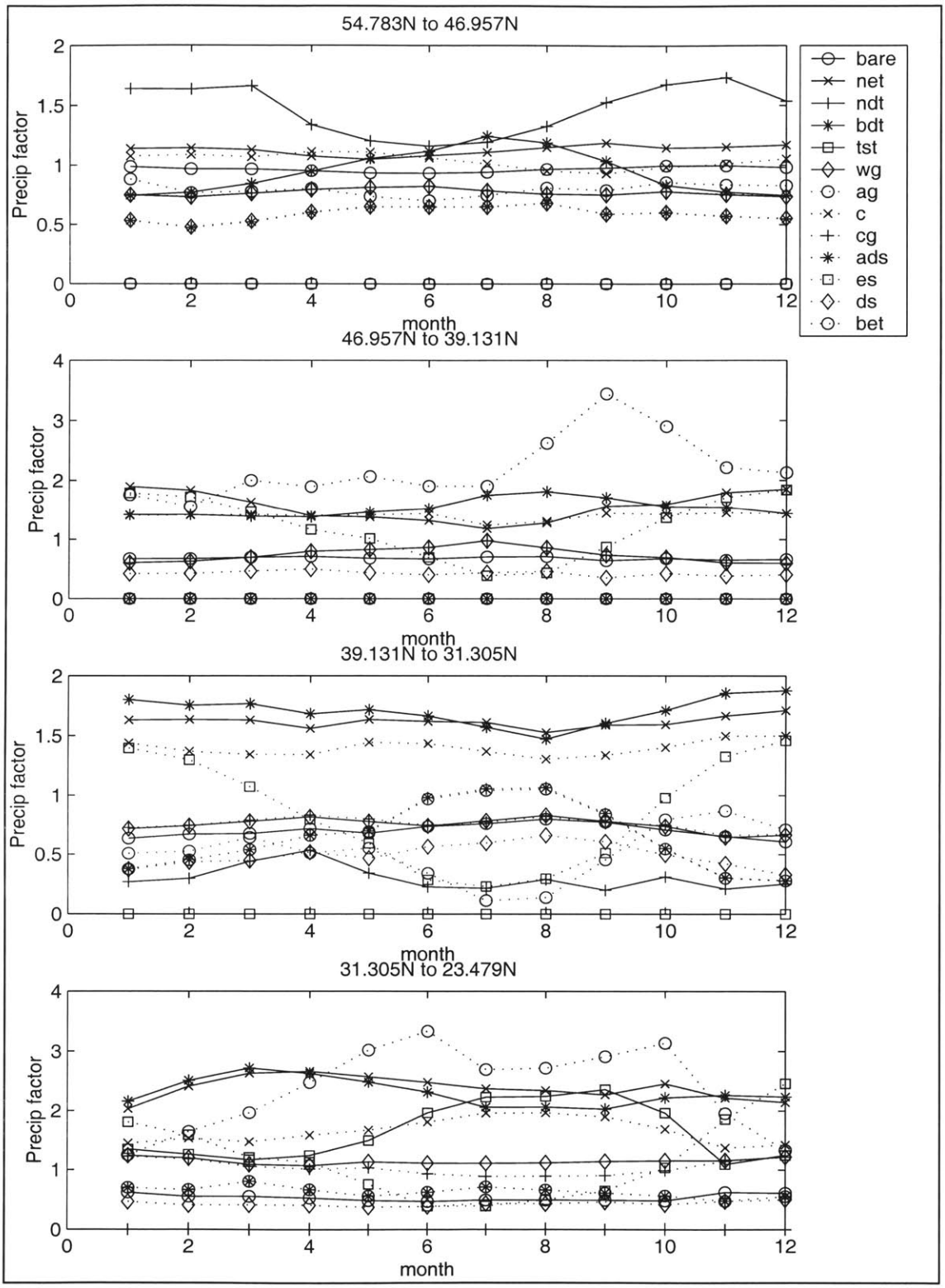

Figure 5.9 **Precipitation factors to be applied to the 13 NCAR fundamental cover types between 54.783N and 23.479N. The abbreviated cover types in the legend are named in full in Table 5.1.**

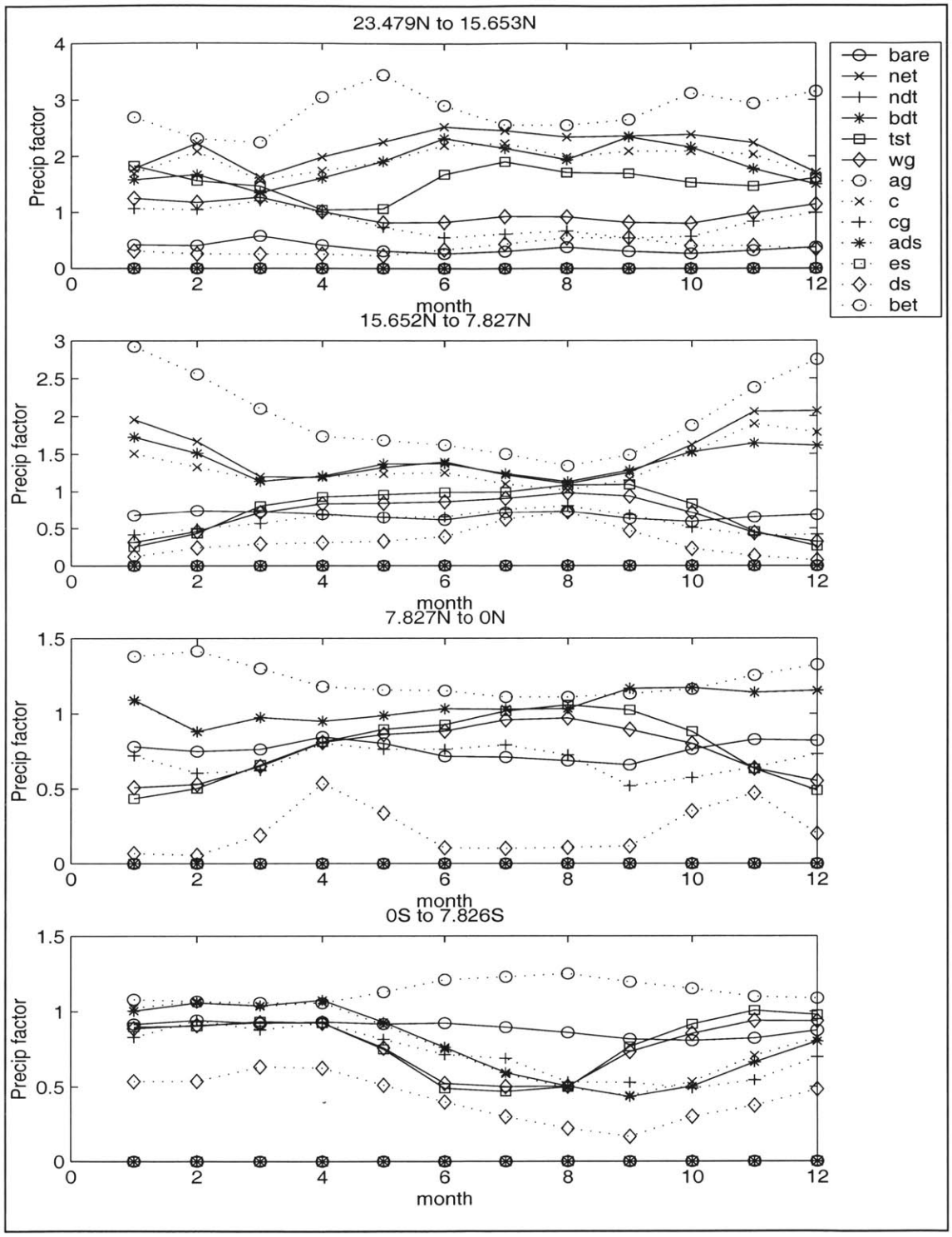

Figure 5.10 Precipitation factors to be applied to the 13 NCAR fundamental cover types between 23.479N and 7.826S. The abbreviated cover types in the legend are named in full in Table 5.1.

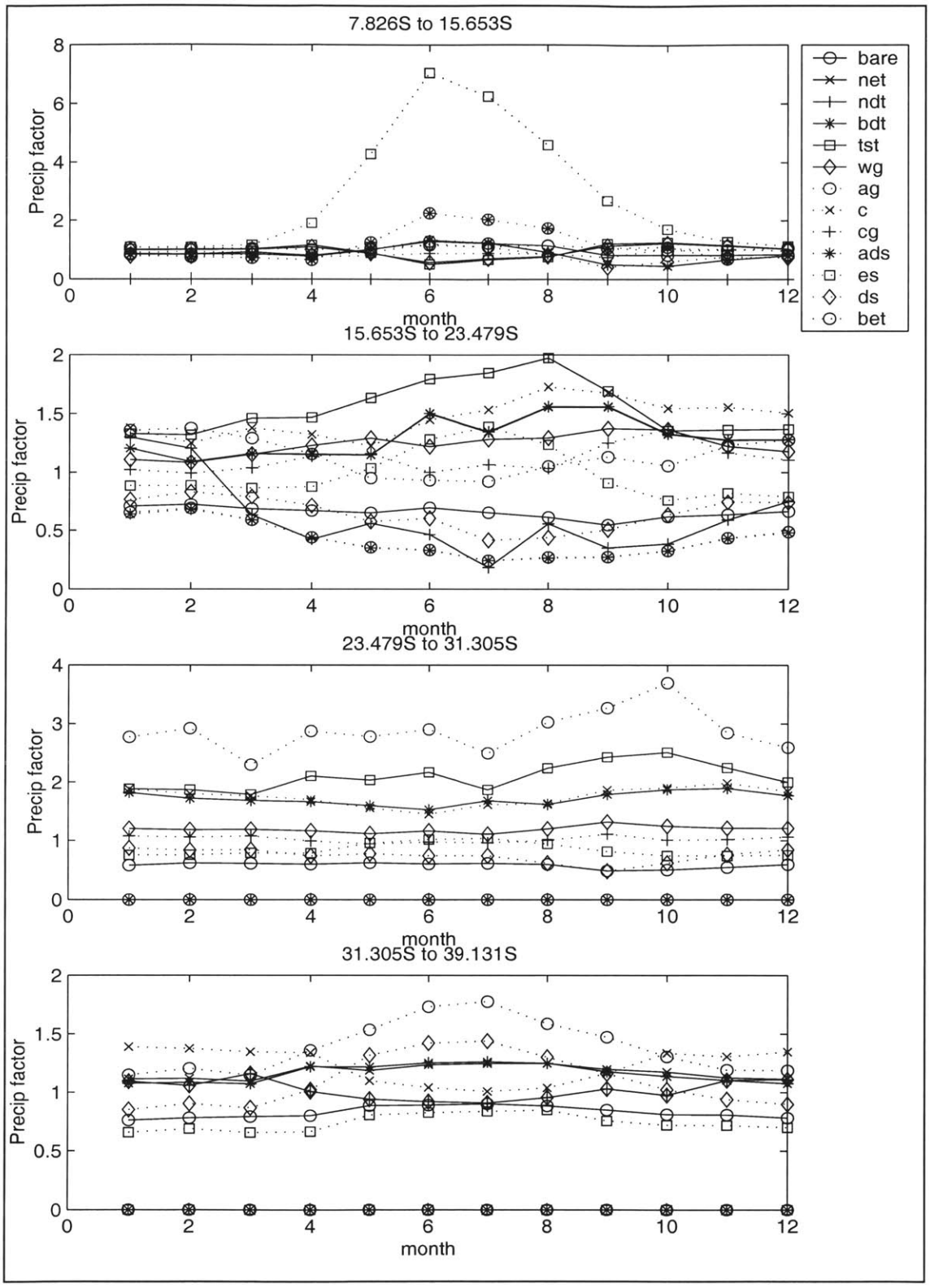

Figure 5.11 **Precipitation factors to be applied to the 13 NCAR fundamental cover types between 7.826S and 39.131S. The abbreviated cover types in the legend are named in full in Table 5.1.**

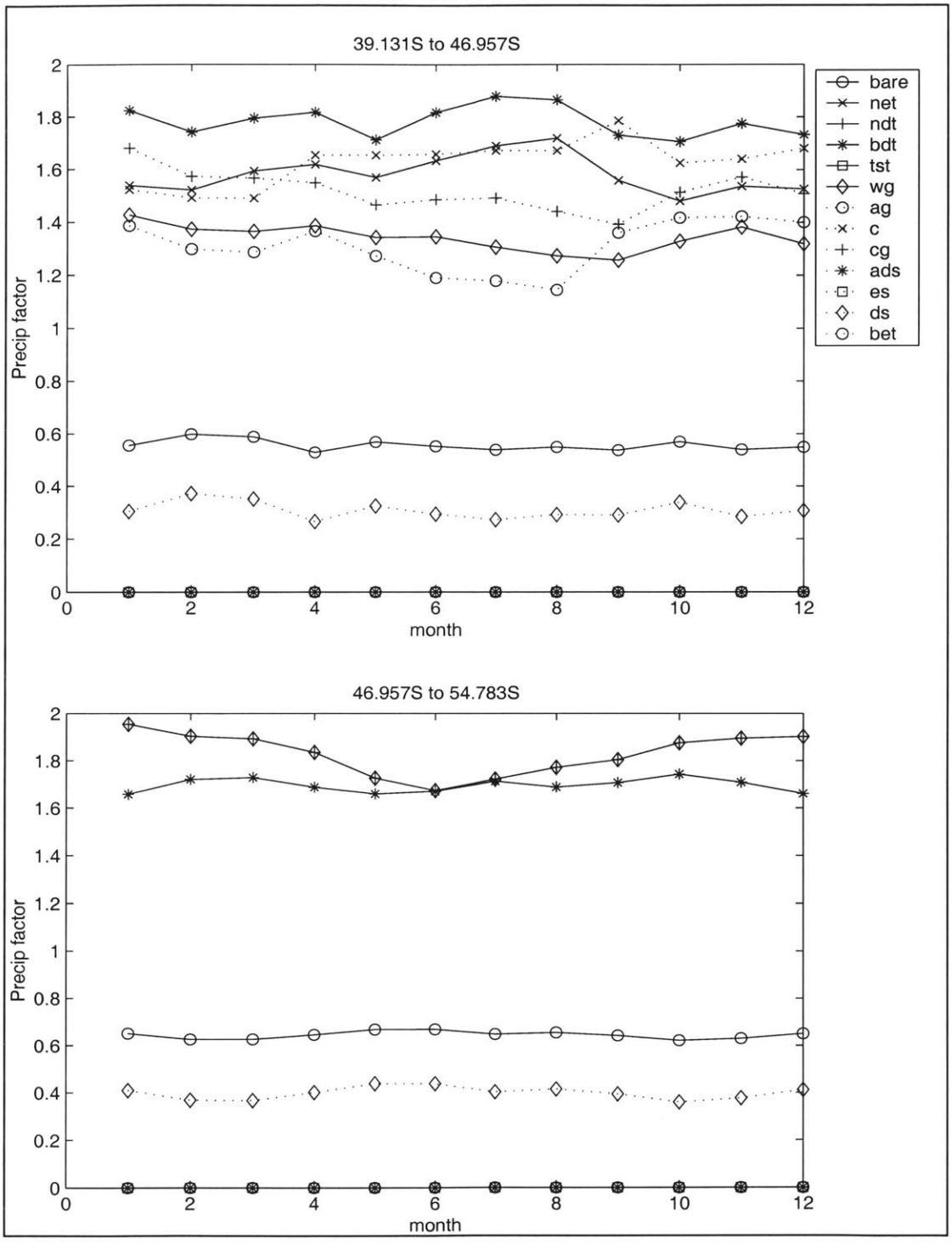

Figure 5.12 Precipitation Factors.Precipitation factors to be applied to the 13 NCAR fundamental cover types between 39.131S – 54.783S The abbreviated cover types in the legend are named in full in Table 5.1.

5.5 Interpretation of the Precipitation Results

A precipitation factor of zero for a certain plant type implies that in that zonal band, that particular plant type receives none of the zonal mean precipitation, either because that cover type does not occur, or because it is actually dry.

If the mean monthly precipitation over the particular cover type exactly equals the zonal mean precipitation, the precipitation factor will be unity. Obviously, between 62.609S and 90S, where the only cover type is land ice, the factor will always be one.

Consider a zonal band in which all 13 cover types occur, and denote the precipitation factors for some month as F_i where i varies from 1 to 13. If we denote the fractional area of each cover type as A_i, and the mean precipitation as $\overline{P}$, then the following must be satisfied:

$$\sum_{i=1}^{13} F_i \overline{P} A_i = \overline{P} A \qquad (5.2)$$

where A is the total zonal area.

From the expression above, it is clear that if a zone consists primarily of one surface type, its precipitation will be close to one, while that of the other cover type may fluctuate considerably. Consider for example the region between 86.087N and 78.261N, where the dominant cover type is bare. Throughout the year, the precipitation factors for the bare surface are close to unity. A small fraction of the region consists of arctic deciduous

shrub and arctic grass. While the precipitation over these areas may be almost four times the zonal mean, the fractional area is very small by comparison. Compare these findings to those of 62.609N to 54.783N where there are many cover types, and the precipitation factors are more closely concentrated around unity for any given month.

In some cases, seasonal variation may be clearly identified. Between 15.652N and 7.827N, there is a marked difference between the character of the broadleaf evergreen tree and the bare surface. While the bare surface remains below unity, and varies little through the year, the broadleaf evergreen tree is subject to precipitation of up to three times the zonal mean, and exhibits a clear seasonal cycle, dropping to below 1.5 in August.

Chapter 6

Results From Fifty-year Simulation

6.1 Introduction

In this chapter the results from a fifty-year simulation with the NCAR LSM coupled to the MIT 2D-LO model are presented. They demonstrate that the incorporating a zonally-averaged version of the NCAR LSM into the existing MIT climate model produces a satisfactory climatology.

The figures in this chapter depict the land surface component only. In two zonal bands, between 90°N and 86.087°N, and 50.87°N and 58.696°N, the earth's surface consists entirely of ocean. There is obviously no contribution from the land surface here. The gaps in the following graphs correspond to these regions.

6.2 Net Radiation

Figure 6.1 shows the Annual Mean Net Longwave Radiation and Net Shortwave Radiation, estimated during a 50-year simulation using NCAR LSM coupled with the MIT 2D-LO climate model.

Net Longwave Radiation is given by

$$\vec{L} = -L_{atm}\downarrow + L\uparrow$$

where $L_{atm}\downarrow$ is the downward atmospheric longwave radiation and $L\uparrow$ is the upward longwave (terrestrial) radiation, both in W m^{-2}.

The net longwave radiation is calculated separately for each subgrid land surface type, and for vegetated surfaces includes contributions from the ground and vegetation. The variability in the net longwave radiation corresponds to the variation in land surface type.

The net shortwave radiation is the incident solar radiation less that absorbed at the surface. As we might expect, the peak is at the equator where the incident radiation is greatest. Furthermore, net shortwave radiation is lowest at the poles, where incident radiation is low and albedo may be on the order of 75-90% for fresh snow.

Moreover, the relative magnitudes of the net shortwave and longwave radiation confirm that the land surface model is correctly coupled to the atmospheric model which provides the forcing.

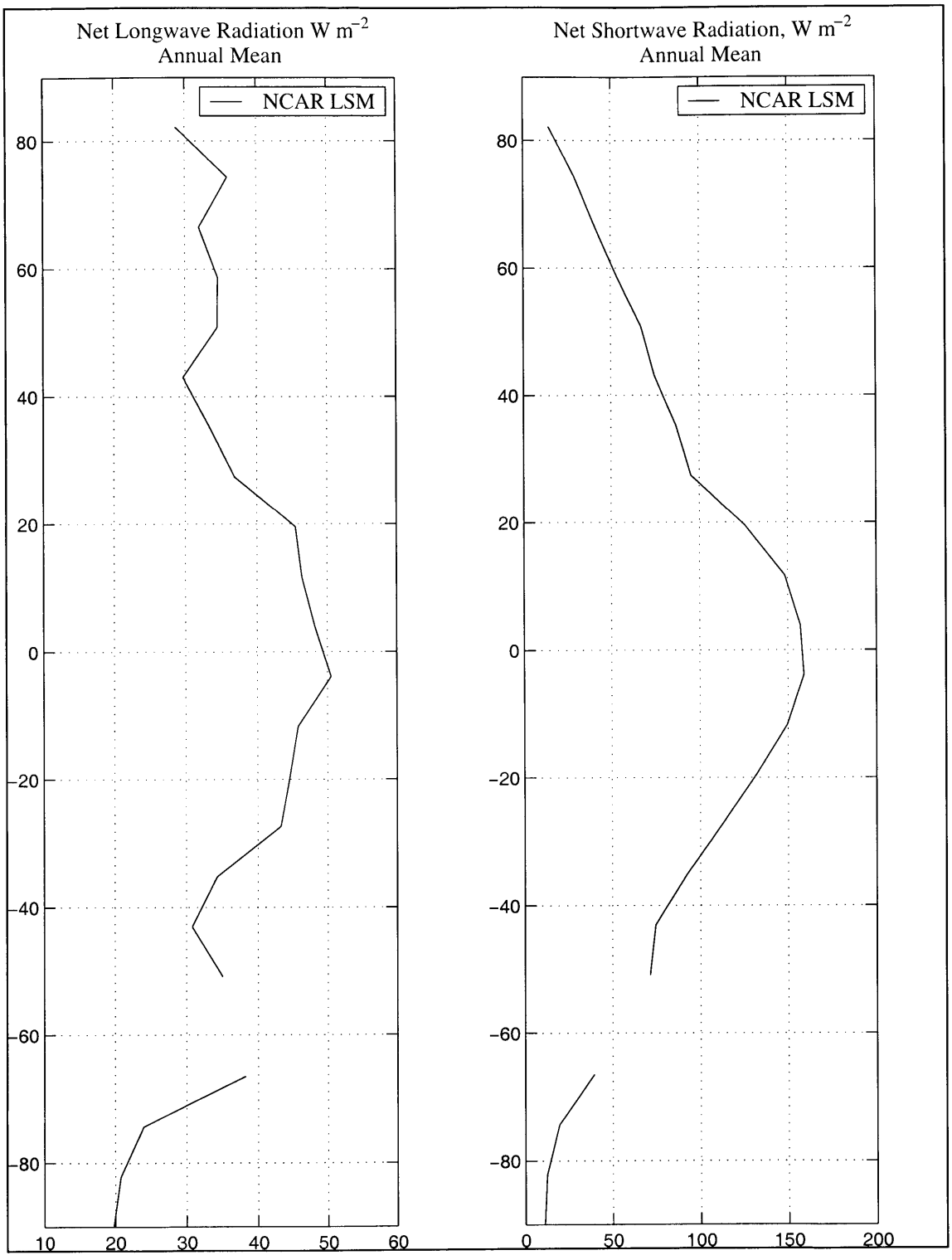

Figure 6.1 **Annual Mean Net Longwave and Shortwave Radiation, in W m^{-2},as a function of latitude, derived from a 50-year simulation replacing the land component of MIT 2D-LO with the NCAR Land Surface Model.**

6.3 Temperature

The results from a fifty-year simulation using NCAR LSM to model the land surface were compared to observations from the datasets of Leemans and Cramer (1991). The observations are the monthly mean values derived from 6,280 stations worldwide between 1941 and 1960. Referring to Figure 6.2, which shows the annual mean air temperature on the left, it seems that the results using the NCAR land surface model are slightly biased with regard to the MIT 2D-LO output, however they are in general consistent with the observations.Where they err from the observations of mean annual temperature, they exhibit a cold bias, which is a common feature of many GCMs (Sokolov and Stone, 1995).

The seasonality in air temperature is shown on the right as the difference between the mean air temperature in July and that in January. The MIT 2D-LO model performs marginally better than NCAR in the northern hemisphere, while the converse is true in the southern hemisphere. There is however, considerably less land mass in the area where NCAR LSM performs poorly, relative to the area where MIT 2D-LO performs poorly, so in general the NCAR LSM leads to a better estimate of air temperature.

Considerably colder conditions exist over Antarctica under the NCAR climate, however data was not available to determine which was closer to the truth. The seasonality in air temperature is also less pronounced under the NCAR model in this region.

Figures 6.3 and 6.4 show the 50-year time series of mean annual air temperature in each of the latitudinal bands. It is apparent that there is a "spin-up" time associated with using the NCAR LSM. In all latitudes, the initial value of the air temperature is higher than the mean value it assumes after about 10 years. The difference is on the order of 2°C for all latitudinal bands except those in the northern high-latitudes where the difference is 5-7°C.

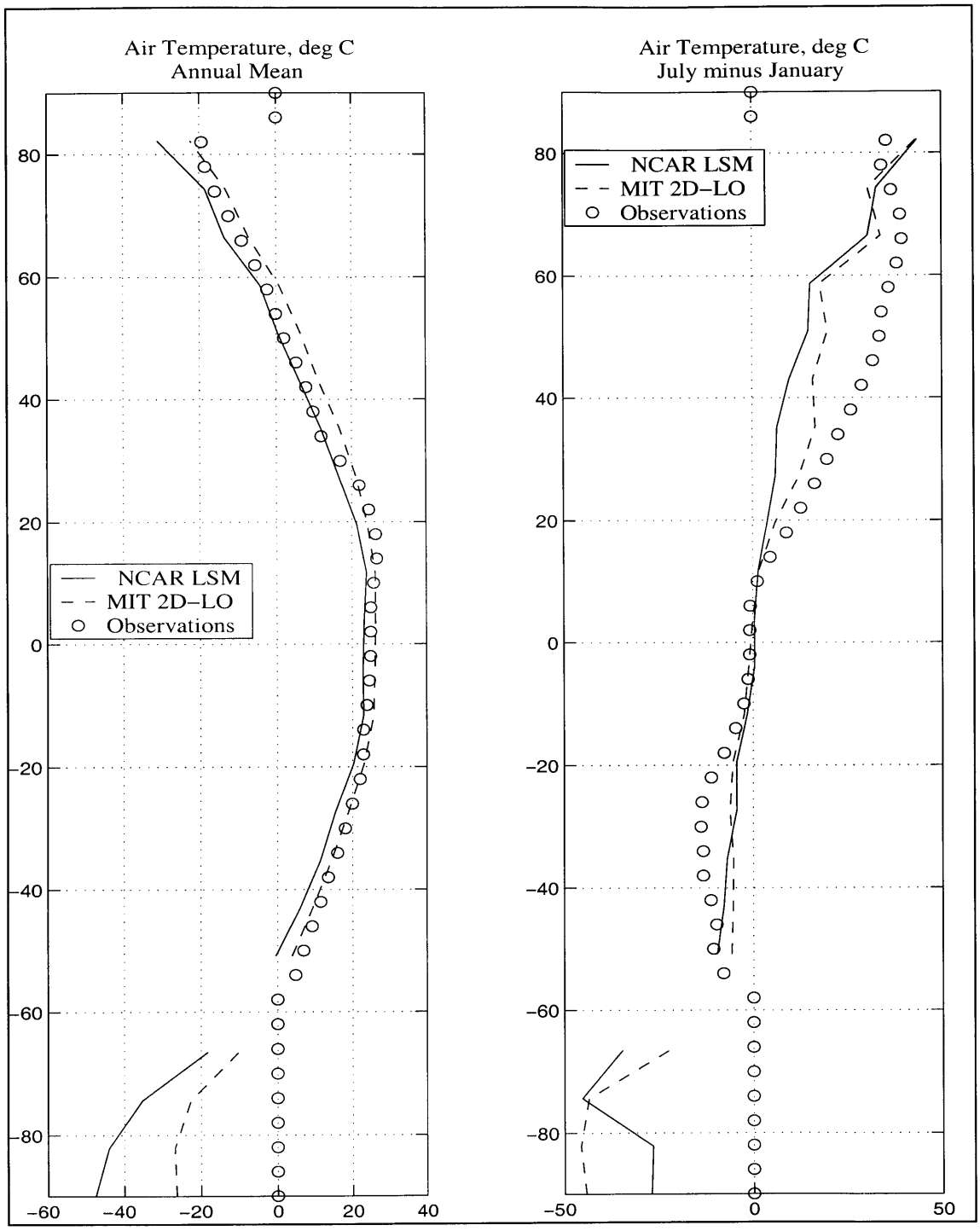

Figure 6.2 **Air temperature at a reference height of 2m in degrees Celsius, as a function of latitude, derived from a 50-year simulation replacing the land component of MIT 2D-LO with the NCAR Land Surface Model. The annual mean is plotted on the right, and seasonality (July-January) on the right. Results are compared to those from the MIT-2D-LO and observations from Leemans and Cramer (1991).**

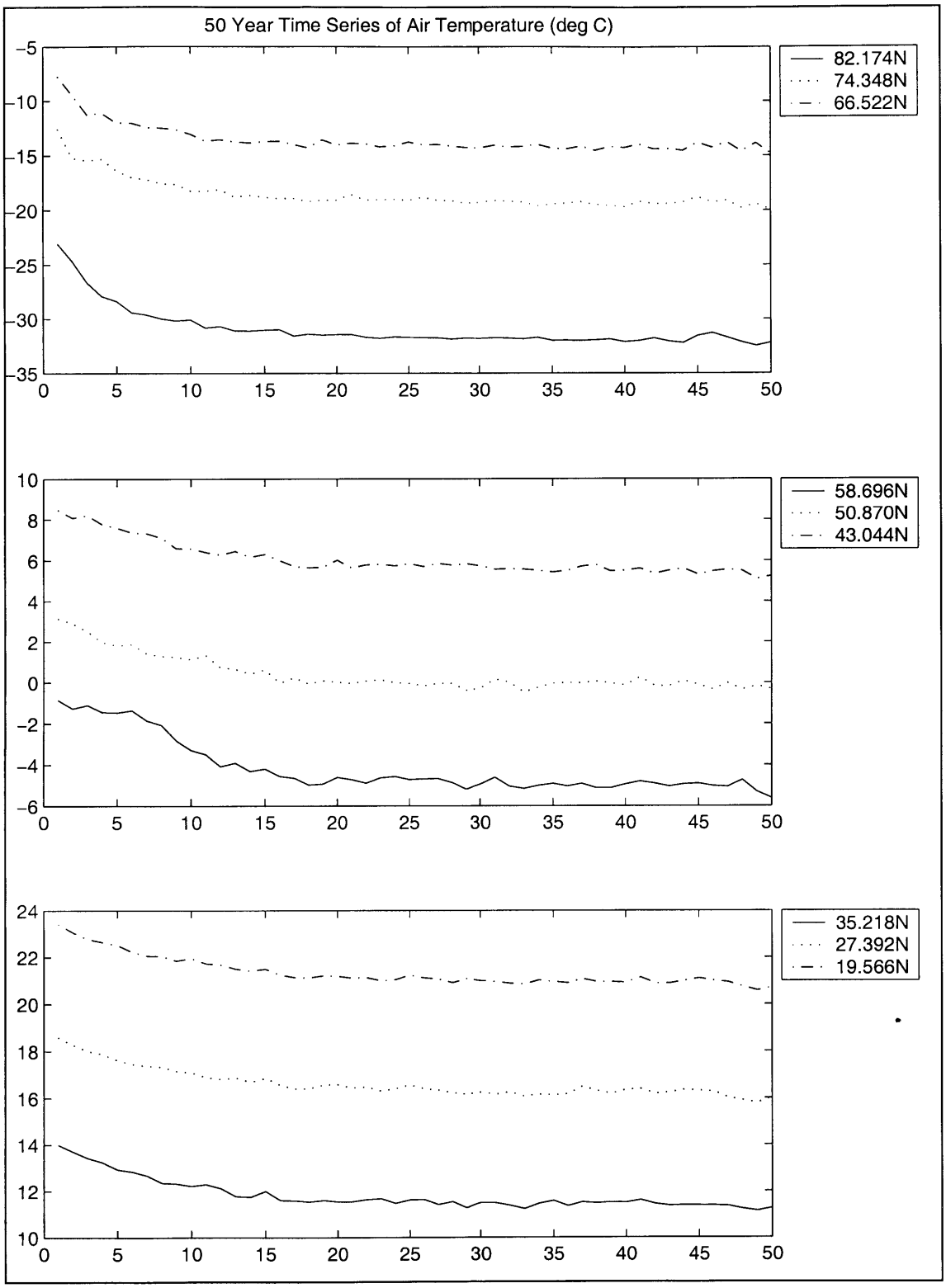

Figure 6.3 **50-year time series of annual mean air temperature in degrees Celsius, modeled using the NCAR Land Surface model over the land portion in MIT 2D-LO.**
Results for zonal bands centered on latitudes 82.174N to 19.566N.

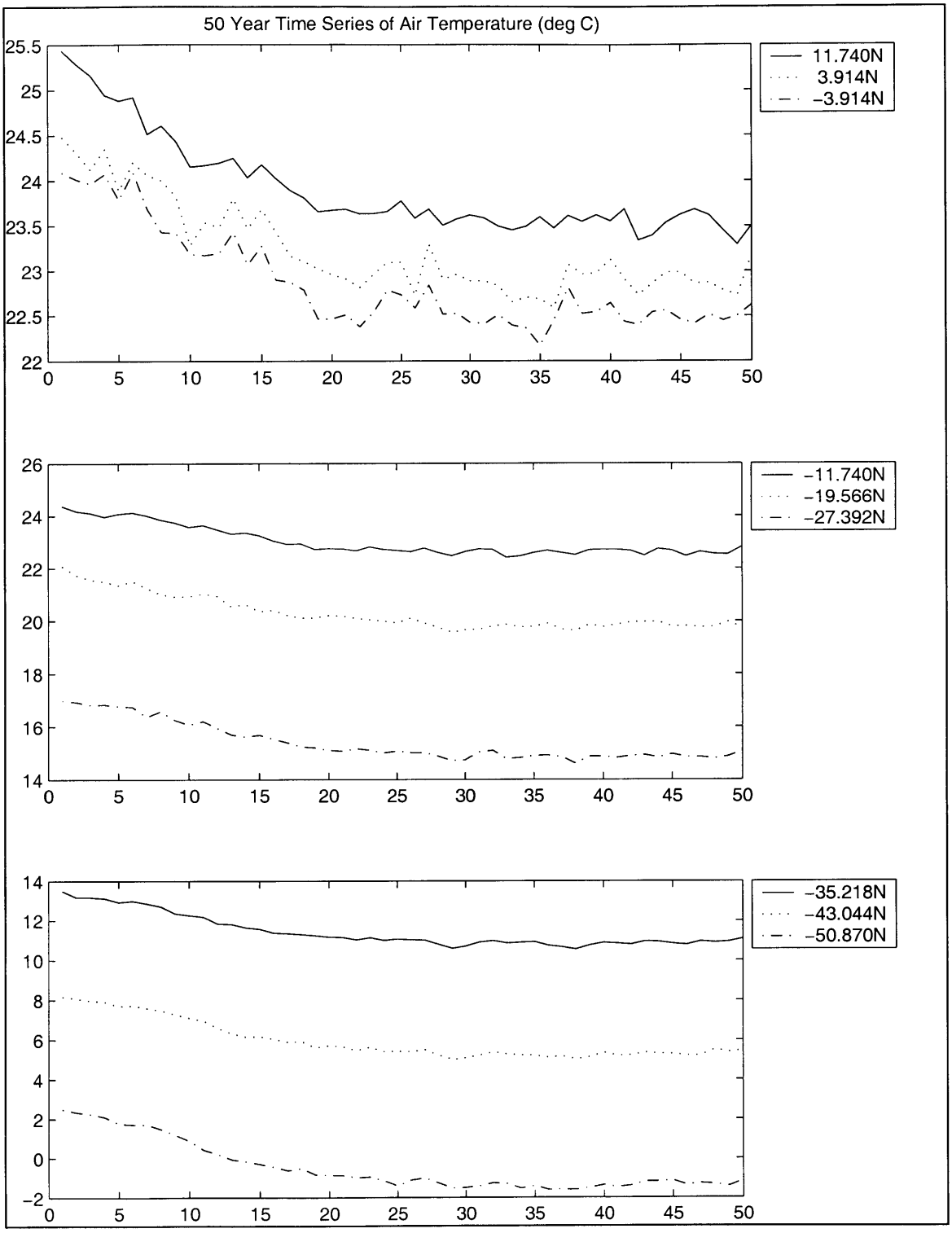

Figure 6.4 **50-year time series of annual mean air temperature in degrees Celsius, modeled using the NCAR Land Surface model over the land portion in MIT 2D-LO.**
Results for zonal bands centered on latitudes 11.740N to –50.870N.

6.4 Precipitation

Results from a fifty year simulation using NCAR LSM were compared to similar output from the MIT 2D-LO model as well as observations from Leemans and Cramer (1991). Observations are derived from precipitation records from 6,090 stations worldwide for the period 1941-1960. Referring to Figure 6.5 which shows the Annual Mean Precipitation on the left-hand side, and the seasonality in precipitation on the right-hand side, we see that there is little difference in the performance of the two models relative to observations. This is because despite the coupling of the models, precipitation is driven by the atmosphere.

In the mean annual precipitation plot, the northward shift in the maximum precipitation is apparent in results from both models. One area where the MIT 2D-LO model outperforms the NCAR LSM is in the zonal band centered at ~4°S. Recall from Figure 6.4 that this region had a particularly noisy air temperature signal. We shall see in Figure 6.7 that this region also exhibits a particularly interesting trend in the 50-year time series of its annual mean precipitation.

Returning to Figure 6.5 to examine the seasonality (July – January) in precipitation, the trace of the observation is pretty intuitive. In the northern hemisphere observations indicate that there is more precipitation in the summer months than in the winter months, with the magnitude of the difference increasing towards the equator. In the northern tropics, the wet season occurs in the northern summer, while in the southern hemisphere

the wet season occurs in the winter months. This is apparent from the observations in the excess of rain in July for the Northern hemisphere, and in January for the Southern Hemisphere. Both the NCAR LSM and the MIT 2D-LO fail to reproduce this clear signal. The seasonal difference in precipitation is grossly underestimated by both models.

Figures 6.6 and 6.7 show the 50-year time series of mean annual precipitation in the different zonal bands. Figure 6.6 displays the time series for zonal bands centered on latitudes from 82.174N to 19.566N. In northern high latitudes, the precipitation, like the temperature in that region appears to decline in the initial 10 year spin-up period. The difference is about 0.1 to 0.2 mm day^{-1}. In northern mid-latitudes, the time series appears to become slightly noisier, but again the difference between the initial precipitation and that later in the series is still about 0.2 mm day^{-1}. In the zonal band centered on 19.566N, the time series is considerably noisier than those further north, and the mean appears to drop by 0.6mm day^{-1} after the spin-up time.

Figure 6.6 displays the time series for zonal bands centered on latitudes from 11.740N to –50.870N. Overall the time-series displays the same features as those in Figure 6.6. However, there is an interesting phenomenon in the bands centred on ± 3.914N. The interannual variability apparent in the time series is much more than at any other latitude. The range of mean annual precipitation varies by up to 2.5mm day^{-1} between consecutive days. Furthermore there is remarkable symmetry between the two time series. This suggests that atmospheric dynamics about the equator may be the cause. While the mean annual precipitation estimated using NCAR LSM at 3.914N is close to both the

observations and more importantly the MIT 2D-LO value, the estimate at –3.914N is considerably lower than both. It is interesting to note that in addition to the temperature, the time series of latent and sensible heat, and CO_2 flux demonstrate the same increased interannual variability at the –3.914N latitude. However no other time series exhibits the symmetry visible in the precipitation model.

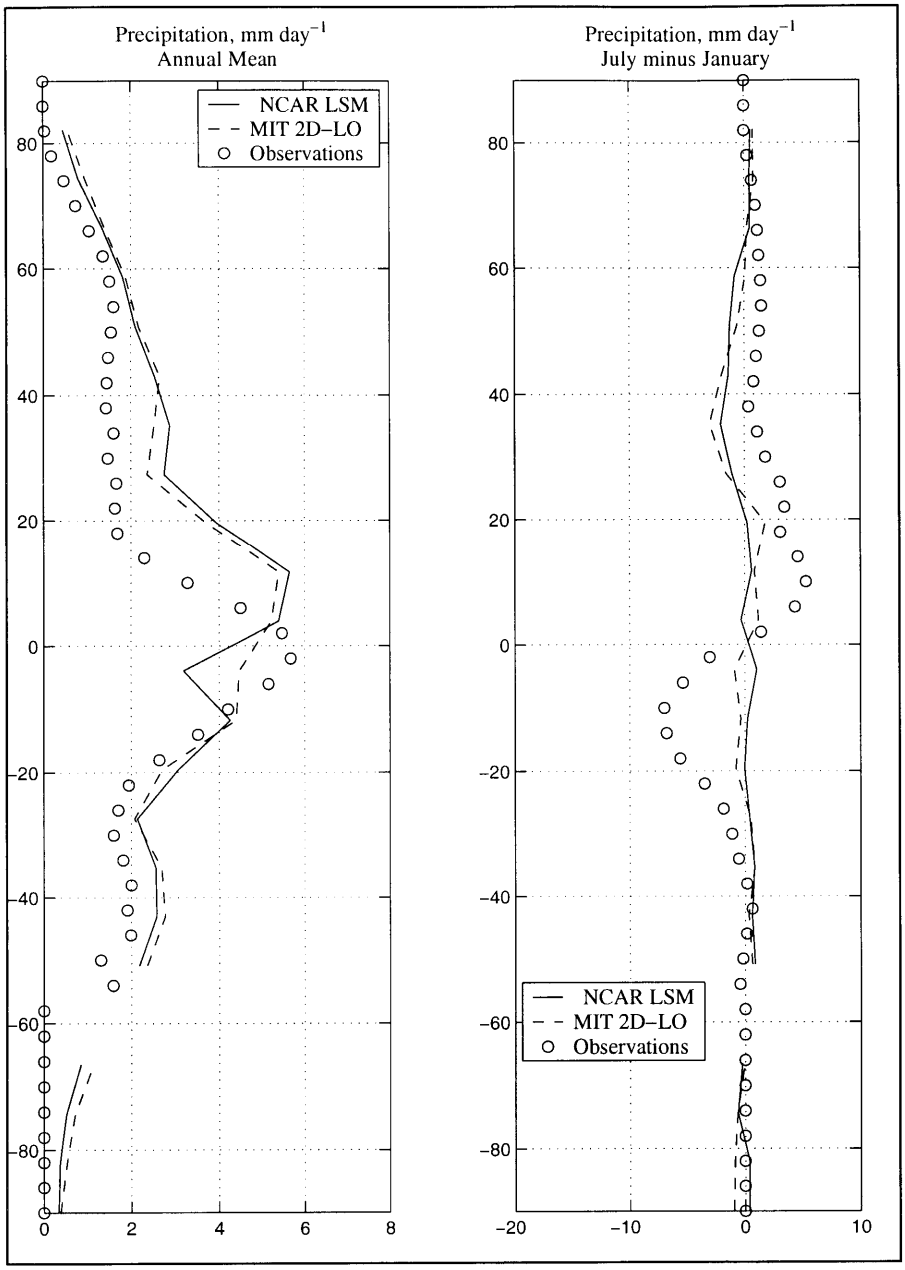

Figure 6.5 **Precipitation in mm day^{-1} as a function of latitude, derived from a 50-year simulation replacing the land component of MIT 2D-LO with the NCAR Land Surface Model.**
The annual mean is plotted on the right, and seasonality (July-January) on the right. Results are compared to those from the MIT-2D-LO and observations from Leemans and Cramer (1991).

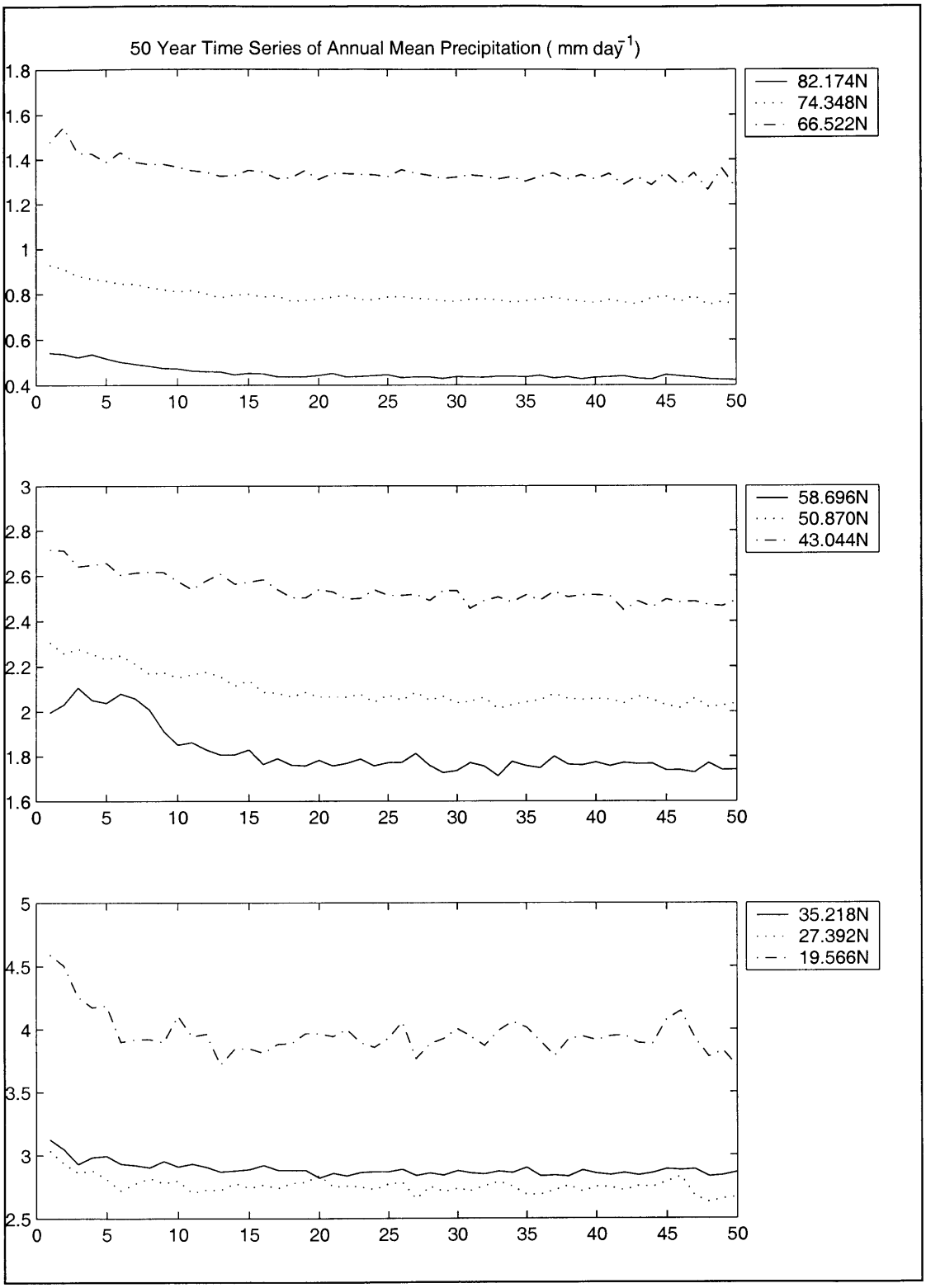

Figure 6.6 **50-year time series of annual mean precipitation in degrees mm day^{-1}, modeled using the NCAR Land Surface model over the land portion in MIT 2D-LO.**
Results for zonal bands centered on latitudes 82.174N to 19.566N.

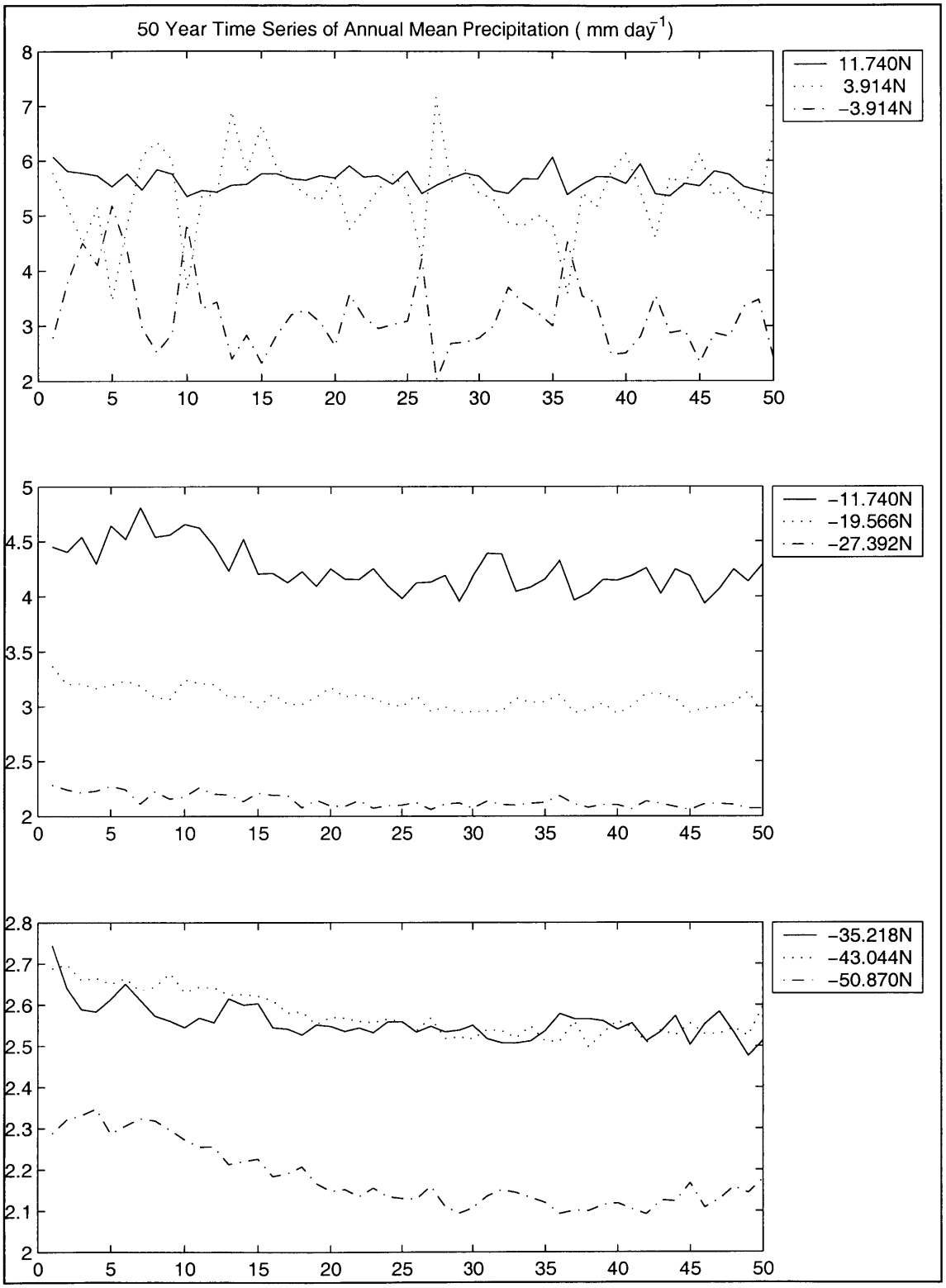

Figure 6.7 **50-year time series of annual mean precipitation in degrees mm day^{-1}, modeled using the NCAR Land Surface model over the land portion in MIT 2D-LO.**
Results for zonal bands centered on latitudes 11.740N to –50.870N.

6.5 Surface Fluxes

It is when we consider the partitioning of energy at the surface between latent and sensible heat fluxes that the performance of the NCAR Land Surface model is better than that of the MIT 2D-LO model. Results from a fifty year simulation using NCAR LSM were compared to similar output from the MIT 2D-LO model as well as observations from Oberhuber (1988). These observations are based on an atlas derived from the COADS (Comprehensive Ocean-Atmosphere Data Set), which as the name suggests was primarily developed to study the ocean, and not the land surface. However, by applying a simple mask the land points can be isolated from the dataset to obtain the fluxes over the land surface. This data is currently used to validate the surface fluxes over the land component estimated by the MIT 2D-LO (Sokolov, personal communication).

6.5.1 Latent Heat Flux

Referring to Figure 6.8 which shows the annual mean latent heat flux on the left-hand side, and the seasonality in latent heat flux on the right-hand side, we see each model has certain areas where it performs better.

In terms of magnitude, both do a reasonable job of capturing the annual mean. The NCAR LSM appears close to the annual mean in the tropics, while the MIT 2D-LO does a better job at higher latitudes. There are bimodal peaks visible in the observations at $\pm$ 30^{o}N. Neither model emulates this feature, with both peaking nearer to the equator.

The seasonal difference in latent heat is not well captured by either model. Observations indicate that latent heat flux in January exceeds that in July by up to 100 W m^{-2} in the northern hemisphere

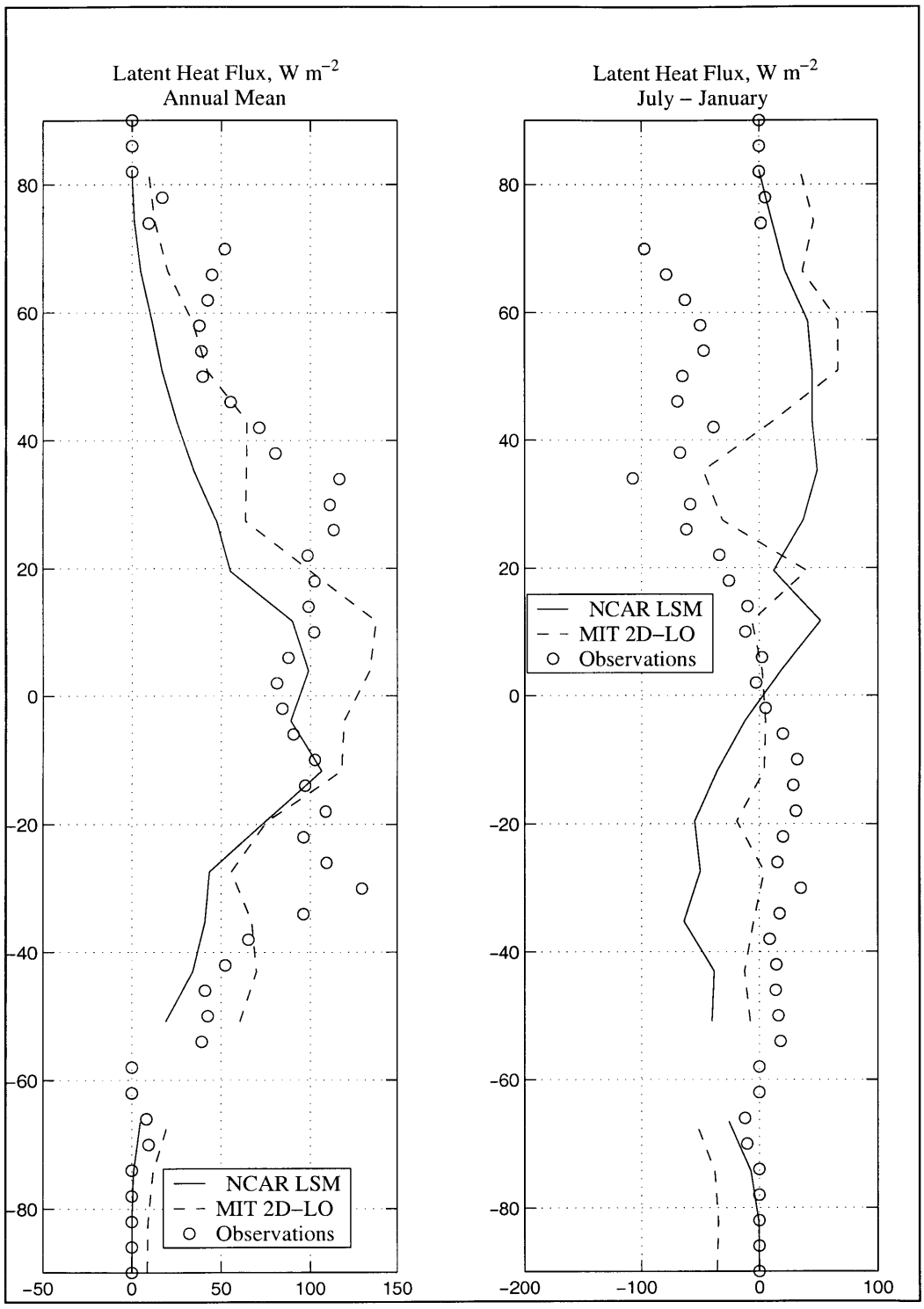

Figure 6.8 **Latent Heat Flux in W m^{-2} as a function of latitude, derived from a 50-year simulation replacing the land component of MIT 2D-LO with the NCAR Land Surface Model. The annual mean is plotted on the right, and seasonality (July-January) on the right. Results are compared to those from the MIT-2D-LO and observations from Oberhuber (1988).**

Figures 6.9 and 6.10 display the time series of annual mean latent heat flux, in W m^{-2} , for zonal bands centered on latitudes from 82.174N to 19.566N and 11.740N to –50.870N respectively.

In Figure 6.9, we see the influence of the spin-up time on mean annual latent heat flux in the northern hemisphere. The annual mean decreases dramatically in the first five years, and appears to level off following about 10 years of spin-up time. The difference between the initial value and this reduced value varies between about 2 W m^{-2} for the zonal band centered at 43.044N to 12 W m^{-2} for the band centered at 19.566N.

In Figure 6.10, we have the same time series between 11.740N and –50.870N. The particularly large interannual variability we witnessed near the equator in the time series of precipitation and temperature, appears to have manifested itself in the time series of latent heat flux too. The time series at –3.914N is particulary interesting. The variability between consecutive years is as high as 25 W m^2. One could argue that visually there appears to be more symmetry between the series at ± 3.914N in the first 15 years of the time series than in the latter part. The minimum in year 5 at +3.914N is followed by a maximum in year six at –3.914N, the minimum in year 7 at –3.914N is followed by a maximum at +3.914N. Between years 10 and 15, minima and maxima in the time series at –3.914N correspond to maxima and minima in the same year at 3.914N. This symmetry appears to diminish as interannual variability in the time series at +3.914N decreases over time.

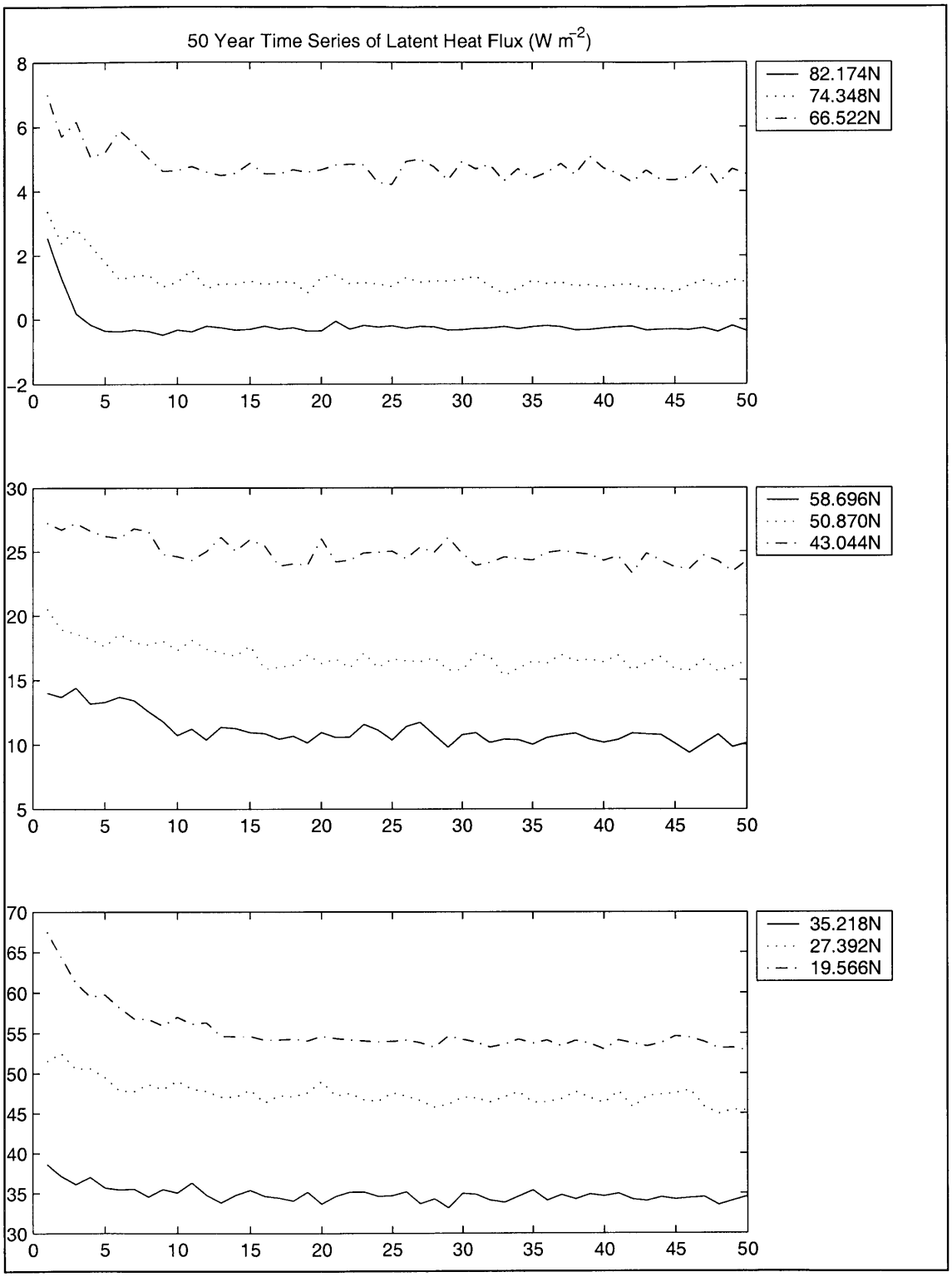

Figure 6.9 **50-year time series of annual mean latent heat flux in W m^{-2}, modeled using the NCAR Land Surface model over the land portion in MIT 2D-LO.**
Results for zonal bands centered on latitudes 82.174N to 19.566N.

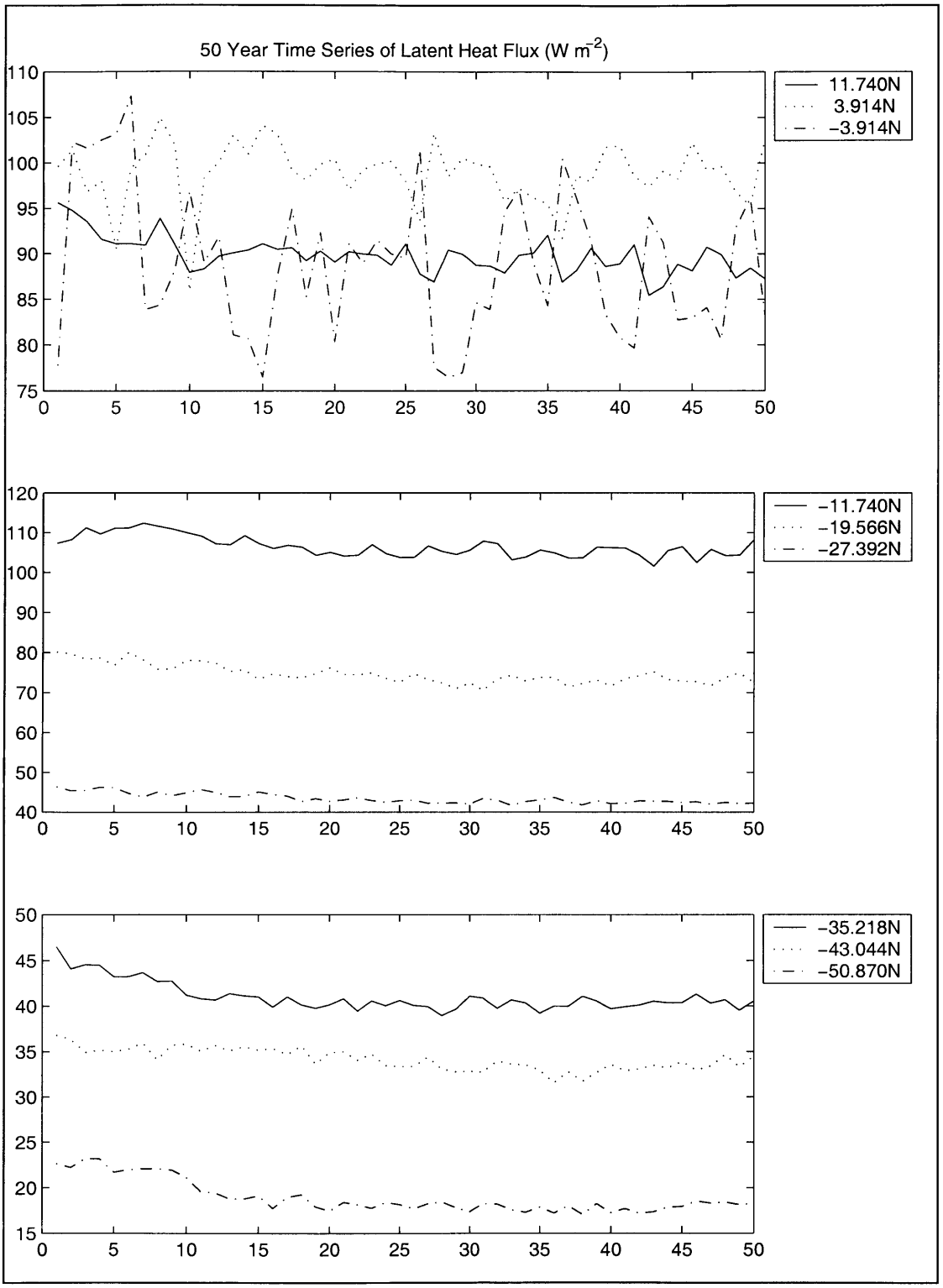

Figure 6.10 **50-year time series of annual mean latent heat flux in W m^{-2}, modeled using the NCAR Land Surface model over the land portion in MIT 2D-LO.**
Results for zonal bands centered on latitudes 11.740N to –50.870N.

6.5.2 Sensible Heat Flux

Figure 6.11 shows the annual mean sensible heat flux on the left-hand side, and the seasonality in sensible heat flux on the right-hand side. It is clear that the estimates of sensible heat flux from the NCAR LSM are a considerable improvement on those from the MIT 2D-LO.

The MIT 2D-LO hugely overestimates the annual mean flux, with a maximum value of 70 W m^{-2} at about –25°N. The peak in observations (Oberhuber, 1988) at this latitude is close to 12 W m^{-2}. The results from the MIT 2D-LO model rise steadily from 60°N to 30°N, where it dips in the tropics and rises again at –25°N. From here, the annual mean decreases steadily approaching the south pole. The observations demonstrate a quite different trend. Mean annual sensible heat flux is typically less than 10 W m^{-2}, with small peaks at +32°N, -30°N and –70°N. The maximum occurs at 70°N, where annual mean sensible heat flux is 40 W m^{-2}. The estimates from the NCAR LSM are considerably closer to the observations than those from MIT 2D-LO. Peaks are apparent at +32°N, and -30°N, although the global maximum at 70°N is not captured. The magnitude of the annual mean is at least on the same order as the observations, typically less than 20 W m^{-2}. North of 70°N, both models underestimate the annual mean, with the MIT-2D LO performing marginally better.

Just like the case of latent heat flux, the seasonal difference in sensible heat is not well captured by either model. Observations indicate that sensible heat flux in January exceeds that in July by up to 100 W m^{-2} in the northern hemisphere. Neither model captures this

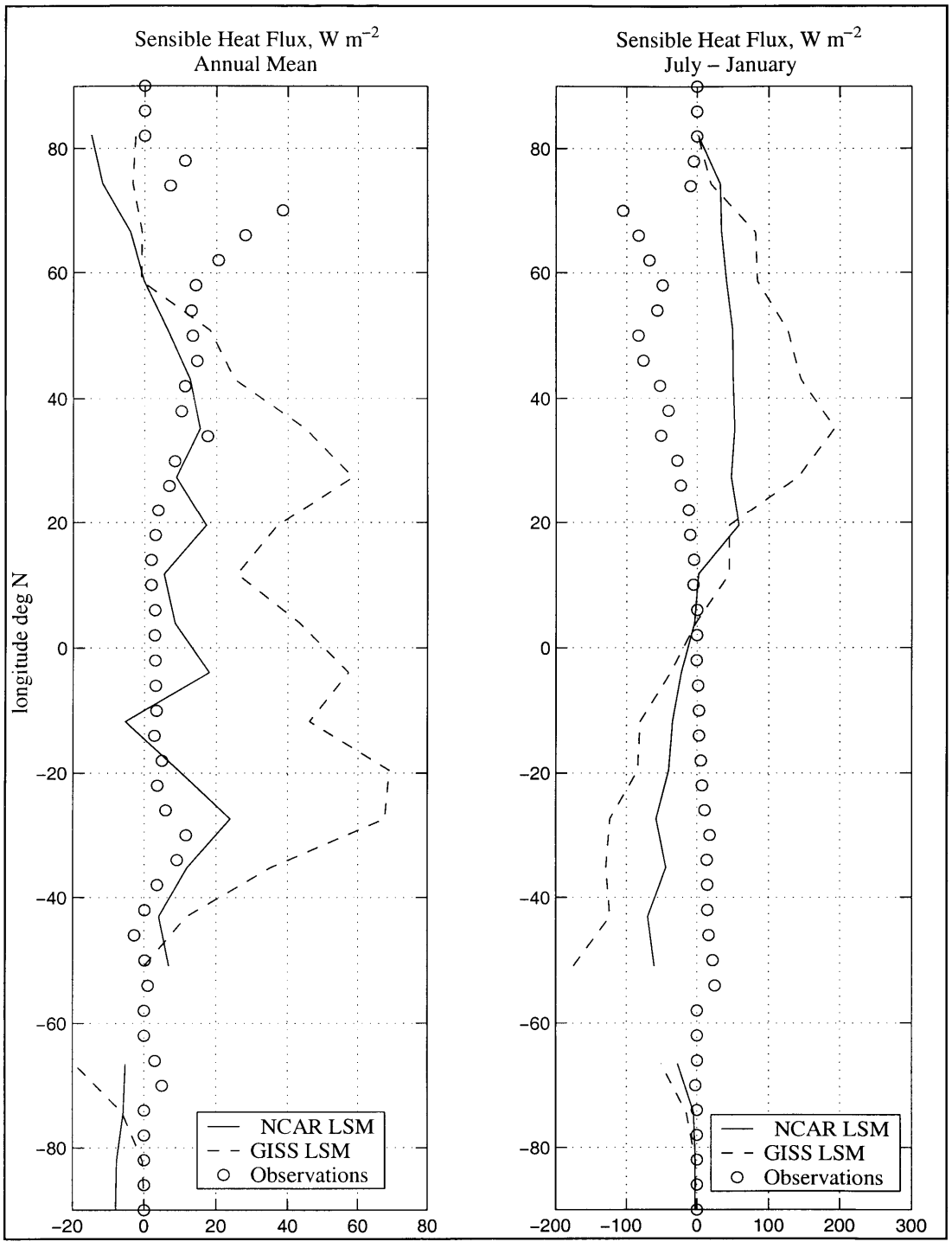

Figure 6.11 **Sensible Heat Flux in W m^{-2} as a function of latitude, derived from a 50-year simulation replacing the land component of MIT 2D-LO with the NCAR Land Surface Model. The annual mean is plotted on the right, and seasonality (July-January) on the right. Results are compared to those from the MIT-2D-LO and observations from Oberhuber (1988).**

trend correctly. In contrast to the latent heat flux case, both models have the incorrect sign at all latitudes. The results from NCAR LSM may be considered an improvement on those from MIT 2D-LO as the magnitude is halved at all latitudes, so it is closer to observations, although still clearly far from correct.

The magnitude of the sensible heat flux estimated from the GISS model is far too high. The annual mean given by the NCAR model may not capture the small occasional peaks of the data, but the values are at least of the same order. In the seasonality plot, we see that both models estimate a more discernable cycle than the observations. However, the magnitude of the flux using the NCAR model is closest to that observed.

Figures 6.12 and 6.13 display the time series of annual mean sensible heat flux, in W m^{-2}, for zonal bands centered on latitudes from 82.174N to 19.566N and 11.740N to – 50.870N respectively.

In Figure 6.12, we see the influence of the spin-up time on mean annual sensible heat flux in the northern hemisphere. Like the case for latent heat flux, the annual mean changes dramatically in the first five years, and appears to level off following about 10 years of spin-up time. The difference between the initial value and later value varies between about 1-2 W m^{-2} for the zonal band centered at 43.044N to 10 W m^{-2} for the band centered at 82.174N. Following spin-up, annual mean sensible heat actually increases in the latitudinal bands between 43.044N and 19.566N.

In Figure 6.13, we have the same time series between 11.740N and –50.870N. With the exception of the band centered at –3.914N, annual mean sensible heat flux tends to increase following the spin-up period. Again, the difference is typically on the order of a few W m^{-2}.

Again, the time series at –3.914N is particularly interesting. The variability between consecutive years is as high as 15 W m^2. By virtue of the relationship between latent and sensible heat, it is no surprise that in this sensitive latitude band, the time series of sensible heat looks remarkable like the image of the time series of latent heat flux. The magnitude of interannual variability may differ, but the pattern is almost identical.

Again, one could argue that visually there appears to be more symmetry between the sensible heat time series at ± 3.914N in the first 15 years of the time series than in the latter part. The maximum in year 5 at +3.914N is followed by a minimum in year six at –3.914N, the maximum in year 7 at –3.914N is followed by a minimum at +3.914N. Between years 10 and 15, minima and maxima in the time series at –3.914N correspond to maxima and minima in the same year at 3.914N. This symmetry appears to diminish as interannual variability in the time series at +3.914N decreases over time.

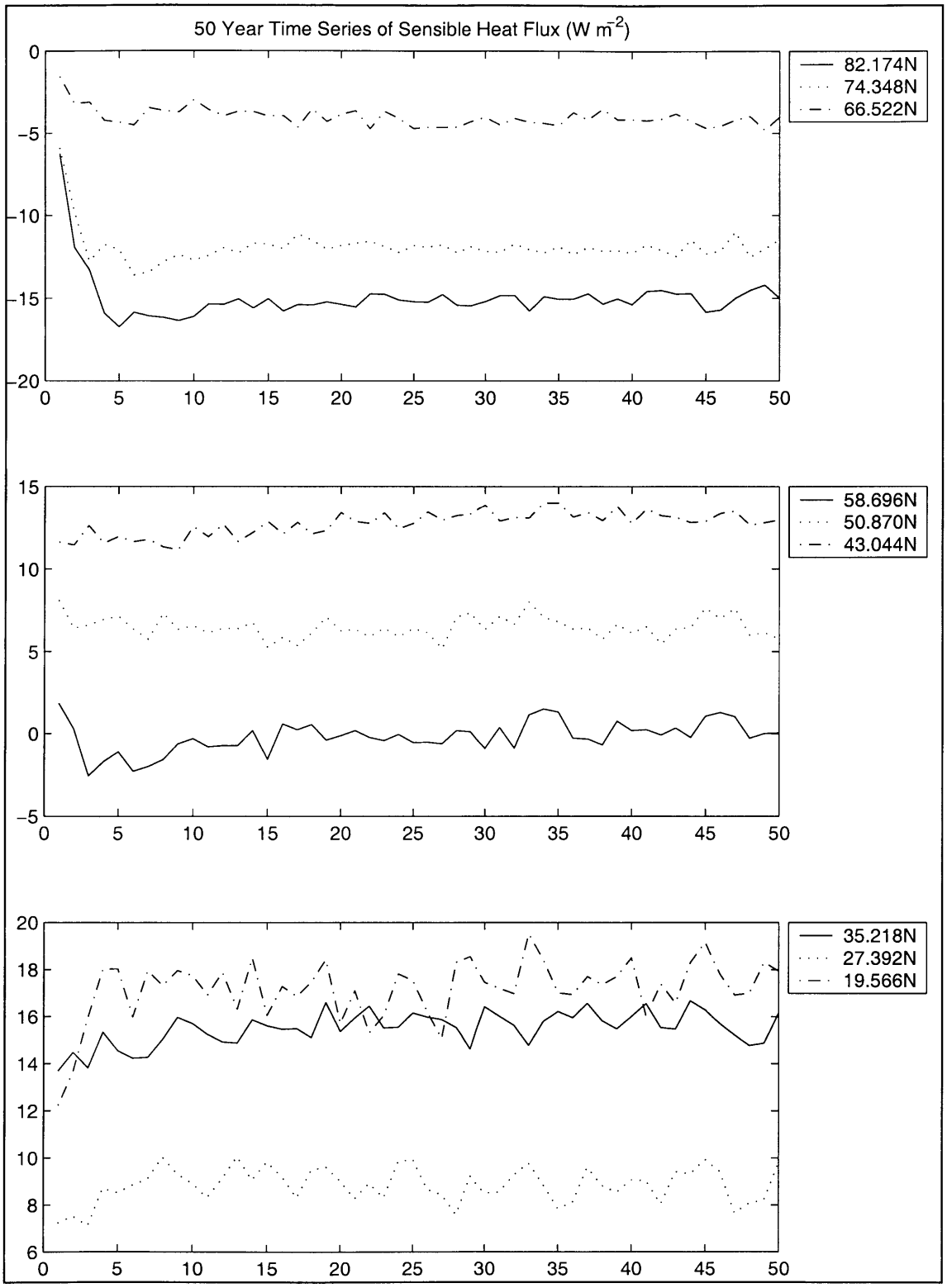

Figure 6.12 **50-year time series of annual mean sensible heat flux in W m^{-2}, modeled using the NCAR Land Surface model over the land portion in MIT 2D-LO.**
Results for zonal bands centered on latitudes 82.174N to 19.566N.

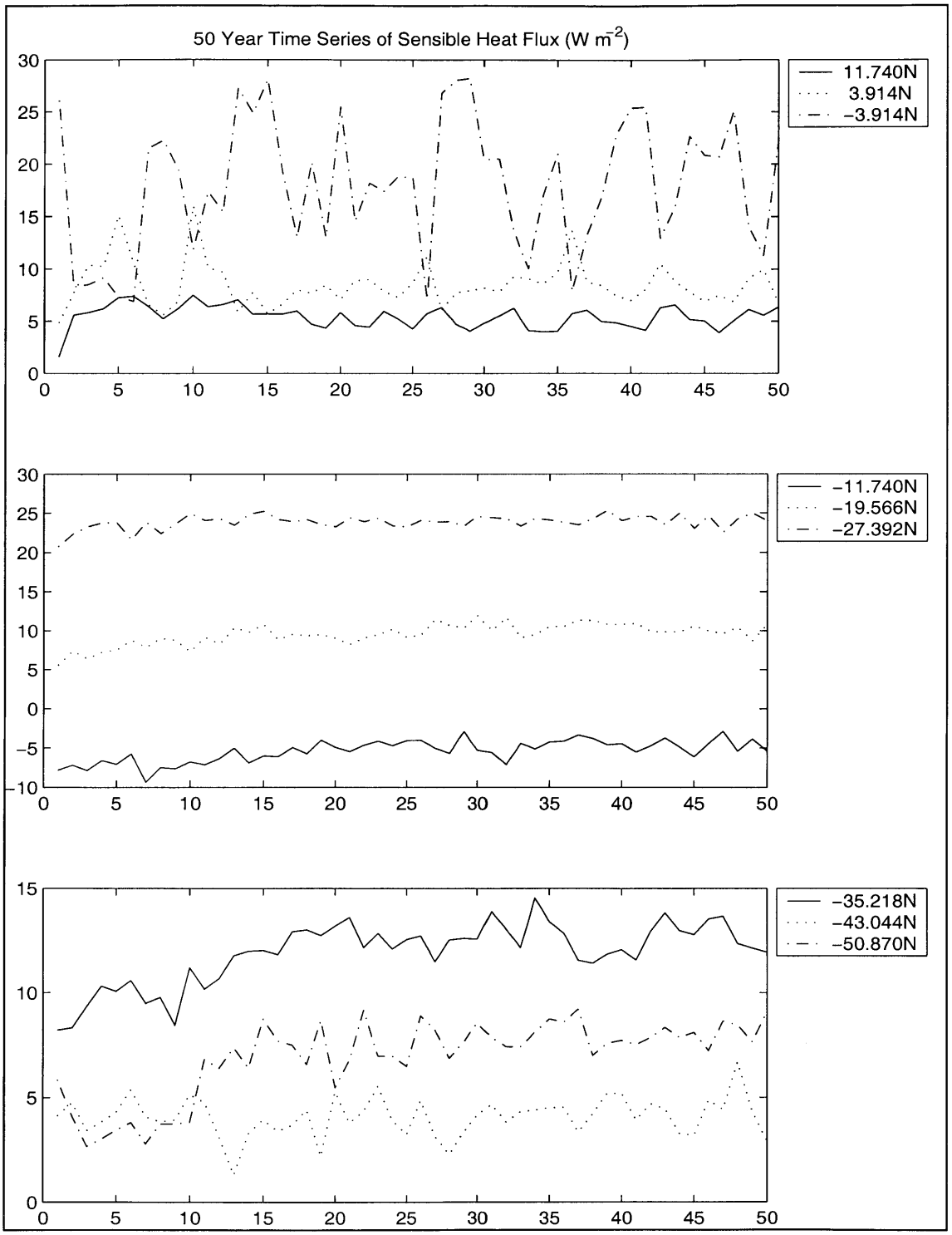

Figure 6.13 **50-year time series of annual mean sensible heat flux in W m^{-2}, modeled using the NCAR Land Surface model over the land portion in MIT 2D-LO.**
Results for zonal bands centered on latitudes 11.740N to –50.870N.

6.6 Carbon dioxide

The objective of this project was to introduce the NCAR LSM into the MIT IGSM, with a view to tightening the coupling between the climate component and the terrestrial ecology model. The primary benefit of using the NCAR LSM is that in additional to producing the usual fluxes, i.e sensible and latent heat, it also produces the carbon dioxide flux to the atmosphere at each timestep. So, the interaction between the hydrologic cycle and the carbon cycle is theoretically captured at each time step. Figure 6.14 illustrates the net carbon dioxide flux in g m^{-2} in each latitudinal band as it varies during the year. Figure 6.15 illustrates the annual mean carbon dioxide flux to the atmosphere from the land surface, and the seasonality in the flux. Figures 6.16 and 6.17 show the 50 year time series of net CO_2 flux from the land surface at different latitudes. Here we shall use the term "source" to indicate that CO_2 loss during plant and microbial respiration exceeded CO_2 uptake during photosynthesis, and "sink" to indicate the contrary. Typically there are a multitude of other factors at play in creating a sink or source, but they are beyond the scope of this model.

In Figure 6.14, the net CO_2 flux is exhibiting the seasonal pattern we intuitively expect. During summer, net CO_2 is negative indicating uptake by the vegetation while in winter net CO_2 is positive indicating that the land is a net source of CO_2. In the northern hemisphere, there is a sink between May and August, and a source between September and April. In the southern hemisphere the land acts as a sink between October and March, with a source between April and September. The largest sink occurs in December and

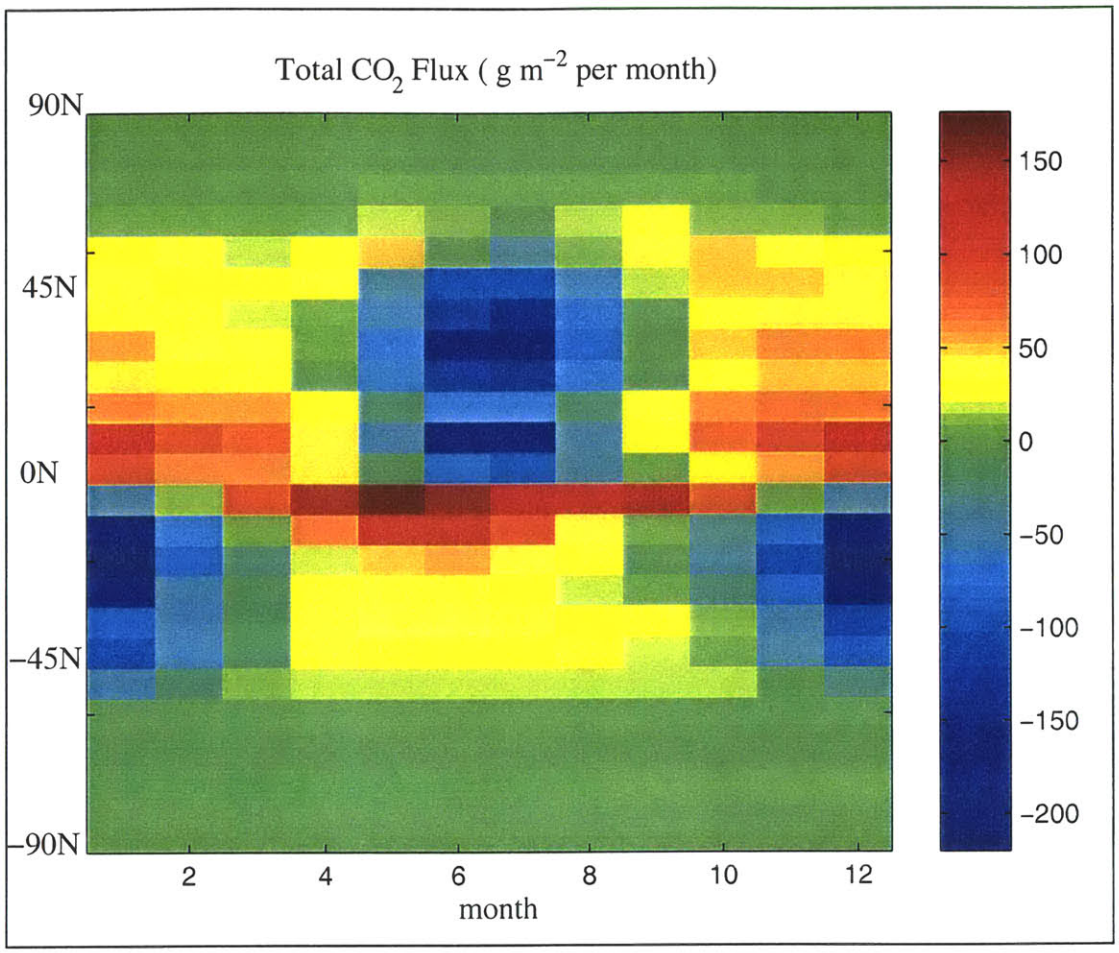

Figure 6.14 Net CO_2 flux to the atmosphere in g m^{-2}, as a funcion of latitude on the y-axis and month of year on the x-axis.

January in the southern hemisphere, and the largest source occurs in May just south of the equator. Recall from Figure 6.8 that in both hemispheres we witnessed an excess of latent heat flux in the summer months over the winter months in the NCAR LSM results. When the stomates of the plant leaves open to assimilate carbon dioxide, water evaporates from the leaf. So we expect CO_2 assimilation to be correlated with periods of greater latent heat flux.

There is a particularly striking contrast in total net CO_2 flux directly above and below the equator. In May, net flux in the band centered at +3.914N is near zero, while that in the

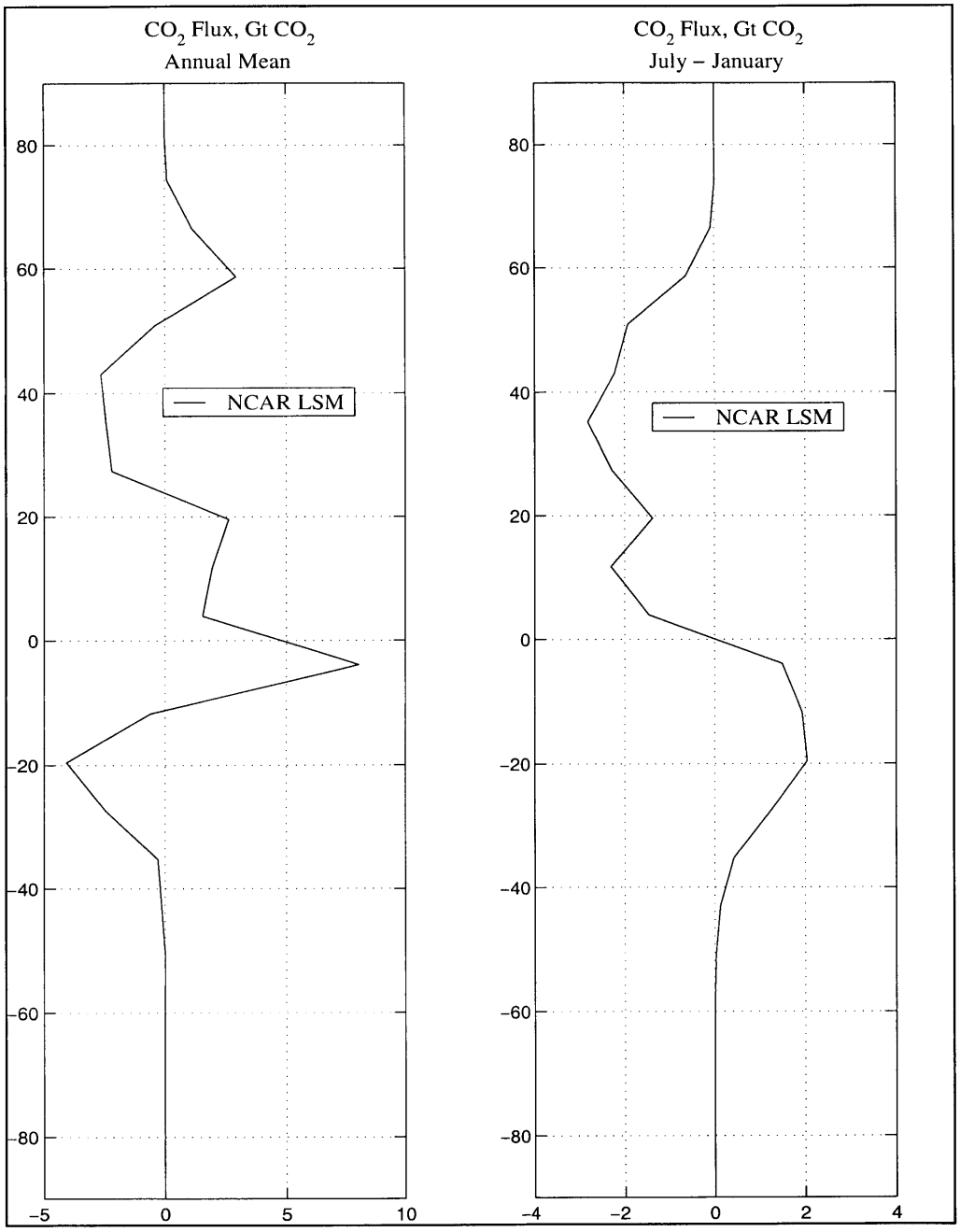

Figure 6.15 **Net CO_2 flux in Gt CO_2 as a function of latitude, derived from a 50-year simulation replacing the land component of MIT 2D-LO with the NCAR Land Surface Model.**
The annual mean is plotted on the right, and seasonality (July-January) on the right.

band centered on –3.914N exceeds 150 g m^{-2}. In June, the northern grid cell acts as a sink of –50 to –100 g m^{-1} of CO_2, while the southern cell is a source of almost 150 g m^{-2}. The same feature occurs in July to a lesser extent.

Figure 6.15 illustrates the annual mean carbon dioxide flux to the atmosphere from the land surface, and the seasonality in the flux. If we study first the annual mean CO_2 flux, it is apparent from the results of NCAR LSM that there are two areas where the land surface acts as a source and two areas where it acts as a sink. The sources are between 75°N and 50°N, and 25°N to –12°N. The sinks are between 50°N and 25°N, and –12°N and –50°N. When summed over all land points, the land surface acts, on average, as a source of 3.2856Gt of CO_2 (≡ 0.89Gt C) per year.

Bonan (1998) ran the NCAR LSM coupled to three different versions of the NCAR CCM3 and obtained vastly different results. Using one atmospheric model, the land surface appeared as a small (0.004Gt CO_2) source, and using two more advanced versions of the CCM the surface appeared to be a sink of 0.015-0.029Gt CO_2. The disparity in these results is attributed to the extreme sensitivity of land-atmosphere CO_2 exchange to the simulated climate. Furthermore it is suggested that as the vegetation types are time-invariant as well as the leaf, stem and root carbon pools, situations may arise where the simulated fluxes are inconsistent with the prescribed vegetation.

The seasonality in net CO_2 flux is also illustrated in Figure 6.15 as the difference between the net flux in July and that in January. In the northern hemisphere the magnitude of the

sink in July is greater than the magnitude of the source in the January. In the southern hemisphere the magnitude of the sink in January exceeds that of the source in July.

At present the terrestrial biosphere is a net sink of approximately 1.4Gt C per year due to land management practices, higher carbon dioxide and nitrogen deposition and potentially recent changes in climate. Although, historically the terrestrial biosphere has been a source of carbon to the atmosphere. From 1850 to 1998, 230 (+60) Gt C is estimated to have been taken up in approximately equal amounts by the oceans and the terrestrial ecosystem. On average, this amounts to the terrestrial ecosystem acting as a source of 1.55Gt C per year. Recall that we estimated net CO_2 flux, as defined by NCAR LSM, as a source of 0.89Gt C per year. This is simply the difference between uptake from photosynthesis and losses through plant and microbial respiration.

While net global terrestrial carbon flux and oceanic uptake of carbon can be quantified independently using molecular oxygen measurements, isolating the net CO_2 flux as we have defined it is not simple. Net terrestrial uptake of carbon is influenced by direct effects of land use and land-use change, such as deforestation, agricultural abandonment and regrowth. It is also subject to the response of terrestrial ecosystems to CO_2 fertilization, nutrient deposition, climatic variation and disturbance such as fires, wind-throws and major droughts. Validating the net CO_2 flux estimated using NCAR LSM against net global terrestrial carbon flux data would only be meaningful if the other processes were accounted for. This would be possible for example, if the NCAR LSM was used with the proposed dynamic Terrestrial Ecology Model (Prinn, NSF 00-22).

Our estimated mean annual net CO_2 flux is at least comparable to the historic value, and its spatial and seasonal variation consistent with what we intuitively expect.

Figures 6.16 and 6.17 display the time series of annual mean net CO_2 flux , for zonal bands centered on latitudes from 82.174N to 19.566N and 11.740N to –50.870N respectively. We see the same trends in the time series as we saw for other estimated quantities.

In the northern latitudes (Figure 6.16), net CO_2 flux rises from the initial value for the spin-up period of approximately 10 years. The difference between the initial value and that attained after spin-up varies between 5 g m^{-2} for the band centered at 82.174N and 250 g m^{-2} for the band centered at 19.566N.

In Figure 6.17, it appears that the CO_2 value takes longer to stabilize than the other quantities we have seen. In the bands centered on –11.740N and –35.218N the net CO_2 flux only appears to level off after 30 years. This is excessive in a 50 year simulation. As before, interannual variability is greatest in the latitude band centered on –3.914N, where it is as high as 1000g m^{-2} between consecutive years.

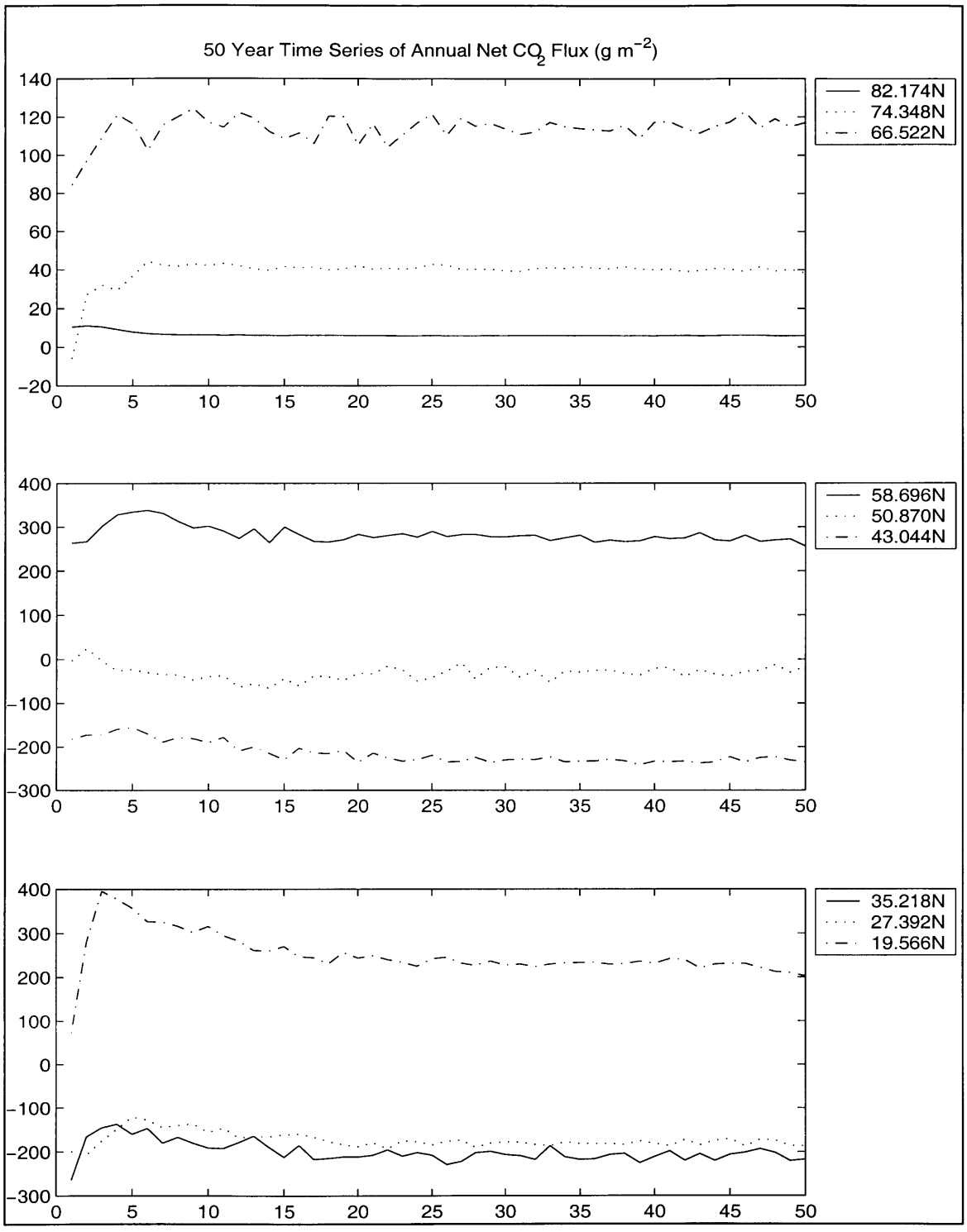

Figure 6.16 **50-year time series of annual mean CO_2 flux in g m^{-2}, modeled using the NCAR Land Surface model over the land portion in MIT 2D-LO. Results for zonal bands centered on latitudes 82.174N to 19.566N.**

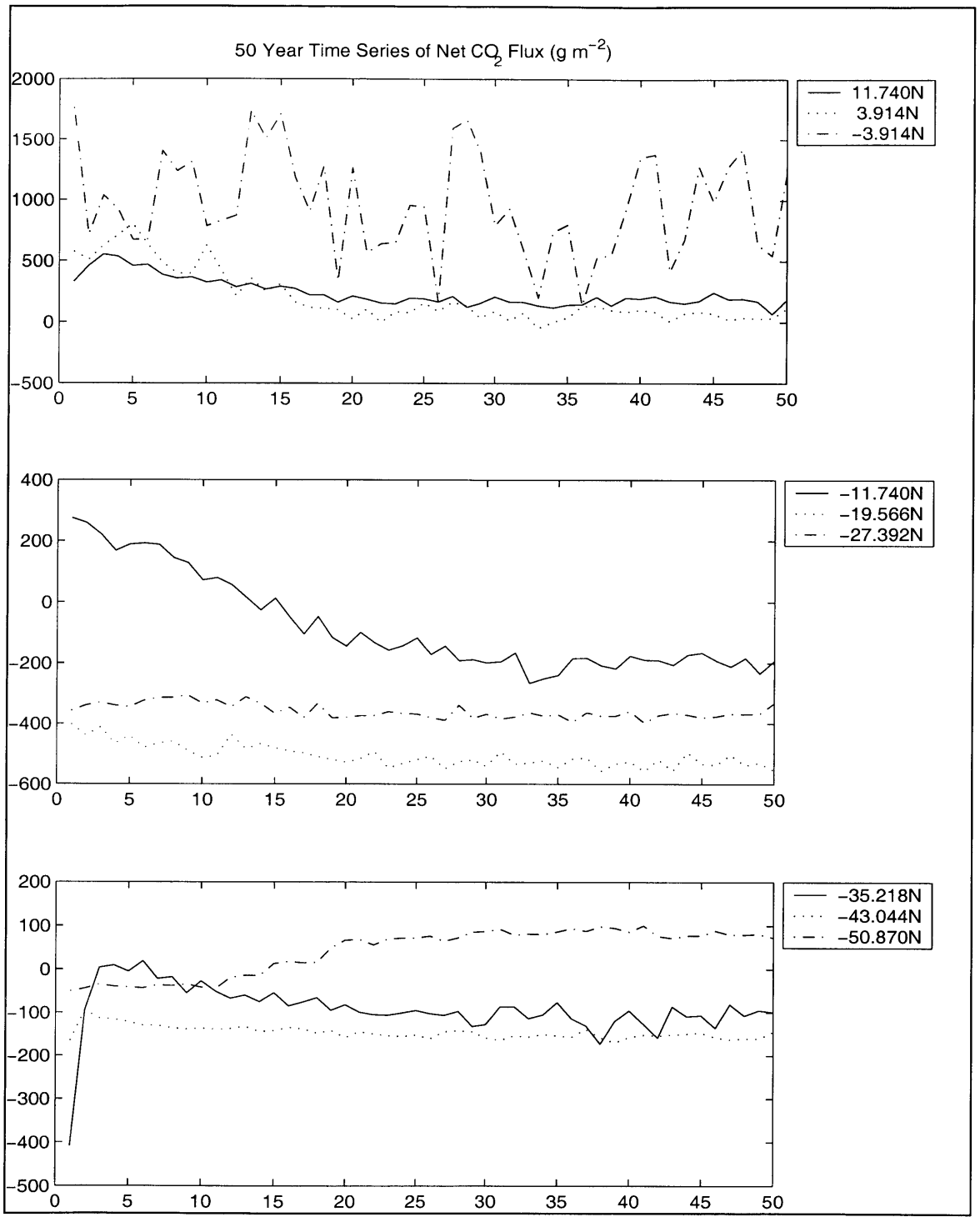

Figure 6.17 **50-year time series of annual mean CO_2 flux in g m^{-2}, modeled using the NCAR Land Surface model over the land portion in MIT 2D-LO. Results for zonal bands centered on latitudes 11.740N to –50.870N.**

Chapter 7

Conclusions

7.1 Successful coupling of NCAR LSM and GISS code

The primary conclusion is that the NCAR LSM could be coupled within the MIT climate-chemistry model framework. A feasibility study (deSilva, 1998) using data from the FIFE experiment had earlier demonstrated the capability of the NCAR LSM to improve latent and sensible heat flux estimates over a test site 15km by 15km. This study used the NCAR LSM in off-line mode, reading in atmospheric forcing data from a file and outputting the fluxes in the standard NCAR output files. As the experiment was on a small scale, the site could be described in terms of the NCAR suface type and soil color, so no changes were required to the model inputs, outputs or architecture. The objective of this research was to determine if the NCAR LSM could be successfully introduced into the MIT IGSM. It was found that by running the NCAR LSM as an offline subroutine, and making the changes to model input and architecture discussed in Chapter 4, it could be used successfully to model the land and land-ice components within the MIT coupled climate-chemistry model.

The results of a fifty-year simulation, presented in Chapter 6, indicate that a satisfactory climatology could be obtained by using the NCAR LSM instead of the GISS routine over the land and land ice components. Furthermore, the estimates of surface fluxes obtained using NCAR LSM improved on those obtained from GISS. Moreover, the NCAR LSM also estimates the flux of carbon dioxide from the land surface to the atmosphere, such

that it is consistent with the energy balance and the level of evapotranspiration. At the very least, this estimate can be used to assess the performance of the Terrestrial Ecology Model.

7.2 Potential expansion of the scope of the climate model

Through attempting to couple the NCAR LSM to the GISS model, several features of the NCAR LSM were noteworthy regarding its potential future application within the MIT IGSM. In particular, the NCAR LSM code is very modular and clean, thereby facilitating adaptation. This leads to the possibility of expanding the role of the climate model to include estimation of biogeochemical fluxes in addition to standard climatological outputs.

Each component of the land surface model, consists of one central calling routine and a number of subroutines. For example, consider the calling sequence of **surphy.F**, the surface biophysics routine, which calculates energy fluxes and temperatures. Its calling sequence is shown below in Figure 7.1.

In addition, the naming of variables and subroutines is quite transparent, with descriptions of each variable given in each subroutine, making it easy to trace the algorithm development. This may prove quite useful if the LSM is included within the MIT IGSM. Processes which are omitted or poorly represented for our problem can be easily isolated and corrected.

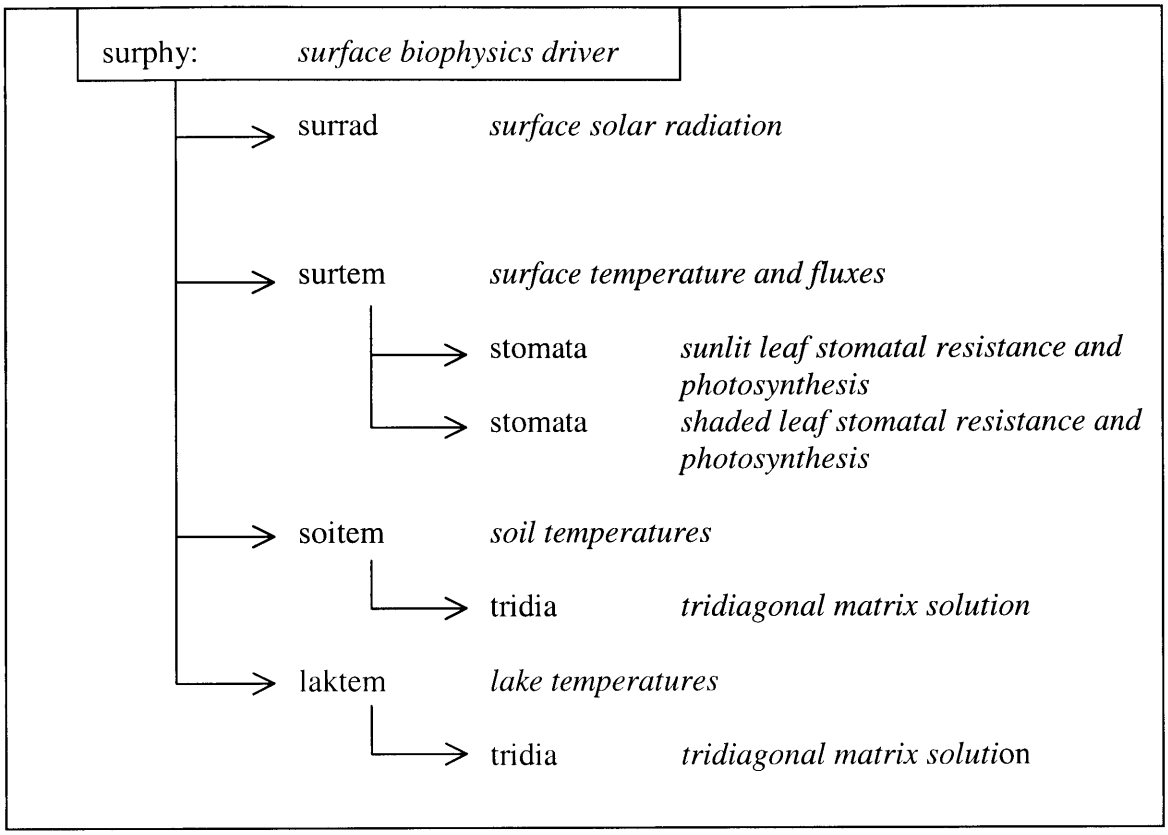

Figure 7.1 Calling sequence of surphy.F

7.3 Computational Efficiency

A feasibility study by deSilva (1998) found that the NCAR LSM took twice as much CPU time as the hydrological modules of the MIT-2D-LO and the TEM. This was based on using the NCAR LSM in off-line mode, forcing it with data from a file, and outputting the results to history files. In this mode, the NCAR LSM required twice as many inputs and wrote out five times as many outputs as the other models. Furthermore, the writing of history files at each time step involves a huge demand on CPU time in terms of I/O. By coupling the NCAR LSM within the MIT IGSM to perform the hydrology calculations over land, we avoid inputting and outputting huge amounts of data, by simply

transferring it in common blocks between the NCAR LSM and the atmospheric component of the climate model. This dramatically reduces the I/O, thereby cutting the CPU time substantially. Furthermore by using NCAR LSM, we can potentially eliminate the need for asynchronous TEM integrations which would lead to huge CPU savings.

Highly efficient coding of NCAR LSM results in little discernable increase in CPU requirements for hydrological parameterization calculations. By calling the NCAR LSM as a subroutine to model the land and land ice components instead of using the existing GISS code, improved flux estimates and additional detail could be obtained without increasing the demand on CPU. Further improvements could be made in terms of efficiency if the model were to be used in a full MIT IGSM simulation. This involves simply optimizing the number of points to process in each call to **lsm** so that it is large enough to take advantage of vectorization, yet small enough to have a sufficient number of processes to multi-task. This is achieved by altering just one variable in the pre-processor file, **preproc.h**.

7.4 Further Research

Having shown that the NCAR LSM may be successfully incorporated into the MIT climate model, many topics for further research arise.

The method of estimating CO_2 flux is very sensitive to the choice of overlying atmospheric model (Bonan, 1998). Perhaps an alternative CO_2 scheme could prove

robust. As the code is quite modular and transparent, it would be easy to replace the current algorithm with alternatives to assess their performance.

At present, the land cover type assignment is time-invariant. It would be interesting to allow these to vary with time to reflect natural and anthropogenic land-use change. In particular, it could allow the net terrestrial CO_2 flux to include the effects of land-use change. As the hydrologic cycle and carbon cycle are more closely coupled in NCAR LSM than in the current MIT IGSM, this might be a particularly useful tool in assessing the influence of land-use change on the global water cycle and vice versa.

Leaf, stem and root carbon pools are time invariant in the current version of the NCAR LSM. This may result in simulated fluxes that are inconsistent with the land cover type (Bonan, 1998). It would be interesting to allow them to vary with time.

Essentially, further research should be directed towards incorporating the features of the TEM into the NCAR LSM, such as more complete modeling of the carbon and nitrogen cycles. This would enable us to study the interactions between fully coupled water, carbon and nitrogen cycles. It would also allow these coupled fluxes to influence the distribution of vegetation cover and vice versa.

Bibliography

Akima, H., 1978. A method of bivariate interpolation and smooth surface fitting for irregularly distributed data points, ACM Transactions on Mathematical Software 4:148-159.

Betts, A. K. and J.H. Ball, 1998. FIFE Surface Climate and Site-Averaged Dataset 1987-89. Journal of Atmospheric Sciences, 55(7):1091-1108.

Bonan, G.B., 1996. A Land Surface Model (LSM Version 1.0) for Ecological Hydrological, and Atmospheric Studies: Technical Description and User's Guide. Climate and Global Dynamics Division, National Center for Atmospheric Research, Boulder, Colorado. NCAR Technical Note NCAR/TN-417+STR.

Bonan, G.B., 1996a. Sensitivity of a GCM simulation to subgrid infiltration and surface runoff. Climate Dynamics, 12:279-285.

Bonan, G.B., 1997. The Land Surface Climatology of the NCAR Land Surface Model Coupled to the NCAR Community Climate Model. Journal of Climate, 11:1307-1326.

Choudhury, B.J., and J.L. Monteith, 19888. A four-layer model for the heat budget of homogeneous land surfaces. Quart. J. Roy. Meteor. Soc. 114:373-398.

Cogley, J.G., 1991. GGHYDRO – Global hydrographic Data Release 2.0. Trent Climate Note 91-1, Dept. Geography, Trent University, Peterborough, Ontario.

Collatz. G.J., Ribas-Carbo, M., and Berry, J. A. 1992. Coupled photosynthesis–stomatal conductance model for leaves of C_4 plants. Aust. J. Plant Physiol. 19:519-538.

Collatz, G.J., Ball, J.T., Grivet, C., and Berry, J.A., 1991. Physiological and environmental regulation of stomatal conductance, photosynthesis, and transpiration: a model that includes a laminar boundary layer. Agric. For. Meteorol. 54:107-136.

Deardorff, J., 1978.Efficient prediction of ground surface temperature and moisture, with inclusion of a layer of vegetation', J. Geophys. Res. 83 (C4), 1889-1903.

DeSilva, R., Intercomparison os Soil Hydrology Modules in the MIT Integrated Global Systems Model for Analysis of Climate Issues, Master's Thesis, Massachusetts Institute of Technology, May 1998.

Dickenson, R.E., Henderson-Sellers, A., and Kennedy, P.J., 1993. Biosphere-Atmosphere Transfer Scheme (BATS) version 1e as coupled to the NCAR Community Climate Model. NCAR Technical Note/TN-387+STR, National Center for Atmospheric Research, Boulder, CO.

Entekhabi, D., and Eagleson, P.S., 1989. Land surface hydrology parameterization for atmospheric general circulation models including subgrid scale spatial variability. Journal of Climate 2:816-831.

Green, P.J. and Sibson, R., 1978. Computing dirichlet tessellations in the plane, The Computer Journal 21:168-173.

Hansen, J., et al., 1983. Efficient three-dimensional global models for climate studies: Models I and II, Mon. Wea. Rev., 111:609-662.

Jacoby, H.D., and R.G.Prinn, 1994. Uncertainty in Climate Change Policy Analysis. MIT Joint Program on the Science and Policy of Global Change, Report No. 1, December 1994.

Jones, P.D., Wigley, T.M.L., and Wright, P.B., 1986. Global temperature variations between 1861 and 1984, Nature 322:430-434.

Kineman, J.J., M. Ohrenschall, J. Klaus, J. Ikelman (eds.), 2000. Global Ecosystems Database Version II Documentation, Metadata, and User's Guide. In: Global Ecosystems Database Version II: Database, User's Guide, and Dataset Documentation. US Department of Commerce, National Oceanic and Atmospheric Administration, National Geophysical Data Center, Boulder, Colorado. KGRD No. 35. HTML digital files on CDROM and the World Wide Web.

Leemans, R. and W.P. Cramer, 1991. The IIASA database for mean monthly values of temperature, precipitation and cloudiness of a global terrestrial grid. Research Report RR-91-18 November 1991, International Institute of Applied Systems Analyses, Laxenburg. 61pp.

Oberhuber, J.M., 1988. An Atlas based on the "COADS" dataset.
Max Planck Institute for Meteorology, Report 15, MPI.

Olson, J.S., Watts, J.A. and Allison, L.J., 1983. Carbon in live vegetation of major world ecosystems. ORNL-5862. Oak Ridge National Laboratory, Oak Ridge, TN.

Pielke, R.A., Climate Prediction as an Initial Value Problem, Bull. Amer. Meteor. Soc., Volume 79, 1998.

Prinn, R., H. Jacoby, A. Sokolov, C. Wang, X.Xiao, Z, Yang, R.Eckaus, P. Stone, D. Ellerman, J. Melillo, J. Fitzmaurice, D. Kicklighter, G. Holian, and Y. Liu, 1999. Integrated global system model for climate policy assessment: feedbacks and sensitivity studies, Climatic Change, 41(3/4): 469-546.

Ramankutty, N., and J. A. Foley, 1999, Estimating historical changes in global land cover: Croplands from 1700 to 1992, Global Biogeochemical Cycles, 13: 997-1027.

Sellers, P.J., 1985. Canopy reflectance, photosynthesis and transpiration. Int. J. Remote Sensing, 6:1335-1372.

Sokolov, Andrei P., and Peter H. Stone, 1995. Description and Validation of the MIT Version of the GISS 2D-Model. MIT Joint Program on the Science and Policy of Global Change, Report No. 2, June 1995.

Watson, Robert T., Ian A. Noble, Bert Bolin, N.H. Ravindranath, David J. Verardo and David J. Dokken (Eds.). Land-use, Land-use change and Forestry, 2000: Special Report of Intergovernmental Panel on Climate Change. Cambridge University Press, UK. pp 375.

Webb, R.S., Rosenzweig, C.E., and Levine, E.R. 1993. Specifying land surface characteristics in general circulation models: soil profile data set and derived water-holding capacities. Global Geochemical Cycles 7:97-108.

Yao, M.S., and P.H. Stone, 1987. Development of a two-dimensional zonally averaged statistical-dynamical model. Part 1: The parameterization of moist convection and its role in the general circulation. J. Atmos. Sci. 44:65-82.

Appendix A

fsurdatsd

This is the input file used to describe the global land surface in NCAR LSM Version 1.0, when coupled to the MIT IGSM.

Its contents are described in Sections 3.2 and 5.2.

```
1    1    1    1    1    1    1    1    1    1    1    1
1    1    1    1    1    1    1    1    1    1    1    1
-90.0000  180.0000 24 24  33.  33.  34.   0.   0.
-82.1740  180.0000 23 23  33.  33.  34.   0.   0.
-74.3480  180.0000 22 22  33.  33.  34.   0.   0.
-66.5220  180.0000 21 21  33.  33.  34.   0.   0.
-58.5960  180.0000  0  0   0.   0.   0.   0.   0.
-50.8600  180.0000 19 19  33.  33.  34.   0.   1.
-43.0440  180.0000 18 18  33.  33.  34.   0.   1.
-35.2180  180.0000 17 17  33.  33.  34.   0.   4.
-27.3920  180.0000 16 16  33.  33.  34.   0.   3.
-19.5660  180.0000 15 15  33.  33.  34.   0.   2.
-11.7400  180.0000 14 14  33.  33.  34.   1.   1.
 -3.9140  180.0000 13 13  33.  33.  34.   1.   3.
  3.9140  180.0000 12 12  33.  33.  34.   0.   2.
 11.7400  180.0000 11 11  33.  33.  34.   0.   2.
 19.5660  180.0000 10 10  33.  33.  34.   0.   1.
 27.3920  180.0000  9  9  33.  33.  34.   0.   1.
 35.2180  180.0000  8  8  33.  33.  34.   0.   1.
 43.0440  180.0000  7  7  33.  33.  34.   2.   1.
 50.8600  180.0000  6  6  33.  33.  34.   2.   5.
 58.5960  180.0000  5  5  33.  33.  34.   2.  10.
 66.5220  180.0000  4  4  33.  33.  34.   2.   3.
 74.3480  180.0000  3  3  33.  33.  34.   1.   1.
 82.1740  180.0000  2  2  33.  33.  34.   0.   0.
 90.0000  180.0000  0  0   0.   0.   0.   0.   0.
```

Appendix B

NCAR LSM Copyright Notice

The copyright notice for the NCAR Land Surface Model follows.

NCAR Land Surface Model, Version 1.0

Copyright © 1996

University Corporation for Atmospheric Research

All rights reserved.

DISTRIBUTION TERMS AND CONDITIONS NOTICE

Copyright © 1996 University Corporation for Atmospheric Research National Center for Atmospheric Research Climate and Global Dynamics Division.

This software, the Land Surface Model (LSM), version 1, was developed by the Climate and Global Dynamics Division (CGD) Climate Modeling Section (CMS) of the National Center for Atmospheric Research (NCAR), which is operated by the University Corporation for Atmospheric Research (UCAR) and sponsored by the National Science Foundation (NSF).

Access and use of this software shall impose the following obligations and understandings on the user. The user is granted the right, without any fee or cost, to use,

copy, modify, alter, enhance, and distribute this software, and any derivative works thereof, and its supporting documentation for any purpose whatsoever, except commercial sales, provided that this entire notice appears in all copies of the software, derivative works and supporting documentation. Further, the user agrees to credit UCAR/NCAR/CGD in any publications that result from the use of this software or in any software package that includes this software. The names UCAR/NCAR/CGD, however, may not be used in any advertising or publicity to endorse or promote any products or commercial entity unless specific written permission is obtained from UCAR/NCAR/CGD.

The LSM materials are made available with the understanding that UCAR/NCAR/CGD is not obligated to provide (and will not provide) the user with any support, consulting, training, or assistance of any kind with regard to the use, operation and performance of this software, nor to provide the user with any updates, revisions, new versions, or "bug fixes".

This software is provided by UCAR/NCAR/CGD "as is" and any express or implied warranties, including but not limited to, the implied warranties of merchantability and fitness for a particular purpose are disclaimed. In no event shall any damages whatsoever, including but not limited to claims associated with the loss of data or profits, which may result from an action in contract, negligence or other tortious claim that arises out of or in connection with the access, use or performance of this software.